00720

AISC E&R Library
7266

1135

Strength and Stiffness of Semi-Rigid Composite Connections

by

Douglas Ammerman

and

Roberto Leon

authors

key words:
1. semi-rigid connections
2. connections

DEPARTMENT OF CIVIL AND MINERAL ENGINEERING
INSTITUTE OF TECHNOLOGY

UNIVERSITY OF MINNESOTA

RR1135

7266

00721

Strength and Stiffness of Semi-Rigid Composite Connections

Preliminary Report

by

Douglas Ammerman

and

Roberto Leon

Department of Civil and Mineral Engineering

University of Minnesota

Minneapolis, Minnesota

submitted to the

American Institute of Steel Construction
Chicago, Illinois

September 7, 1985

00722

ABSTRACT

The experimental results of two tests on composite semi-rigid connections are reported. The connections were made up of bolted top and seat angles, double web angles, and a composite concrete floor slab. Two tests were conducted, one for gravity load and one for lateral load. The test specimen were similar to the semi-rigid connections tested by another investigator, with the addition of a 4 in. slab, 60 in. wide and containing 8 #4 grade 60 rebars. The composite specimen showed strengths approximately three times and initial stiffnesses eight to ten times larger than those of the bare connection. The initial stiffness of the system was almost that of a rigid connection, and was maintained up to about 30% of the plastic capacity of the composite beam. At ultimate the connections achieved over 75% of the beam plastic capacity and showed no strength deterioration up to rotations of 0.040 radians. In the cyclically loaded specimen some stiffness deterioration occurred after the slab steel yielded at an interstory drift of 1.5%. No slippage of the slab with respect to the beam, slippage of the reinforcing bars, or web crippling in the column was observed. The test showed semi-rigid composite connections (1) possess very large ductilities, (2) are inherently redundant and therefore very safe, (3) can provide large moment transfer across interior joints and (4) can provide the neccessary stiffness to resist lateral loads.

00723

TABLE OF CONTENTS

Chapter 1 INTRODUCTION	1
1.1 General	1
1.2 Advantages of Composite Semi-Rigid Frames	1
Chapter 2 Experimental Design	4
2.1 General	4
2.2 Test Specimen	4
2.3 Material Properties	8
2.4 Load History	8
2.5 Instrumentation	9
Chapter 3 EXPERIMENTAL RESULTS	13
3.1 Gravity Load Test	13
3.2 Cyclic Load Test	18
Chapter 4 ANALYTICAL STUDY	23
4.1 General	23
4.2 Finite Element Model	23
4.3 Modelling of Connection Angle	24
Chapter 5 CONCLUSIONS	26
5.1 Gravity Load Test	26
5.2 Cyclic Load Test	27
5.3 Implications for Design	29
5.4 Summary	30
REFERENCES	31

00724

LIST OF TABLES

Table 1 .- Crossectional Properties 33

Table 2 .- Material Properties 34

Table 3 .- Load History SRCC1M 35

Table 4 .- Load History SRCC1C 36

Table 5 .- Selected Stiffnesses SRCC1M 38

Table 6 .- Peak-to-Peak Stiffness SRCC1C 39

Table 7 .- Selected Stiffnesses SRCC1C 41

Table 8 .- Envelope Stiffness SRCC1C 42

Table 9 .- Hysteresis Loop Areas 43

00725

LIST OF FIGURES

Figure 1 - Test specimen 44

Figure 2 - Specimen in loading frame 45

Figure 3 - Connection details 46

Figure 4 - Slab details 47

Figure 5 - Load history - SRCC1M 48

Figure 6 - Instrumentation in the connection 49

Figure 7 - Strain gages in the connection angles 50

Figure 8 - Shear strain instrumentation 51

Figure 9 - Complete Load-Deflection curve SRCC1M 52

Figure 10 - Complete Moment-Rotation curve 53

Figure 11 - Load-Deflection curve (GL2) 54

Figure 12 - Moment-Rotation curves (GL2) 55

Figure 13 - Load-Deflection curve (GL3) 56

Figure 14 - Moment-Rotation curve (GL3) 57

Figure 15 - Load-Deflection curve (GL4) 58

Figure 16 - Slab cracking patterns 59

Figure 17 - Specimen before slab was cast 60

Figure 18 - Specimen in loading frame before test 60

Figure 19 - Instrumentation in the connection area 61

Figure 20 - Specimen deformed at end of GL2 61

Figure 21 - Right connection (GL2) 62

Figure 22 - Left connection (GL2) 62

Figure 23 - Right connection at end of test (GL4) 63

00726

Figure 24 - Left connection at end of test (GL4) 63

Figure 25 - Column web yielding at LS 30 64

Figure 26 - Details of connection SRCC1C 65

Figure 27 - Load history SRCC1C 66

Figure 28 - Loading scheme for SRCC1C 67

Figure 29 - Complete Load-Deflection curve SRCC1C 68

Figure 30 - Load-Deflection curve LL1 69

Figure 31 - Load-Deflection curve LL2 70

Figure 32 - Load-Deflection curve LS 61-94 71

Figure 33 - Load-Deflection curve LS 94-127 72

Figure 34 - Load-Deflection curve LS 127-160 73

Figure 35 - Load-Deflection curve LL3 74

Figure 36 - Load-Deflection curve LL4 75

Figure 37 - Complete Moment-Rotation curve SRCC1CL 76

Figure 38 - Moment-Rotation curve, left LL1 77

Figure 39 - Moment-Rotation curve, left LL2 78

Figure 40 - Moment-Rotation curve, left LS 61-94 79

Figure 41 - Moment-Rotation curve, left LS 94-127 80

Figure 42 - Moment-Rotation curve, left LS 127-160 81

Figure 43 - Moment-Rotation curve, left LL3 82

Figure 44 - Moment-Rotation curve, left LL4 83

Figure 45 - Complete Moment-Rotation curve SRCC1CR 84

Figure 46 - Moment-Rotation curve, right LL1 85

Figure 47 - Moment-Rotation curve, right LL2 86

Figure 48 - Moment-Rotation curve, right LS 61-94 87

00727

Figure 49 - Moment-Rotation curve, right LS 94-127 88

Figure 50 - Moment-Rotation curve, right LS 127-160 89

Figure 51 - Moment-Rotation curve, right LL3 90

Figure 52 - Moment-Rotation curve, right LL4 91

Figure 53 - Comparison of left and right M-ø curves 92

Figure 54 - Comparison of left and right M-ø curves 93

Figure 55 - Idealized loop - bare steel connection 94

Figure 56 - Idealized loop - composite connection 94

Figure 57 - Yielding of column web 95

Figure 58 - Opening of slab cracks 95

Figure 59 - Seperation of tension angle 96

Figure 60 - Specimen in loading frame 96

Figure 61 - Instrumentation at flange angle 97

Figure 62 - Cracking of slab - LS178 97

Figure 63 - Moment rotation curves SRCC1ML and SRCC1CR 98

Figure 64 - Moment vs. Rotation - GL 2&3, LL 1&2 99

Figure 65 - Model for semi-rigid conneciton 100

Figure 66 - Finite Element mesh of connection 101

Figure 67 - M-ø curves - Experimental vs. Analytical 102

Figure 68 - Stress - Strain model for seat angle 103

Figure 69 - Stress - Strain model for web angles 104

Figure 70 - Finite Element mesh for seat angle 105

Figure 71 - M-ø curves for bare connection 106

00728

Chapter 1

INTRODUCTION

1.1 General

The advent of plastic design for steel structures can result in substantial savings in materials in multi-story steel frames if one considers the connections to be semi-rigid. The main reason for this is plastic design allows both the use of the section's properties at ultimate capacity and recognition of the continuity in the structure provided by the semi-rigid connections and composite floor slabs. The development of a method to predict the moment capacity of these connections is important not only for economy in future construction but also for strengthening and evaluating existing structures. Many of the simple connections in use today are in reality semi-rigid; the additional capacity provided is not taken into account in design because of the lack of a reliable data base on which to formulate analysis and design recommendations.

1.2 Advantages of Composite Semi-Rigid Frames

The use of semi-rigid connections in steel frames can lead to substantial savings and improved structural performance for a combination of the following reasons:

(a) The designer can adjust the level of restraint at the end of the beams and columns. Thus, the beams need not be designed with simple connections, nor do the columns need to be assumed to have pin connections at their end.

00729

The material savings due to (a) a redistribution of forces in the beams, and (b) the decreased effective length of the columns can be as high as 15% over current design practices.

(b) With the utilization of plastic design for steel frames, semi-rigid connections offer the possibility of "tuning" the structure to maximize its structural efficiency. Thus, the designer would be able to force the structure to form a large number of plastic hinges almost simultaneously, at a load close to the collapse load but without excessive deflections.

(c) The additional stiffness and strength provided by semi-rigid connections, and their use with composite floor slabs to provide additional continuity over the columns, will result in decreased drifts and reduced non-structural damage under lateral loads. Moreover, semi-rigid composite connections offer the possibility of concentrating energy dissipation in well-defined areas.

(d) Many of the common connection details in use today could be considered semi-rigid. In areas where seismic risk has been recently upgraded, and where strength evaluation and retrofitting are needed, the use of the additional strength and stiffness provided by these connections can lead to a more realistic and economical assessment of the structure's response to low to moderate seismic loads.

00730

The advantages described above are not currently usable because the utilization of Type 3 connections requires the designer to know their moment-rotation characteristics accurately. Two alternatives are currently possible. The first is based on the use of empirical curves derived from statistical analysis of the few available tests. The second alternative is to actually test some of the connections, and utilize the data obtained in the laboratory in the design process. The first alternative provides an approximation at best, and offers very limited reliability since the statistical database is small and the number of variables involved is large. The experimental alternative is expensive and outside the capabilities of most design firms. It has been used in cases where a more accurate estimate of the strength and stiffness of the structures were required, but seldom as a design tool

This project, of which this document represents a progress report, aims at clarifying the variables influencing the strength and ductility of semi-rigid composite connections through a three-pronged approach. The first approach is to generate the necessary experimental data to derive a comprehensive model of semi-rigid connection behavior. The second is to use the model derived above in actual analysis and design to assess its viability as a design office tool. Finally, an economic assessment of the impact of semi-rigid connections will be made through the comparative design of simple building configurations utilizing simple, semi-rigid and rigid connections. At this stage of the project stage one is almost completed and stage two has begun.

00731

Chapter 2

EXPERIMENTAL DESIGN

2.1 General

The first phase of this project was intended to provide some baseline data to compare the behavior of a semi-rigid connection with and without a composite slab. Given the time and economic constraints, it was decided to use a connection similar to those tested by Radziminski et al.(1,2) for which the moment-rotation characteristics of the non-composite connection were well known. It was recognized that by adding a slab to Radziminski's test specimen without any other modifications some A.I.S.C. design criteria might not be met. The possibility of making meaningful comparisons, however, overrode these objections.

2.2 Test Specimen

2.2.1 Gravity Load Test

The first specimen tested is shown in Figure 1, and will be labelled SRCC1Mx (semi-rigid composite connection, number 1, monotonic loading, x = L or R for left or right side). It consisted of a W14 x 99 column, approximately 12.5 ft. high with two W14 x 38 approximately 10.0 ft long beams framing into it along the strong axis. A composite slab was cast on shored forms above the beam to simulate a continuous floor slab across an interior column.

The column was considerably stronger than the beams in flexure because the decision to avoid stiffeners in the joint area required a heavy column section to remain within the b/t ratios allowed by AISC specifications. Due to material

00732

availability, Radziminki's column, a W12 x 96, was substituted with a W14 x 99. It was recognized that this could lead to problems with web buckling if the specimen developed the full negative capacity of the beams. However, to avoid adding another variable to the test, the addition of stiffeners was ruled out. The flange to thickness ratio for these specimens was 9.3, while the span to depth ratio was 8.0. Both of these were intended to model typical conditions in steel construction.

It was anticipated the column would behave essentially as a fixed end for the gravity load case. Given this assumption, different connection details were used on each side of the column. On the right side a connection very similar to that labelled 14S1 by Radziminski was used. As shown in Figure 3, this connection consisted of a L6 x 4 x 3/8 at the top and bottom, and 2 L4 x 3-1/2 x 1/4 in the web. The top and bottom angles had an 8 in. length along the beam flange, and were connected by two pairs of 3/4 in. ASTM A325 heavy hex bolts. All holes were 1/16 in. oversized to minimize construction problems, thus introducing the possibility of connection slippage. The gage length in the column was only 2 1/2 in. with a single pair of bolts. All bolts were tightened with a calibrated torque wrench to 350 ft-lbs, and no washers were used.

The web angles had originally been designed to sustain 1 1/2 times the shear the member would experience at its A.I.S.C. allowable uniform load as a simply supported beam with a span equal to the length of the test beam (1). It was decided to maintain them in order to eliminate one possible source of differences.

00733

The connection on the left side was similar, except it lacked the upper angle. This specimen was then topped with a 4 in. concrete slab 60 in. wide and contained 8 #4 reinforcing bars with a nominal cover of 1.0 in. (See Fig. 4). This amount of reinforcement was chosen because it provides about the same strength (A^*f_y) as the flange angle which was omitted on the left connection. The 10' long beam approximates a span of 20' for which the AISC specifications give a maximum effective width of 60". Since any kind of horizontal shear failure was deemed to be undesirable, a large number of 5/8" x 2-1/2" shear studs were welded to the beam sections to provide the necessary composite action. A total of 19 studs were present on each side, at a spacing of 6"; this represents about twice as many as required by the current AISC specifications.

The specimen had originally been designed so the connection would be able to transmit some, but not all, of the moment the beams could develop. Radziminski's results indicated the connection transmitted about 670 kip-in at a rotation of 0.024 radians. This corresponds to about 30% of the plastic capacity of the beams. It was anticipated since the behavior of the specimen without the slab was governed by the yielding of the top angle and its bolts in tension, the reinforcing steel in the slab would play a major role in the behavior of the composite specimen. It would seem the right hand side connection, with the top angle included, would have a much larger steel area available in tension, and thus a larger moment capacity. Calculations showed, however, the neutral axis at ultimate will lie very close to the top of the beam flange, and therefore the top angle would not be able to carry very large tensile loads until the slab steel yielded significantly or fractured. Once

00734

this occured, it was anticipated the left connection would lose most of its load-carrying capacity, while the right side would be able to transfer the loads to the upper angle and thus sustain the loads through much larger deformations.

The possible sectional properties to be used for analysis are described in Table 1. The sections compared are the steel beam alone, the full composite beam, the connections with and without the full slab, and the connections with a partial slab. The last case would seem to be the most realistic since it represents the angle connections, the reinforcing bars, and the slab section outside the column. It should be noted that for most cases the neutral axis fell somewhere between the bottom of the slab and the top of the beam web. It appears, therefore, the upper angle on the right connection does not become important until conditions at ultimate are considered. The top angle on the right side was maintained because it was desirable to test one connection which was identical to Radziminski's except for the addition of the composite slab. From Table 1, it is seen first cracking of the slab was anticipated at about 675 kip-in of moment, with a corresponding deflection of about 0.07 in. Yield of the top reinforcing steel was anticipated at a moment of 2167 kip-in for the left connection and 2477 kip-in for the right one. This would correspond to a deflection of about 0.7 in., and was calculated assuming the connection would behave rigidly; thus no allowance for the semi-rigidity of the joint is incorporated. The plastic moment capacity of the composite beam was calculated at 3470 kip-in by considering the slab reinforcement and the beam section to have completely plasticized.

00735

2.2.2 Cyclic Load Test

The test setup for the cyclic test was similar to that used for the monotonic test except load was applied at the bottom of the column instead of at the beam ends. The actuators at the beam ends were replaced by rigid links which were instrumented to form load cells. For reasons of symmetry under lateral load both sides had the same connection. The connection tested was the same as the left connection for the monotonic test (without the top flange angle).

In this test the bolts were tightened using turn of the nut method instead of using a calibrated torque wrench as in the previous test and hardened washers were used under the nuts.

2.3 Material Properties

The specimen was constructed of A36 steel in the beams, columns, and connection angles, grade 60 steel for the reinforcing bars, and concrete with a nominal strength of 4000 psi. The actual material properties obtained from the fabricator and from coupon tests are summarized in Table 2. It seems the properties were very similar to those of Radziminski's tests and direct comparisons are possible.

2.4 Load History

The load histories are summarized in Tables 3 and 4, and shown in Fig. 5 for the gravity load test and Fig. 27 for the lateral load test.

00736

2.41 Gravity Load Test

The first specimen was considered to be part of a braced frame, and thus loaded only under gravity loads. Four load histories were run on this specimen:

GL1 : an elastic cycle to check the instrumentation and obtain some initial values of rotational stiffness. This cycle corresponded to a total deflection of about 0.15 inches at each end, or a total moment of about 340 kip-in. at each side of the column.

GL2 : this was intended to be the main test for the structure, and was carried out by applying equal loads to both beam ends in a load-control mode. This test was conducted until two phenomena occured. One was a series of loud noises, possibly indicating slippage of the bolted joints; the other was the formation of a large crack on one of the nuts in the bottom left connection. These phenomena will be discussed in detail later. Since the latter was unexpected and could have lead to an early failure, the specimen was unloaded and the nut replaced and retightened (See Table 3).

GL3 : this was the same test as GL2, except no further problems were encountered and the beams deformed until a total beam end displacement of about 2.5 inches was achieved. This corresponded to the ultimate capacity of the left connection. The right connection, which was still showing a strength gain with increased deformation was then taken to a maximum deflection of 4.1 in. without any indication of failure.

00737

GL4 : this last test was conducted to determine the ultimate strength of the right connection, and was carried out by holding the left beam in its unloaded position and deflecting the right one until failure occured.

2.4.2 Cyclic Test

The specimen was subjected to a slowly applied cyclic load to determine the strength and hysteretic behavior of this type of connection. The loading was carried out using deflection control, with the assembly being subjected to two load cycles at each level of displacement. The initial load was in the direction which caused negative moment in the right connection and positive moment in the left connection, henceforth to be called positive displacement.

LL1 : At the start of the test the specimen was subjected to several cycles in the elastic range, as determined from the monotonic tests. This portion consisted of two cycles at a displacement of 0.20 in. and two cycles at a displacement of 0.50 in., corresponding to interstory drifts of 0.14% and 0.34% respectively.

LL2 : After these elastic cycles the amplitude of the cycles was increased to bring the connection into the non-linear range. Two cycles were run at each of the folllowing deflections: 1.00 in., 1.50 in., and 2.00 in.

LL3 : At this point deflections in the positive direction were increased to 4.00 in. but the stroke on the hydraulic actuators limited the deflection in the negative direction to 3.00 in. Three cycles of load were run at these deflections to see if the increased damage had any effect on the third

00738

hysteresis loop or if it would remain essentially the same as the second loop. These deflections correspond to a maximum story drift of 2.76% in the positive direction and 2.07% in the negative direction.

LL4 : The final portion of the test was composed of a monotonic loading in the positive direction. This loading was conducted using the same loading scheme as used in test SRCC1M, except the load on the left beam was upward instead of downward.

2.5 Instrumentation

2.5.1 Gravity Load Test

The specimen was instrumented with Schaevitz linear variable differential transformers (LVDT's) to measure deflections above and below the joint (See Fig. 6). These measurements were used to calculate the connection rotations, and were measured with reference to a fixed frame welded to the top and bottom beam flanges at a distance of 12 in. from the column flange. MicroMeasurements strain gauges were used to monitor stresses in the reinforceing bars, in the beams, and in the connection angles. The locations of these are shown in Figures 6 and 7. A Kaye datalogger and Cresent external amplifiers were used to automatically collect the data. All deflection measurements were also checked with Fowler dial gages accurate to 0.0005 inches. Dial gages were also used to monitor the relative slip of the slab with respect to the beam at each end of the test specimen.

00739

The load data was obtained from Strainsert load cells, and checked against the line pressures read by Enerpac dial pressure gages. Very good agreement was found between the two. Beam end deflections were monitored by LVDT's, dial gages, and by levels located about 60 ft. from the specimen. No significant differences were found between the readings from the LVDT's and the dial gages. The former are used on all calculations.

2.5.2 Cyclic Test

The instrumentation of this specimen was similar to that of test SRCC1M for measurement of rotations. LVDTs were also used to measure the interstory drift and any possible slip between the flange angles and the flange of the beams. The average shear strain in the panel zone of the column was also measured using a pivoting frame connected at three corners of this zone and measuring the change in the length of the hypotenuse of the triangle formed by this frame with a LVDT (See Fig. 8). The readings for the load cells and LVDTs were taken automatically with a Keithley DAS Series 500 Measurement and Control System using Schaevitz amplifiers for the LVDTs. The strain gage data was taken manually with Vishay strain indicators and switch and balance units. With load cells at the end of each beam and at the bottom of the column it was possible to determine the moments for each connection independently of the determination of the lateral load applied.

00740

Chapter 3

EXPERIMENTAL RESULTS

3.1 Gravity Load Test

3.1.1 General

In this section, the preliminary experimental results will be discussed. The performance of SRCC1M will be described with the aid of figures and graphs, and the reader is encouraged to refer to them during this discussion. In Figures 9 and 10 the complete load-deflection and moment-rotation curves are presented for comparison purposes. The individual curves for tests GL2 and GL3 are presented in Figures 11 through 15. Selected values for stiffnesses and moments to compare with the bare connection data are shown in Table 5. The cracking patterns for the slab are shown in Fig. 16, and selected photos of the test appear in Figs. 17 through 25.

3.1.2 Behavior of Specimen

During load history one (GL1) the behavior of the specimen was entirely elastic, with no slab cracking or yield observed. It was noted the loading system had about 1/16 in. of slack, and therefore any calculations for stiffness at this stage (total deflection of 0.1 in.) would not be meaningful. This load run was used to insure the proper behavior of the instrumentation. Perfectly elastic behavior was observed up to a moment of 340 kip-in on each connection.

00741

The initial loading during GL2 closely followed the curves for GL1 to a moment of about 500 kip-in (load stage 6, or LS6) when first cracking was observed on the left beam. The initial stiffnesses measured were about 68 kip/in for the right beam and 31 kip/in for the left one. The corresponding rotational stiffnesses were 2.26×10^6 kip-in/radian for the right connection and 2.00×10^6 for the left connection. By comparison specimen 14S1, without a composite slab, had only 1.95×10^5 kip-in/radian.

The cracks observed at LS6 on the left side of the slab began at the column flange tips and extended outwards to the slab edge. The crack penetrated through the slab and corresponded with a signifcant jump on the strain readings from the reinforcing bar strain gages. Similar cracking occured on the right beam at LS7; it should be noted cracking of the slab occured earlier than calculations anticipated. This was probably due to a zone of weakness created by the column flange tip and a hole left in the slab to facilitate lifting of the specimen after testing.

Beginning with loading to LS9 (moment of about 700 kip-in) loud noises were heard, signifying the beginning of the slippage of the left bottom angle. At this point the bolts were carrying approximately 10.4 kips of shear each, above the allowable load of 7.7 kips given by A.I.S.C. specifications. Increasing the load resulted in more loud noises and the beginning of a pronounced loss of stiffness, particularly for the left beam. At LS10 the web angle on the right connection began to show some separation from the column flange, and a second set of longitudinal cracks began to open in the slab. At LS14 it was noticed the nut in one of the bolts connecting the left beam flange and the connection

00742

angle showed a large crack. The deformations in this nut indicated it had ceased to work in friction, transferred its load to the remaining three bolts, and caused substantial slip of the connection by exceeding the frictional capacity of the remaining bolts. No local yielding or damage was observed as a result of this nut cracking. It was decided to unload the specimen and replace the nut in order to avoid an undesirable local failure. The unloading branch of the curves for this test indicated essentially elastic unloading for the left beam, but a much lower stiffness (about 23 kip/in) for the right beam. The unloading resulted in residual deformations due to the bolt slippage. These were particularly large for the left beam, about 0.57 in., and about a third of that, 0.19 in., for the right one. When the damaged nut was removed it was clear the angle had slipped considerably and the bolts were acting in bearing rather than friction.

After the nut was replaced and retightened to 350 ft-lbs of torque, the specimen was reloaded, and this load run labelled GL3. The first noises were heard at LS27, or about the same load level at which loading had been stopped during GL2. At this point the behavior of the two connections began to diverge. The left connection had slipped completely during GL2 and therefore followed a reloading curve without a plateau until the slab rebars began to yield at a load of about 1800 kip-in. After this the stiffness decreased significantly, and its ultimate strength was achieved at a total rotation of about 0.030 radians, corresponding to a moment of 2080 kip-in and a beam end deflection of 2.5 in. The right connection on the other hand had not slipped as much and therefore exhibited a pronounced softening beginning at a load of 1000 kip-in. After the right connection had slipped sufficiently (by LS38, see Fig. 14) the load began to

00743

increase again and a long, essentially linear behavior was achieved as the rebar progressively yielded. The ultimate capacity was reached at 2365 kip-in with a rotation of about 0.024 radians, and a beam end deflection of 4.1 in.

It was noticed the noises stopped after LS39, when the right connection began to work in bearing and the stiffness of that side began to increase again. Also of interest is the fact some yielding of the column web began to occur at LS30, with the formation of yield bands inclined at about 50 degrees, beginning near the points where the compression angles were connected to the beam. Assuming the moment was about 1250 kip-in at this point, and the force in the flange about 80 kips, the column web still complied with the A.I.S.C. equations (1.15-2) and (1.15-3) with a d_c of 11.25 in. (less than 22.9 required if 5/3 factor is used) and a t_f of 0.78 in. (where 0.71 in. is required). Equation (1.15-1) would have begun to require a stiffener when the flange load was about 94 kips (still using the 5/3 factor) or 156 kips (without factor). The latter, which is the most reasonable case since the flange load was well known, would give a moment of about 2500 kip-in or close to the yield capacity of the beams. Beginning with LS38 some localized yielding of the bottom left beam flange was noted near the connection, as well as some yielding in the left web angles. With increase in load, most of the deflection was produced by yielding of the steel reinforcing bars. No visble signs of yielding could be found in the angles except as noted.

The last load run (GL4) was conducted to measure the ultimate capacity of the right connection, as the additional strength provided by the top angle in the connection had not been fully mobilized at this point. For this test the left

08744

beam was held at its deformed position after test GL3. The ultimate capacity was reached at a moment of 2700 kip-in, a rotation of about 0.039 radians and a total deflection of about 7.5 in. Failure occured at LS73 when two of the bolts in the bottom right angle connection to the beam flange fractured in shear, and the whole beam slipped. It ended bearing on the column flange and sustaining about two-thirds of the ultimate load. The horizontal shear load at fracture in the bolts was calculated at about 45 kips or about three times the amount allowed in bearing by the A.I.S.C. specifications. During this last load history, yielding of the left web angle was observed beginning at LS67, and slippage was observed at LS69. The cracks in the slab were very wide at ultimate, with widths of about 3/8 in. for the first crack and 1/8 in. for the second main longitudinal cracks in the right side of the connection. No appreciable slippage of either the slab reinforcement or between the slab and the beam was evident. Removal of the concrete around selected bar ends and shear studs indicated no distress in these areas.

3.1.3 Summary

In summary, the behavior of the specimen can be divided roughly into three phases. The first phase consisted of essentially linear behavior and lasted until the friction capacity of the bolts was exceeded in the bottom angles (LS0 to LS8 for the left, and LS0 to LS15 for the right connection). The second phase comprised the slippge of the bolts until they began to work in bearing (LS8 to LS42 for the left, and LS15 to LS48 for the right). The last phase consisted of a long, almost plastic, curve with no strength deterioration and excellent ductility characteristics. The specimen followed the expected behavior quite closely once a suitable moment-rotation relationship was included

00745

in the calculations. It is thought the slippage phase could be minimized either by reducing the tolerances (not practical) or by increasing the connection frictional capacity with more or larger bolts. This would reduce the slippage phase considerably and enable the connection to achieve its desired moment capacity without any stiffness deterioration.

3.2 Cyclic Load Test

3.2.1 General

The large ductilities and strength evidenced by the gravity load test indicated that it should be possible to use this type of connection to carry some of the lateral loads imposed on structures. Clearly, the lack of full connection rigidity prevents its use in zones of high seismic risk (UBC Zones 3 and 4), but enough strength and stiffness may be present for satisfactory performance under wind loads and small earthquakes (UBC Zones 1 and 2). For this cyclic test the left connection from the gravity load test was chosen.

The details of the connection for this second test are shown in Fig. 26. The load history imposed is given in Fig. 27, and the loading scheme in Fig. 28. The complete load-deformation curve for the test is shown in Fig. 29. Figures 30 through 36 show the loops at different deformation levels to facilitate interpretation. The complete moment-rotation curves are shown in Fig. 37 for the left connection, and in Fig. 45 for the right connection. Figures 38 to 44 show various stages of the moment-rotation curves for the left connection, and corresponding plots for the right connection are shown in Figures 46-52. Figures 53 and 54 show comparisons of the moment-rotation curves when the slab steel began to yield. Photographs at various stages are shown in figures 57 to

00746

62. Stiffnesses and areas of hysteresis loops are reported in tables 6 to 9. While reading this section reference will be made to these figures and tables.

3.2.2 Behavior of Specimen

The initial loading of the specimen consisted of four cycles of load, two each at deflections of 0.2 in. and 0.5 in. at the bottom of the column (LL1). A deflection of 0.5 in. at the bottom of the column corresponds to about 0.34% interstory drift. These cycles resulted in beam end loads of 3 and 9 kips, and no evidence of non-linear behavior. The only damage which occurred during these cycles was the cracking of the slab at the column face. This cracking occurred much earlier than expected, probably the result of shrinkage stresses developed in the three months since the slab was cast.

In this load sequence the maximum moments and rotations achieved were about 600 in-kips and 1.50 milliradians, respectively. By comparison the rotation in the monotonic test at this level of moment was about 0.70 milliradians. This less stiff behavior is most likely due to the earlier cracking of the concrete slab in the cyclic tests and loss of its contribution to stiffness. This loss can be seen by comparing the initial stiffness from this test to that of the monotonic test. The monotonic stiffness was about 2000 kip-in/mR as opposed to only 500 kip-in/mR for the cyclically loaded specimen. If instead of the initial stiffness from the monotonic test we compare stiffnesses after slab cracking had occured, more satisfactory agreement is found. For the monotonic test, at start of GL3 (reloading after the slab had been cracked at GL2), a stiffness of 491 kip-in/mR was computed vs. 488 kip-in/mR for the cyclically loaded one. At the end of this portion of the loading there was no residual deflection and other

00747

than the cracks marked on the slab there was no indication of damage.

The non-linear portion of the load history began with LL2. The first two cycles at an interstory drift of 1.00 in. (0.68%) did not produce any observable distress. However, beginning with the next two cycles at 1.50 in. (1.02%), the first visible signs of damage were evident. This damage was of two types: for the connection loaded with negative moment there was an increasing number of cracks and the existing cracks opened more; for the connection with positive moment the flange angle began to separate from the column face. In this region slip between the flange angles and beam flange began to have an effect on the behavior of the connection and the moment rotation curves deviated from linear. The large non-linearities in this region are due primarily to yielding of the slab reinforcement, as shown in Figs. 53 and 54. This yielding began in the first loop with a deflection of 1.50 in. for the right connection and in the first loop with a deflection of 2.00 in. for the left connection. This indicates a possible influence of the initial direction of loading.

As the loading proceded into LL3, with maximum positive displacements of 4.25 in. and negative ones of 2.91 in., significant hysteresis losses began to occur. The opening up of cracks and the pulling away from the column face of the flange angle were the causes of pinching of the hysteresis loops in this region.

An interesting comparison can be made at this level between the behavior of a bare steel connection and the composite one. For the bare steel connection Radziminski had proposed a three-zone interpretation of the hysteresis loops. This is shown in Fig. 55. Zones 1 and 3 represent the compression angle bearing

00748

against the column, and zone 2 represents the area of low stiffness when the gap between the angle and the column was not closed. For the composite connection, a similar non-symmetrical loop can be drawn as shown in Fig. 56. Consider this loop at point 1, when the deflection is a maximum in the positive direction. The cracks in the slab of the right beam are open and the bottom angle of the left connection is pulled away from the column face. As the specimen is unloaded to point 2 the loop follows an essentially elastic unloading. At point 2 the cracks in the right beam are still open and the left flange angle is still not bearing against the column face. As the specimen is loaded in the negative direction the cracks and seperation of the flange angle close. In this portion of the curve the stiffness is at a minimum. As load is increased after the cracks close and the angle bears the stiffness begins to increase until it reaches a maximum at the maximum negative deflection (point 3). At this point the situation is opposite of point 1, the cracks are in the slab of the left beam and the right connection flange angle is pulled away from the column face. As the beam is unloaded and then reloaded in the positive direction the procedure described above is repeated with left and right reversed. Because the behavior of the composite connection is not symmetrical, the length of the small stiffness portion will depend on whether the slab steel has yielded, and what size cracks were produced in the process.

Even with this detrimental behavior of the connections, as load was increased to the point where the cracks were closed and the flange angle was bearing, the stiffness increased to the same values obtained in the monotonic test for similar levels of rotation. (see Table 8)

00749

As the level of load for each cycle increased there was greater residual deformation at the end of the cycle. At the zero load position in the final set of cycles there was a residual deformation of about 2 in. in the positive direction and 1 in. in the negative direction.

The final monotonic test (LL4) did not produce any new results, except to prove very large rotations can be accommodated by the system and ductile behavior can easily be achieved.

3.2.3 Summary

The results of the cyclic test indicate good lateral load behavior can be obtained with composite semi-rigid connections. The first large non-linearities in the hysteresis loops were noted at an interstory diplacement of 1.5%. Normal design procedures would limit this to 0.5% under most conditions for the type of construction envisioned. The large ductilities and good energy-absorption capacity evidenced by the system, as well as its inherent redundancy will probably make it a very attractive structural system in large areas of the U.S.A.

80758

Chapter 4

ANALYTICAL STUDY

4.1 General

The analytical effort has been centered on two issues. The first is to develop a comprehensive finite element model capable of predicting the monotonic connection behavior. The second, and parallel effort, has been aimed at developing a simplified truss element model for the connection angles in order to reduce the computational effort.

4.2 Finite Element Model

A very complete three-dimensional modelling of the entire test structure was first carried out utilizing the program ADINA. The object in this phase was to replicate the experimental results obtained in the monotonic test, and to derive a model to serve as a baseline for future simplifications. The general model of the connection is shown in Fig. 65. The beam was modelled using 3D elements, the bars and angles utilizing truss elements, and the shear connectors by very stiff 2D beam elements. A mesh for the area next to the connection is shown in Fig. 66.

The model was found to produce results in very good agreement with the experimental ones, as shown in Fig. 67. The material model utilized has a significant bearing on computation time, so a simple linear elasto-plastic relationship was used for the monotonic case. The stress-strain characteristics used for the model are shown in Fig. 68 and 69. Because of this assumption, the model cannot be used for cyclic loading. It can, however, provide an excellent

00751

approximation to the cracked stiffness of the system at a very reasonable cost.

4.3 Modelling of Connection Angle

For the case of cyclic loading, it becomes necessary to develop a very precise stress-strain relationship for the angle in tension if it is to be modelled as a truss element. The angle is attached to the column by A325 bolts, for which a gage distance of at least 2.25 in. is desirable for erection purposes. This results in the angle being loaded in tension along its connection to the beam flange, but almost as a cantilever beam on the leg attached to the column. The relatively small thickness (3/8 in.) of the angles results in a modest section modulus and consequently, in yielding of this cantilever at very low loads. The unfortunate consequence of this yielding is the initial slope and the yield load in tension are much smaller than in compression (see Fig. 68). Most finite element codes can handle this type of material model only as a user-specified constitutive relationship; this signifies a large increase in the input data as well as in CPU time.

Since this yielding affects the rotation of the connection significantly, another finite element model was made of the angle itself in order to determine the load-deformation characteristics of the truss element. The mesh utilized is shown in Fig. 70, and the results for selected geometries are shown in Fig. 71. As can be seen from this last figure, softening of the angle in tension begins very early and will result in large permanent deformations if the force in the beam flange reaches the yield force of the beam. These results refer to the bare connection, without the contribution of the slab or the slab reinforcing bars. Modelling of the latter case is underway, and results are expected to

00752

show that a large portion of the initial gain in stiffness and strength for the composite connection is due to the shifting of the neutral axis caused by the large slab.

00753

Chapter 5

CONCLUSIONS

5.1 Gravity Load Test

This preliminary test leads to the following conclusions:

1) The behavior of a composite connection is similar to that of a non-composite connection, with the slab steel replacing the top angle. The higher strength of the rebar steel, the increased moment arm and the presence of a slab result in a stronger, stiffer and more ductile system. The substitution of the angle with the rebar also results in a much more linear initial behavior.

2) The moment-rotation curves are fairly linear within the range that should be used for service loads, and thus the calculations required might not be as difficult as previously thought. For design purposes, the connection can probably be considered linear with a stiffness similar to those obtained at the beginning of GL3, if shakedown can be assumed to have taken place during GL2. Thus the use of a complex approach, requiring B-splines or polynomials to approximate the moment-rotation characteristics, might not be required for everyday office use.

3) The behavior of the specimen was governed primarily by the yielding of the slab steel. This specimen had only 8 # 4 bars (A = 1.60 in.) for a reinforcement ratio of 0.67 in the slab. Substantial gains in the linearity of the moment rotation curves can be expected if the reinforcement ratio is increased. The strain gauge data available from the slab rebars indicates,

00754

after a cursory examination, the stresses were not distributed uniformly across the slab, but more on a parabolic fashion, with the outermost bars carrying about half as much load up to yield as the innermost ones.

4) Although the forces in the column web were very large, and at the end of the test exceeded AISC allowable values, only very limited yielding was observed. Thus web crippling might not be as severe a problem for semi-rigid connections as with rigid ones.

5) If the slippage of the bolts can be limited, either by increasing their size or number, the linear behavior can probably be extended far beyond what was shown in this test.

6) The use of a top angle provided reserve strength capacity and stiffness at ultimate. The deformations observed in the angles were very small until the end of test GL3.

5.2 Cyclic Load Test

The results of this test lead to the following conclusions:

1) The behavior of a composite connection under cyclic loads is considerably different than similar non-composite connections. The increased strength of the connection makes the "yielding" of the bottom flange angle occur at a moment that is a lower proportion of the yield moment than is the case for a non-composite connection. This charecteristic leads to increased pinching of the hysteresis loops, but the area they enclose is still about twice as large as

007755

enclosed by loops for the same range of rotations in non-composite connections.

2) The envelope of the moment rotation curves from the cyclic test follows the moment rotation curve of the monotonic test very closely. (Fig. 63)

3) The shear strains observed were large enough to cause some yielding in the column web (see Fig. 57), but not nearly as large as those obtained in tests of rigid connections. This suggests the use of web stiffeners may not be required as often in semi-rigid construction as in rigid construction.

4) The behavior of the connection was governed by the plastic bending of the flange angle and the yielding of the rebar. The more important of these at lower levels of load (in the service range) is the bending of the flange angle, as it occurs first for a configuration like the one tested. This problem can be eliminated by using a thicker and/or longer angle, by using a plate welded to the column in place of the angle, or--especially in the case of retrofits--a weld could be added along the top of the leg adjacent to the column. The addition of more reinforcement in the slab along with these modifications would produce a longer linear portion in the moment-rotation curves, and enable the designer to detail a connection capable of developing the full moment capacity of the beam

5) The lack of a top angle did not have an effect in the cyclic test any more than it did in the monotonic case. The removal of this connection element simplifies erection and decreases cost.

00756

6) The hysteresis loops for the third cycle at the maximum deflection did not change appreciably from the loops from the second cycle at this deflection (see Fig.s 43 and 51). This indicates there is no increase in damage as the number of cycles at a given loading increases, suggesting incremental collapse should not be a problem.

7) The direction of first damage did not appear to have any effect on the behavior of the connection. The moment rotation curves obtained for the right connection are the same as those for the left connection.

5.3 Implications for Design

The results of this project indicate that the particular connection configuration tested could be used to provide lateral stability if design drifts are kept below 0.5%. It should be noted, however, that these results are only for one connection, and to generalize them to all of the many possible connection configurations without further testing should be strongly discouraged.

These results suggest the use of semi-rigid composite connections may be an economical way to resist lateral load in low rise structures or to help in the resistance of these forces in larger structures. It should be noted, however, that these connections have only been tested in isolated subassemblies and not as part of a moment resisting frame. A test of this type will be carried out later this year.

00757

If this type of connection is to be used as part of a frame, the analysis must include springs (perhaps non-linear) at the ends of the beams. For linear springs, methods of adapting the most commonly used analysis procedures have been reported, but to incorporate non-linear springs is more difficult.

The most critical aspect of replacing rigid connections with semi-rigid ones is the increased drifts they allow. Most designers do not have a feel for the range of drifts associated with semi-rigid connections. For structures with large lateral loads the moment resistance of a semi-rigid connection may be insufficient to provide the required lateral stability.

5.4 Summary

The use of a structural system based on a semi-rigid composite connection has many advantages. The most important are:

a) The system possesses very large ductilities, and is inherently redundant.

b) The connection details are simple and should not increase cost significantly.

c) Quality control problems are minimized by the simplicity of the connection.

d) The contribution of the slab to the stiffness of the structural system has been demonstrated, and its beneficial influence on column behavior proved.

00758

REFERENCES

(1) Altman, W.G., Azizinamini, A., Bradburn, J.H., and Radziminski, J.B., Moment-Rotation Characteristics of Semi-Rigid Steel Beam-Column Connections, Technical Report, Dept. of Civil Enginnering, University of South Carolina, June, 1982.

(2) Azizinamini, A., Bradburn, J.H., and Radziminski, J.B., Static and Cyclic Behavior of Semi-Rigid Steel Beam-Column Connections, Technical Report, Dept. of Civil Engineering, University of South Carolina, March, 1985.

80759

ACKNOWLEDGEMENTS

The help of the staff at the Department of Civil and Mineral Engineering is gratefully acknowledged. The contributions of Bruce Hennen to the instrumentation and testing of the specimen are particularly appreciated. The materials for the test were donated by LeJeune Steel, Minneapolis, and Mr. Larry Kloiber's advice and suggestions were greatly appreciated. Finally the authors would like to extend their thanks to Dr. Theodore Galambos for his guidance and suggestions during this project.

00760

Table 1 - Crossectional Properties

Type	Case	A ($in.^2$)	I ($in.^4$)	y (in.)	St ($in.^3$)	Sc ($in.^3$)	M (k-in)
W14 x 38	D	11.20	385.0	7.05	54.6	54.6	2613 (1)
Composite	A	45.21	1126.9	13.90	268.2	81.1	
Beam	B	13.57	573.0	8.76	61.4	65.4	3470 (2)
Right	A	44.01	1023.8	14.13	235.7	74.5	
Connection	B	12.37	544.0	9.14	58.3	59.5	2477 (3)
	C	36.34	1039.8	12.66	178.8	82.1	681 (4)
Left	A	41.01	1023.5	14.12	235.0	72.5	
Connection	B	9.37	560.8	7.49	51.0	74.9	2167 (3)
	C	33.34	1054.9	12.51	177.1	84.3	675 (4)

(1) Plastic moment capacity of beam alone.
(2) Plastic moment capacity of beam plus slab reinforcement.
(3) Yield moment based on elastic properties.
(4) Cracking moment based on $7.5\sqrt{f'_c}$ tensile strength.

Cases - A - full slab width plus reinforcement.
B - no contribution from slab, except for reinforcement.
C - slab width outside column flange plus reinforcement.
D - bare beam, no slab or reinforcement considered.

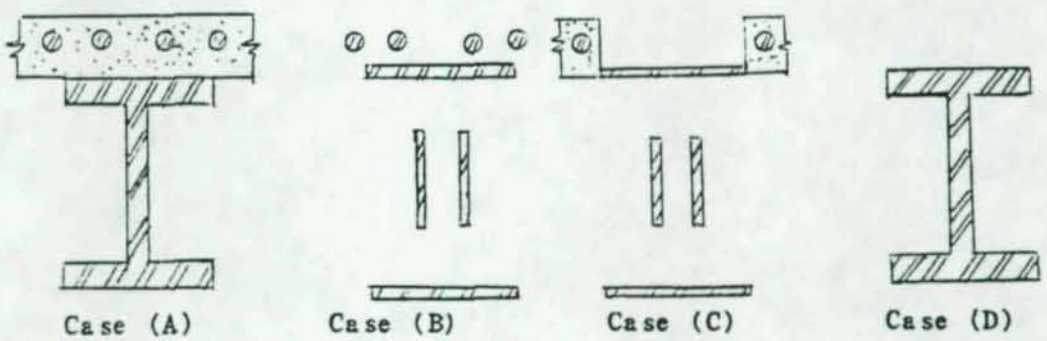

Case (A) Case (B) Case (C) Case (D)

80761

Table 2 - Material Properties

Member	Yield Stress (ksi)	Ultimate Strength (ksi)
Beam	42.5	65.0
Column	42.6	67.0
Angle	43.0	65.6
Rebar	63.0	108.0
	Yield Stress f'c (psi)	Tensile Strength (psi)
Concrete	4490	545

(*) By comparison, Radziminski's test had yield strengths varying from 37.6 to 42.6 ksi for yield and 67.9 to 69.9 ksi for ultimate strength; the author does not specify whether these refer to the angles only or to all structural steel used.

00762

Table 3 - Load History - SRCC1M

Load History	Load Stage	Left Load (kips)	Left Deflection (inches)	Right Load (kips)	Right Deflection (inches)
2	1	0.960	0.046	0.984	0.000
	5	3.980	0.130	3.948	0.057
	9	6.096	0.281	6.032	0.166
	13	8.048	0.372	8.080	0.302
	17	9.680	0.684	10.000	0.634
	18	9.856	0.858	10.352	0.638
	19	0.032	0.580	0.108	0.194
3	21	0.400	0.580	0.400	0.214
	25	6.968	0.858	7.048	0.464
	29	10.416	1.088	10.768	0.685
	33	10.744	1.258	10.980	0.746
	37	11.636	1.202	12.572	1.298
	41	13.212	1.258	14.432	1.865
	45	16.000	2.066	17.368	2.602
	49	18.472	3.623	20.940	4.262
4	61	0.064	2.705	0.256	2.207
	65	13.752	3.484	14.692	3.248
	69	19.152	3.431	22.560	5.249
	72	19.248	3.421	23.920	7.374
	73	13.840	3.497	16.012	8.819

00763

Table 4 - Load History - SRCC1C

Load History	Load Stage	Deflection (in.)	Drift (%)	Lateral Load (kips)
1	1	0.00	0.000	0.0
	9	0.14	0.096	3.2
	13	0.00	0.000	0.0
	19	-0.18	0.124	-3.0
	22	0.00	0.000	-0.1
	24	0.12	0.082	2.9
	26	0.00	0.000	0.0
	28	-0.17	0.118	-2.7
	29	-0.02	0.017	-0.3
	35	0.47	0.324	8.3
	38	0.02	0.017	0.2
	45	-0.52	0.353	-7.9
	48	0.00	0.000	-0.3
	52	0.47	0.320	8.1
	54	0.00	0.000	-0.2
	57	-0.50	0.344	-7.5
	60	0.00	0.000	-0.3
2	68	0.96	0.660	13.1
	70	0.08	0.058	0.2
	79	-0.99	0.677	-13.8
	82	-0.06	0.041	-0.3
	86	0.97	0.667	12.7
	88	0.00	0.002	0.2
	92	-0.97	0.668	-13.2
	94	-0.03	0.022	-0.3
	100	1.63	1.112	15.6
	104	-0.24	0.164	-3.6
	109	-1.55	1.064	-16.8
	113	0.00	0.003	1.1
	117	1.48	1.011	14.2
	120	0.33	0.225	0.1
	125	-1.47	1.008	-15.5
	127	-0.30	0.207	-0.4
	134	2.24	1.534	18.4
	138	0.02	0.013	-2.5
	147	-1.91	1.307	-18.8
	151	-0.64	0.439	-0.3
	155	2.40	1.646	16.9
	157	-0.54	0.367	-6.8
	159	-2.08	1.428	-18.3
	160	-0.48	0.327	-0.3

00764

Table 4 - Load History - SRCC1C (cont.)

Load History	Load Stage	Deflection (in.)	Drift (%)	Lateral Load (kips)
3	164	4.14	2.834	21.6
	173	-0.54	0.373	-7.9
	176	-2.80	1.915	-18.0
	180	0.63	0.430	4.0
	186	4.23	2.895	20.8
	192	-0.27	0.182	-7.3
	195	-2.43	1.665	-17.4
	198	1.03	0.704	3.9
	201	4.25	2.910	20.5
	206	-0.63	0.431	-8.3
	208	-2.45	1.675	-17.3
	213	-0.71	0.483	-0.4
4	251	1.70	1.161	10.0
	289	2.84	1.945	15.4
	318	3.80	2.603	19.4
	348	4.76	3.262	22.3

00765

Table 5 - Stiffness at Selected Points - SRCC1M

Condition	SRCC1MR	SRCC1ML	Radziminski
Initial Stiffness	2260	2000	195
Slope of Secant at 4.0 mR	327	270	109
Slope of Tangent at 4.0 mR	95.2	63.3	53.5
Moment at 4.0 mR	1306	1078	435
Slope of Tangent at 24 mR	40.0	14.0	5.8
Moment at 24 mR	2404	1939	668
Slope of Tangent at 38 mR	9.1	7.5	—
Moment at 38 mR	2640	2173	—

All stiffnesses and slopes are given in kip-in per milliRadian;
All moment are given in kip-in.

00766

Table 6 - Peak-to-Peak Stiffness

Left Connection

Load Stage	End Moment (k-in)	End Rotation (mR)	Stiffness (k-in/mR)	Stiffness/Ideal (%)
0-9	240	0.43	557.0	100
9-19	-232	-0.72	411.7	82
19-24	235	0.41	413.4	83
24-28	-208	-0.68	405.7	81
28-35	625	1.73	346.3	69
35-45	-569	-1.87	332.3	66
45-52	633	1.72	334.9	67
52-57	-516	-1.92	315.5	63
57-68	923	4.02	242.2	48
68-79	-997	-4.35	229.3	50
79-86	936	4.23	225.5	50
86-92	-931	-4.33	218.3	47
92-100	1052	6.42	184.4	62
100-109	-1292	-6.62	179.8	60
109-117	1018	6.17	180.6	59
117-125	-1150	-6.33	173.4	55
125-134	1145	9.65	143.6	73
134-146	-1513	-9.25	140.7	65
146-155	1147	7.53	158.5	63
155-159	-1380	-13.76	118.7	82
159-164	1313	17.65	85.7	80
164-176	-1226	-16.85	73.6	62
176-186	1309	18.03	72.7	69
186-195	-1202	-17.34	71.0	61
195-201	1273	18.52	69.0	67
201-207	-1174	-17.55	67.8	60
207-349	1377	16.11	75.8	64

00767

Table 6 - Peak-to-Peak Stiffness (cont.)

Right Connection

Load Stage	End Moment (k-in)	End Rotation (mR)	Stiffness (k-in/mR)	Stiffness/Ideal (%)
0-9	-238	-0.49	487.7	98
9-19	162	0.61	363.5	73
19-24	-201	-0.47	336.8	67
24-28	157	0.58	341.0	68
28-35	-610	-1.88	310.4	62
35-45	536	1.36	352.5	71
45-52	-565	-1.88	338.8	68
52-57	527	1.34	338.5	68
57-68	-987	-3.72	298.8	60
68-79	926	3.79	254.6	51
79-86	-920	-3.84	242.1	48
86-92	921	3.90	238.0	48
92-100	-1209	-5.65	223.1	63
100-109	1048	6.06	192.9	61
109-118	-1023	-5.14	185.1	48
118-125	1016	5.65	189.1	56
125-134	-1480	-8.30	178.9	74
134-148	1188	8.51	158.8	71
148-155	-1279	-8.89	141.8	63
155-159	1181	8.80	139.0	64
159-164	-1779	-20.27	101.9	100
164-176	1283	12.01	94.9	60
176-186	-1675	-20.51	91.0	93
186-195	1255	12.55	88.7	59
195-201	-1671	-20.86	87.6	91
201-208	1237	12.91	86.1	59
208-350	-1894	-26.38	79.7	100

The Stiffness/Ideal is obtained by multiplying the stiffness by the ductility ratio (assume yield rotations of 4 mR and 3.8 mR for positive and negative moments) and dividing by the elastic stiffness (assume 500 k-in/mR).

00768

Table 7 - Stiffness at Selected Points - SRCC1C

Left Connection

Load Stage	Moment (k-in)	Rotation (mR)	Stiffness (k-in/mR)
68	923	4.021	100.1
96	897	4.088	182.1
154	1030	4.998	75.8
181	675	5.194	65.4
91	-874	-4.110	342.9
107	-920	-4.509	294.4
141	-693	-4.832	143.6
192	-345	-4.825	30.9
134	1145	9.647	9.1
163	1255	10.695	43.1
184	1156	12.079	78.3
200	1110	12.554	83.0
146	-1513	-9.247	83.8
158	-814	-11.080	102.0
174	-623	-10.873	34.9
193	-611	-12.119	34.4

Right Connection

Load Stage	Moment (k-in)	Rotation (mR)	Stiffness (k-in/mR)
68	-987	-3.725	135.2
86	-920	-3.836	357.5
97	-1058	-4.413	325.3
116	-774	-4.279	294.7
129	-755	-4.233	253.4
153	-431	-4.043	87.1
79	926	3.789	69.6
92	921	3.900	139.1
107	962	4.246	138.9
122	790	4.095	179.8
141	935	4.526	141.0
155	-1279	-8.894	209.2
183	-504	-11.417	95.0
199	-460	-11.395	36.4
158	1181	8.796	56.5
175	1243	10.336	33.6
207	1119	10.251	61.3

00769

Table 8 - Stiffness of Envelope - SRCC1C

Left Connection

Load Stage	Moment (kip-in)	Rotation (mR)	Stiffness (kip-in/mR)
0-9	240	0.4	557.0
24-35	625	1.7	296.9
52-68	923	4.0	126.1
86-100	1052	6.4	52.74
117-134	1145	9.6	36.51
155-164	1313	17.7	16.38
0-18	-217	-0.7	326.7
28-45	-569	-1.9	304.0
57-79	-997	-4.3	197.8
92-109	-1293	-6.6	157.8
125-146	-1513	-9.2	124.5

Right Connection

Load Stage	Moment (kip-in)	Rotation (mR)	Stiffness (kip-in/mR)
0-9	-238	-0.5	487.7
24-35	-610	-1.9	287.8
52-68	-987	-3.7	229.1
86-100	-1209	-5.6	159.5
117-134	-1480	-8.3	137.9
155-164	-1779	-20.3	44.02
201-350	-1894	-26.4	40.35
0-19	162	0.6	264.3
28-45	536	1.4	485.8
57-79	926	3.8	162.9
92-109	1048	6.1	59.22
125-148	1188	8.5	60.19
159-176	1283	12.0	31.79

00778

Table 9 - Area Enclosed by Hysteresis Loops

Left Connection

Load Stage	Moment Range (kip-in)	Rotation Range (mR)	Area (kip-in)	Area/Ideal (%)
60-82	1900	8.4	1.33	83
82-94	1900	8.6	.29	14
94-113	2300	13.0	3.65	25
113-127	2200	12.5	1.40	11
127-151	2700	18.9	17.63	57
151-160	2500	21.4	6.61	10
160-179	2500	34.5	21.20	28
179-197	2500	35.4	19.15	25
197-213	2400	36.1	15.87	20

Right Connection

Load Stage	Moment Range (kip-in)	Rotation Range (mR)	Area (kip-in)	Area/Ideal (%)
60-82	1900	7.5	1.19	-
82-94	1800	7.7	.26	-
94-113	2300	11.7	2.48	15
113-127	2100	10.8	.96	12
127-151	2700	16.8	7.69	30
151-160	2500	17.7	5.65	20
160-179	3100	32.3	27.69	40
179-197	2900	33.1	14.27	20
197-213	2900	33.8	13.06	18

The ideal area is calculated by assuming elastic-perfectly plastic behavior with a yield moment of 1500 kip-in at a rotation of 4 mR in the positive direction and a yield moment of 1300 kip-in at a rotation of 3.8 mR in the negative direction.

00771

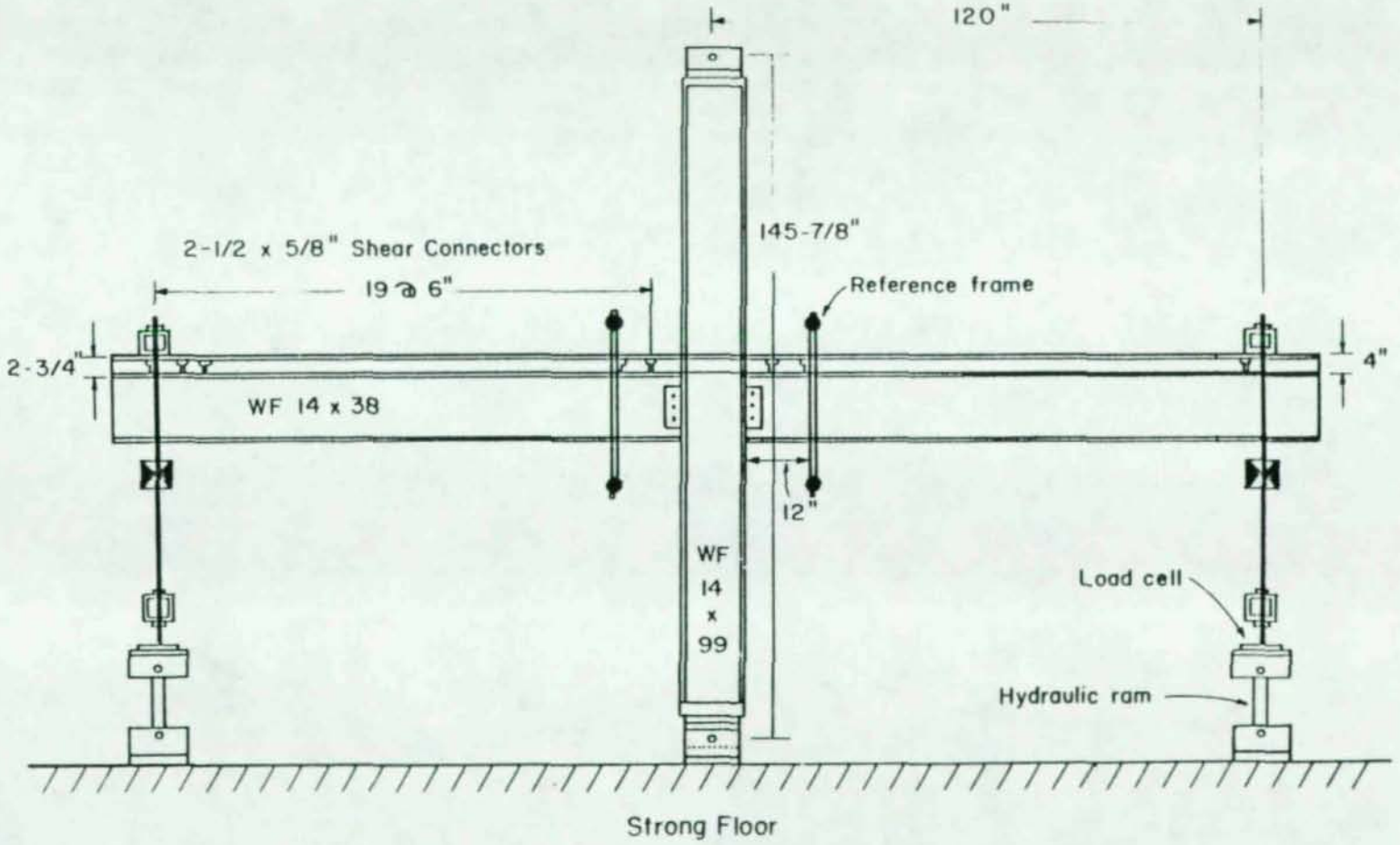

Figure 1.- Overall view of test specimen.

00772

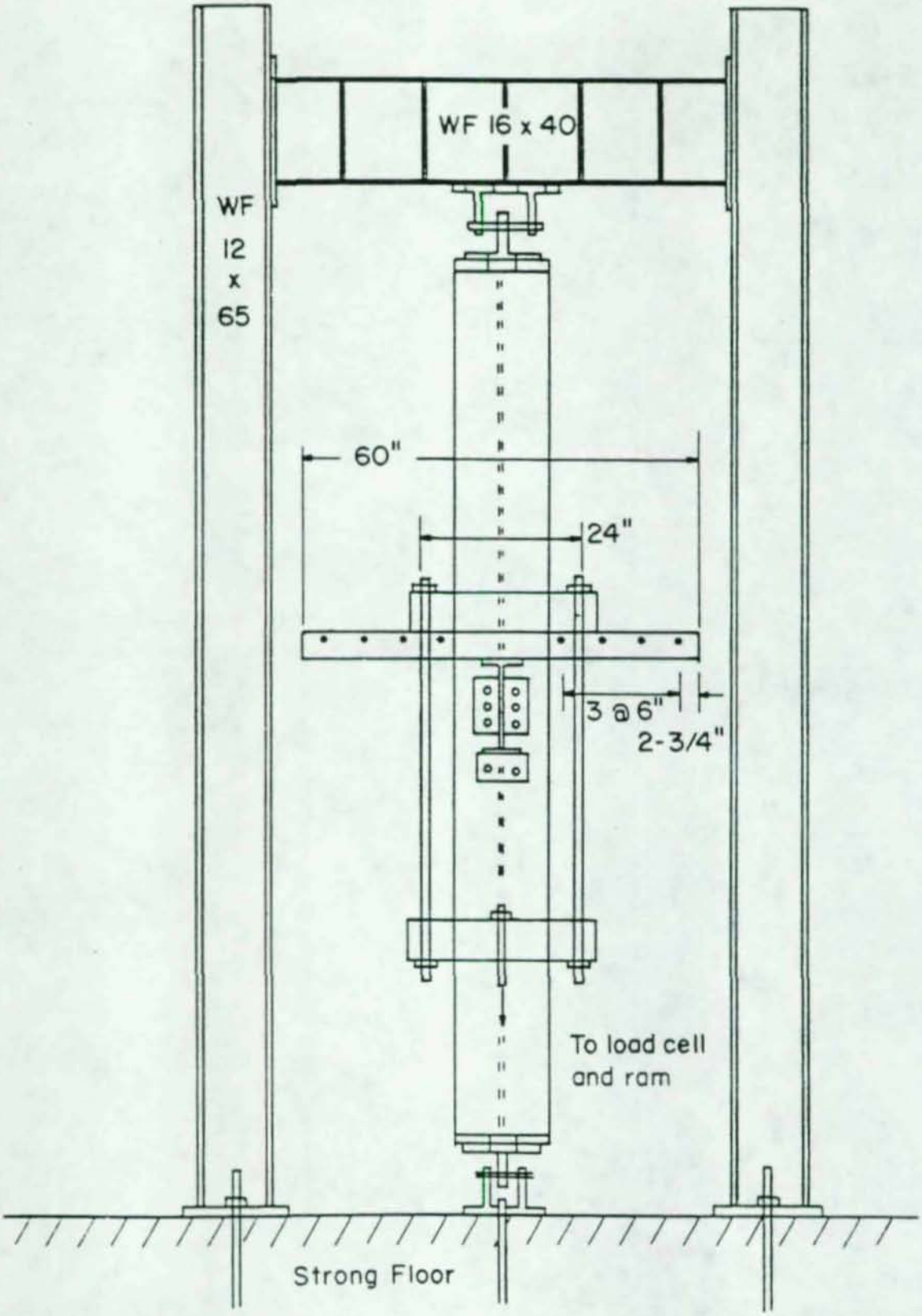

Figure 2 - Specimen in loading frame

00773

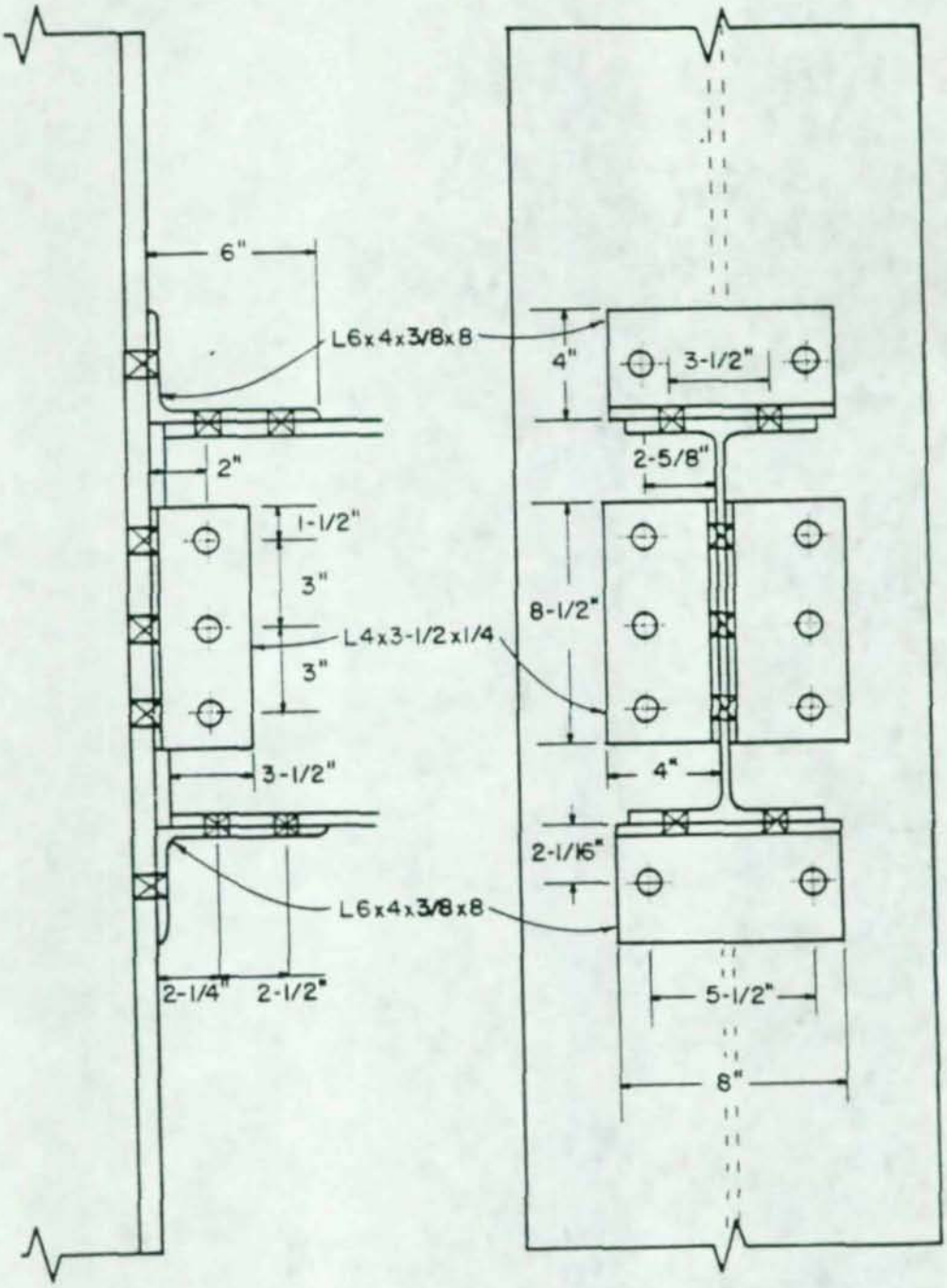

Figure 3 - Details of connection SRCC1MR

00774

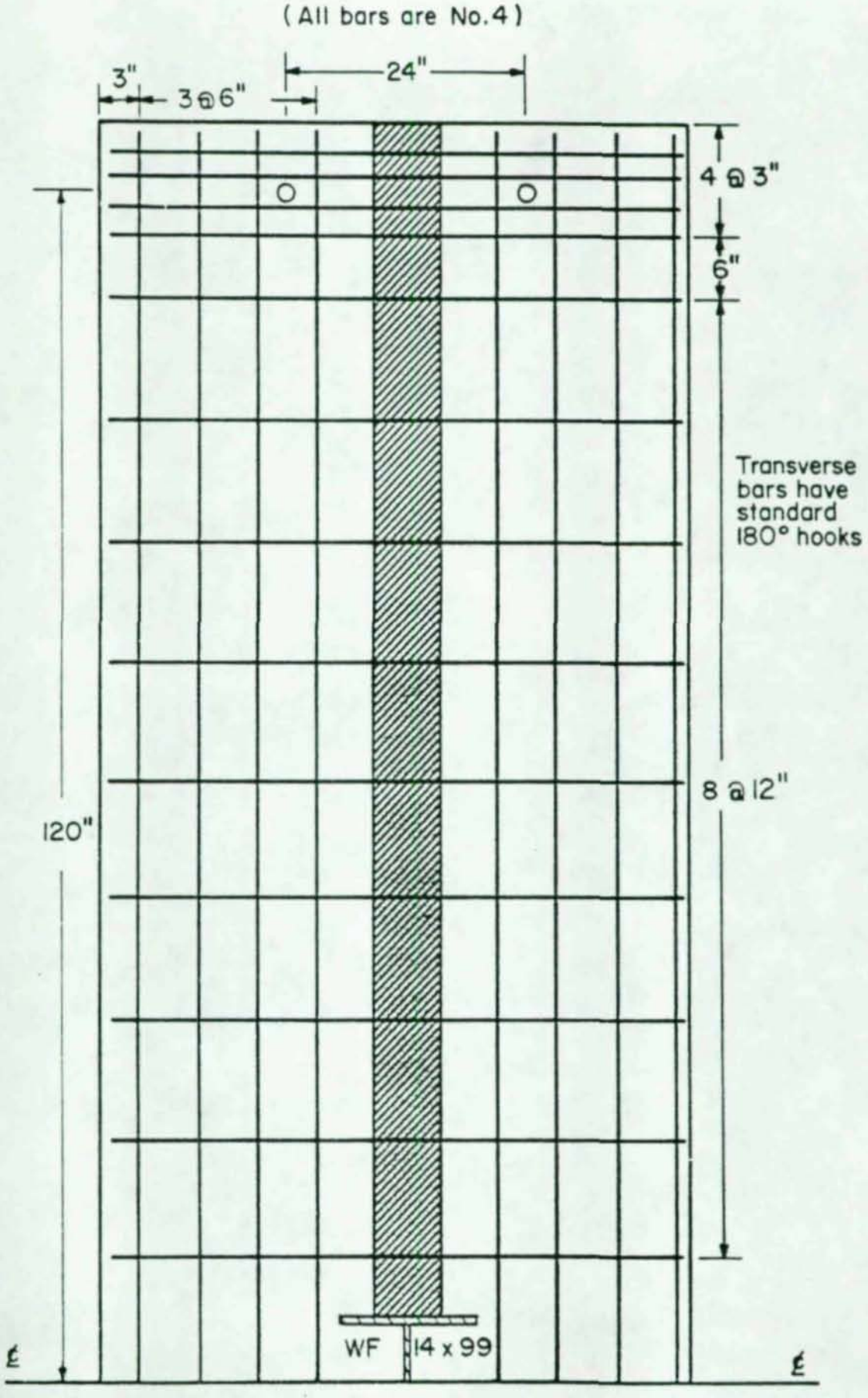

Figure 4 - Details of slab

FIGURE 5 - LOAD HISTORY FOR GRAVITY LOAD TEST - SRCC1M

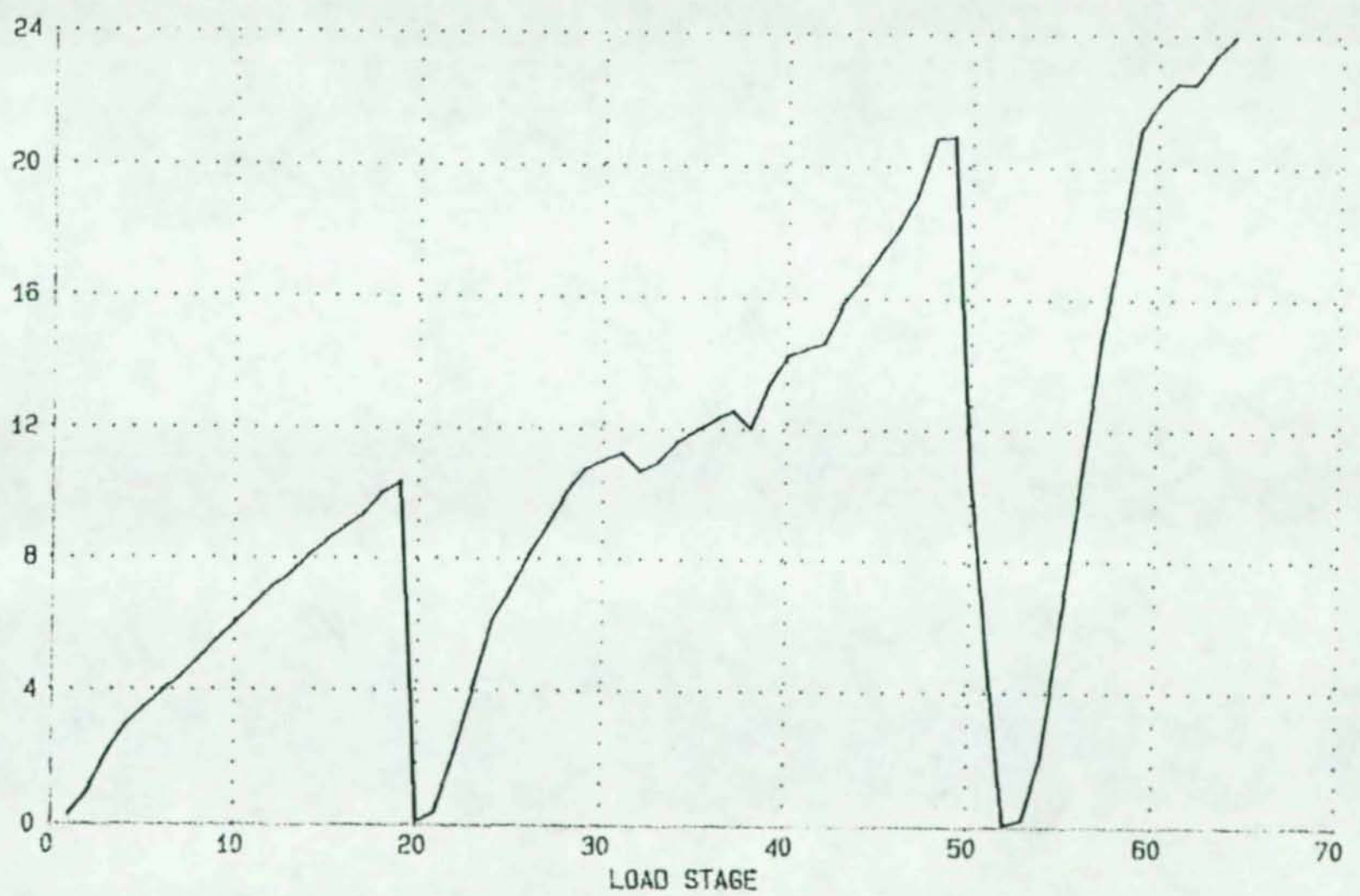

00776

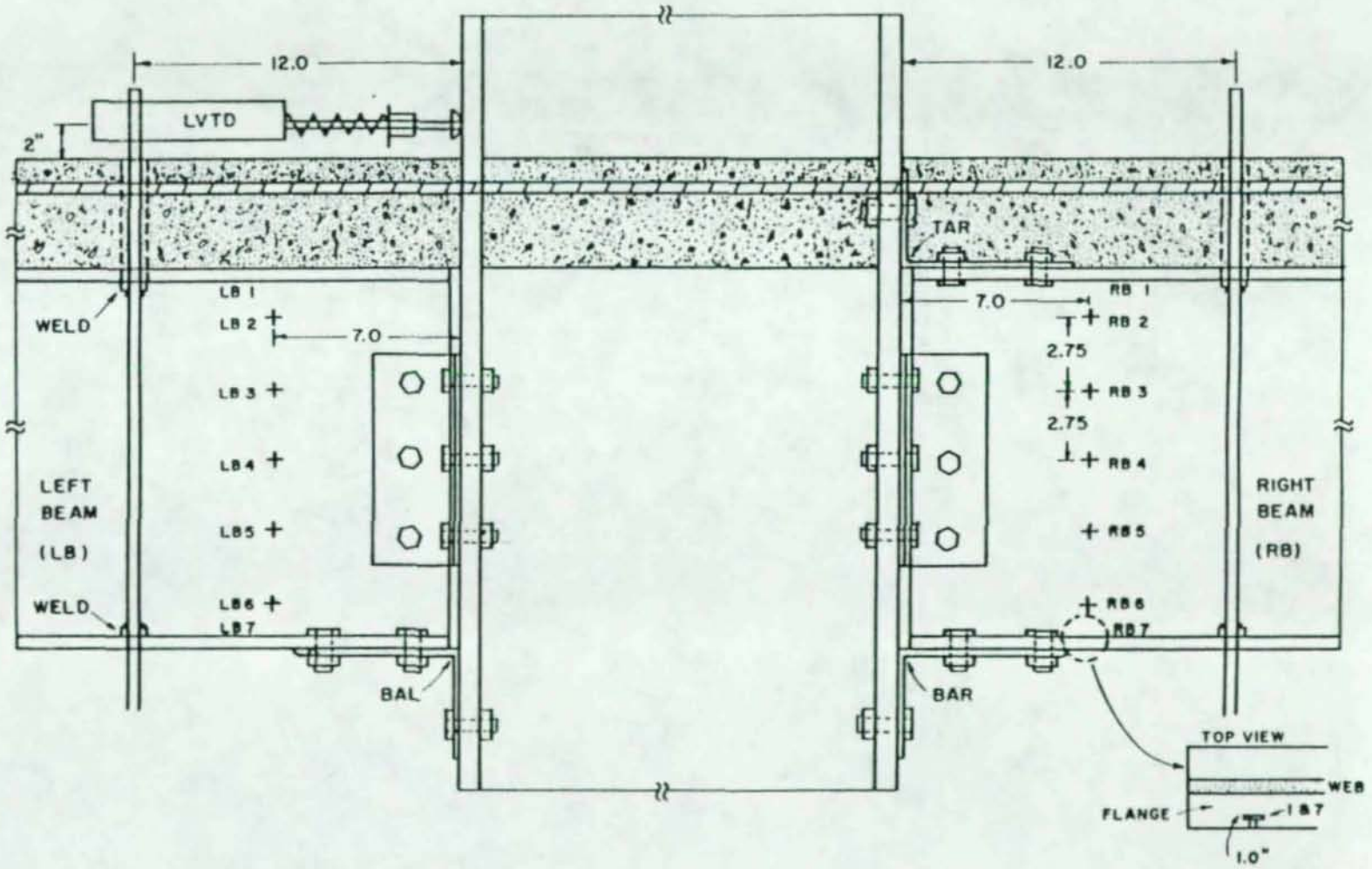

Figure 6 - Instrumentation in the connection area

80777

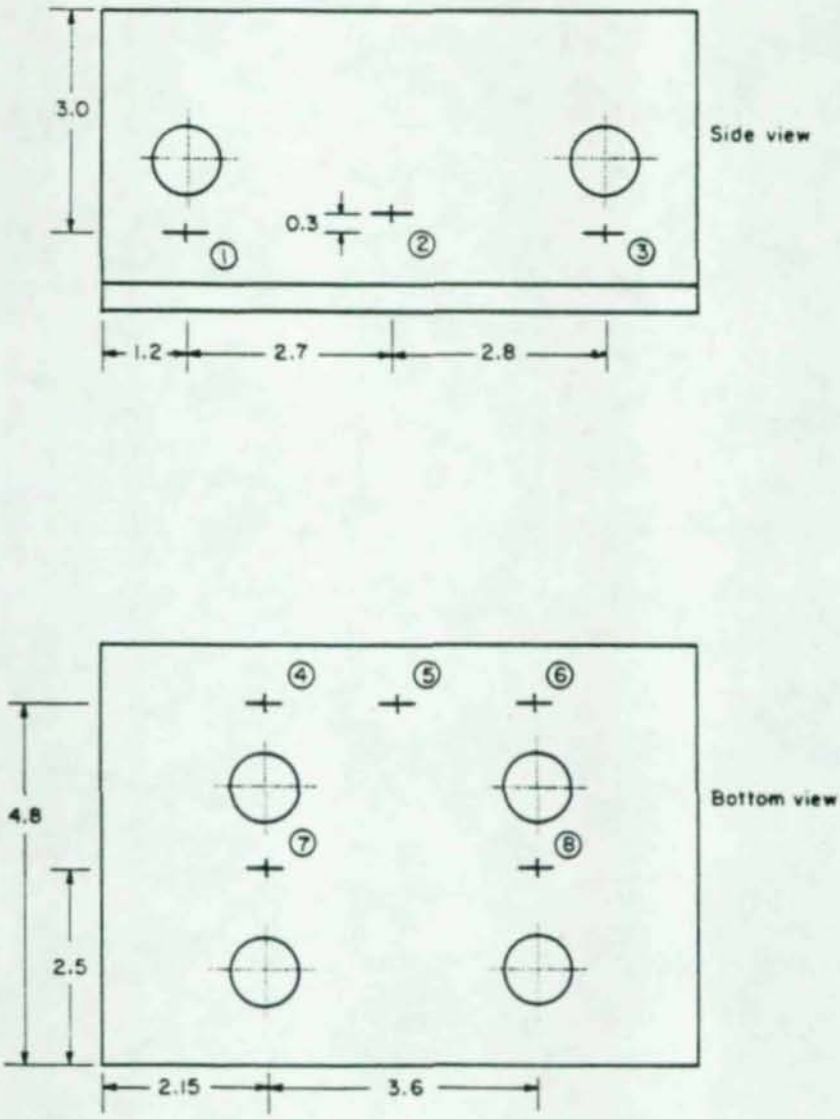

Figure 7 - Strain gages on the flange angles

00778

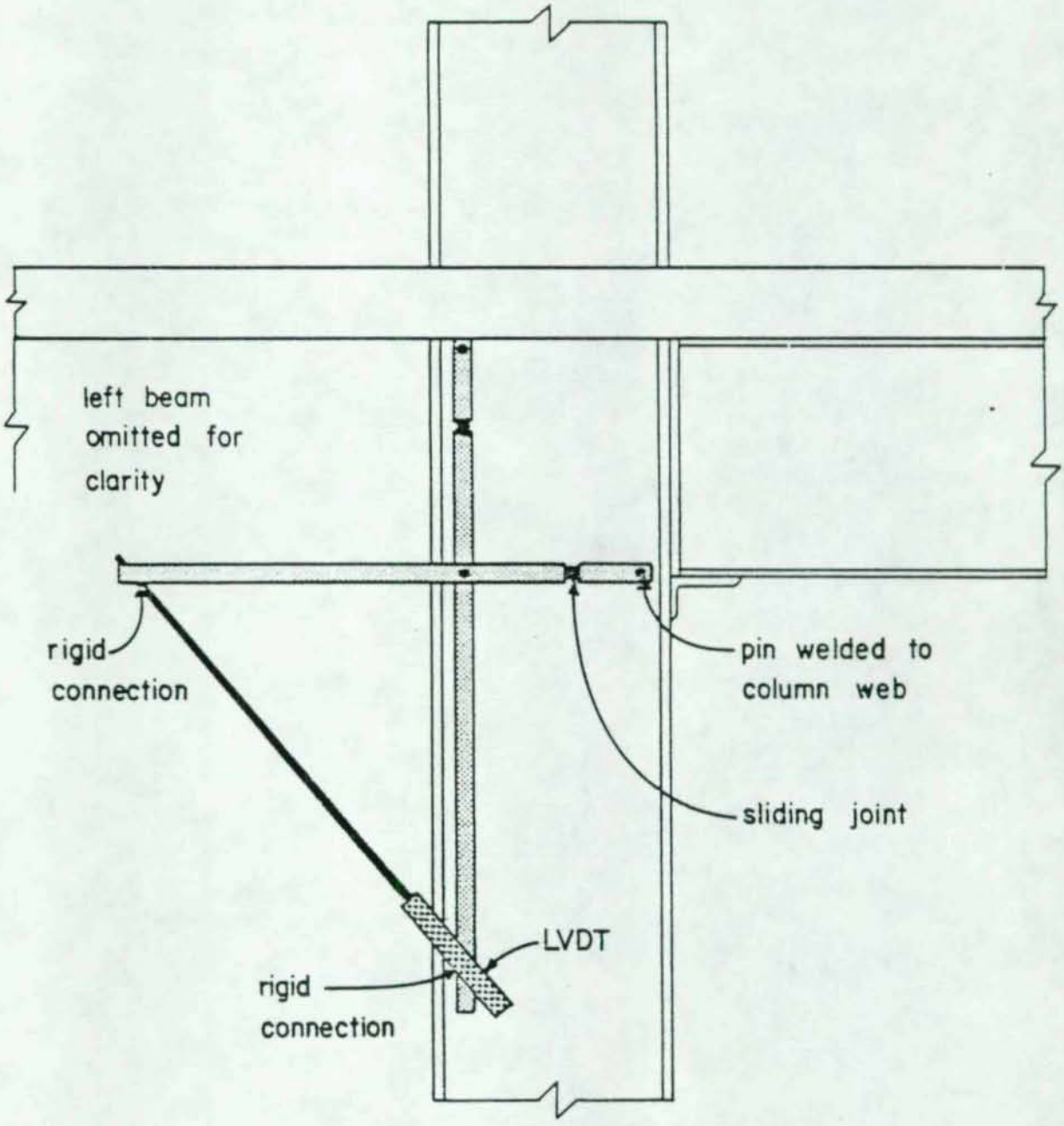

Figure 8 - Shear strain instrumentation

FIGURE 9 - COMPLETE LOAD-DEFLECTION CURVES - SRCC1M - GL2, GL3, AND GL4

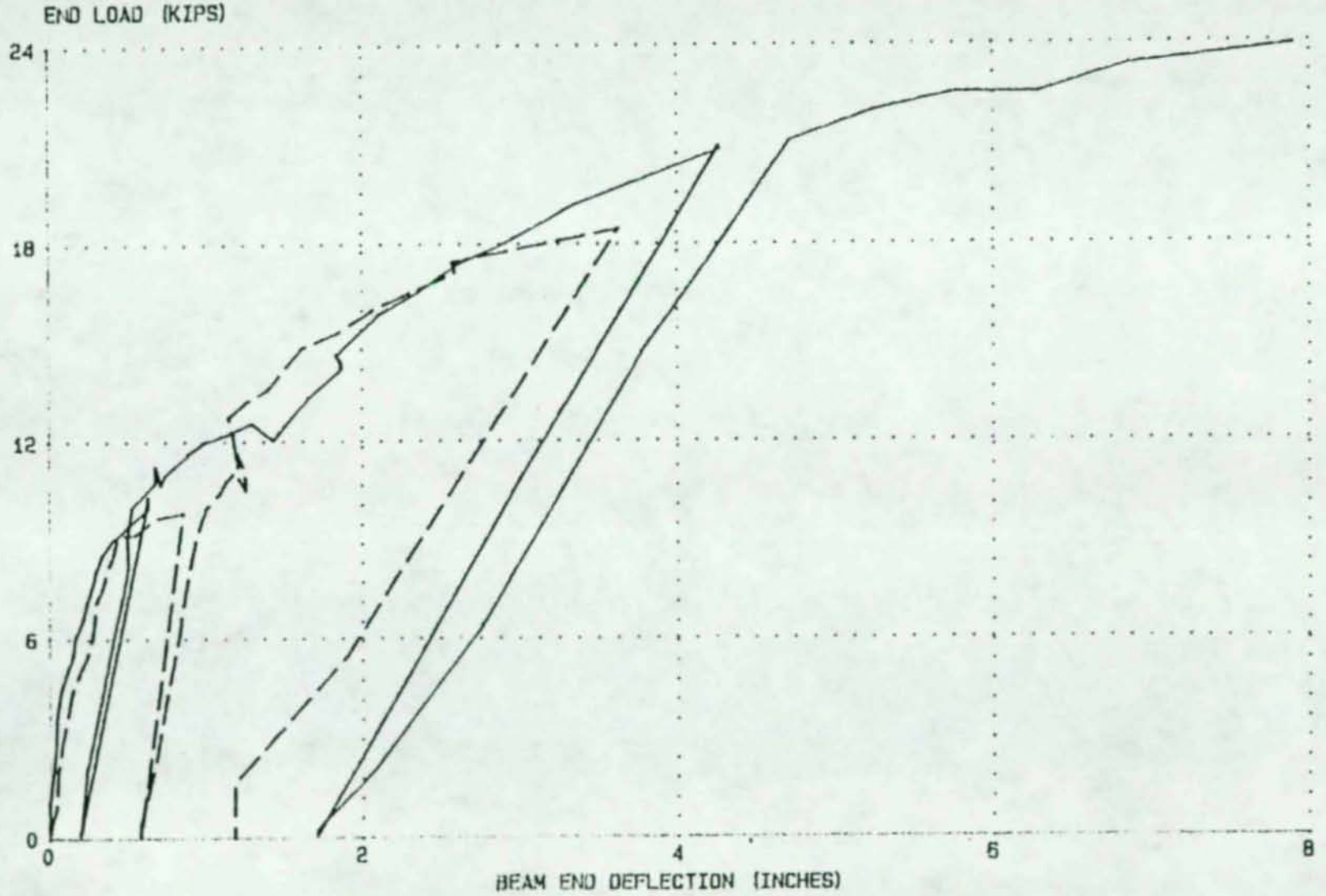

FIGURE 10 - COMPLETE MOMENT-ROTATION CURVES FOR SRCC1M - GL2, GL3, AND GL4

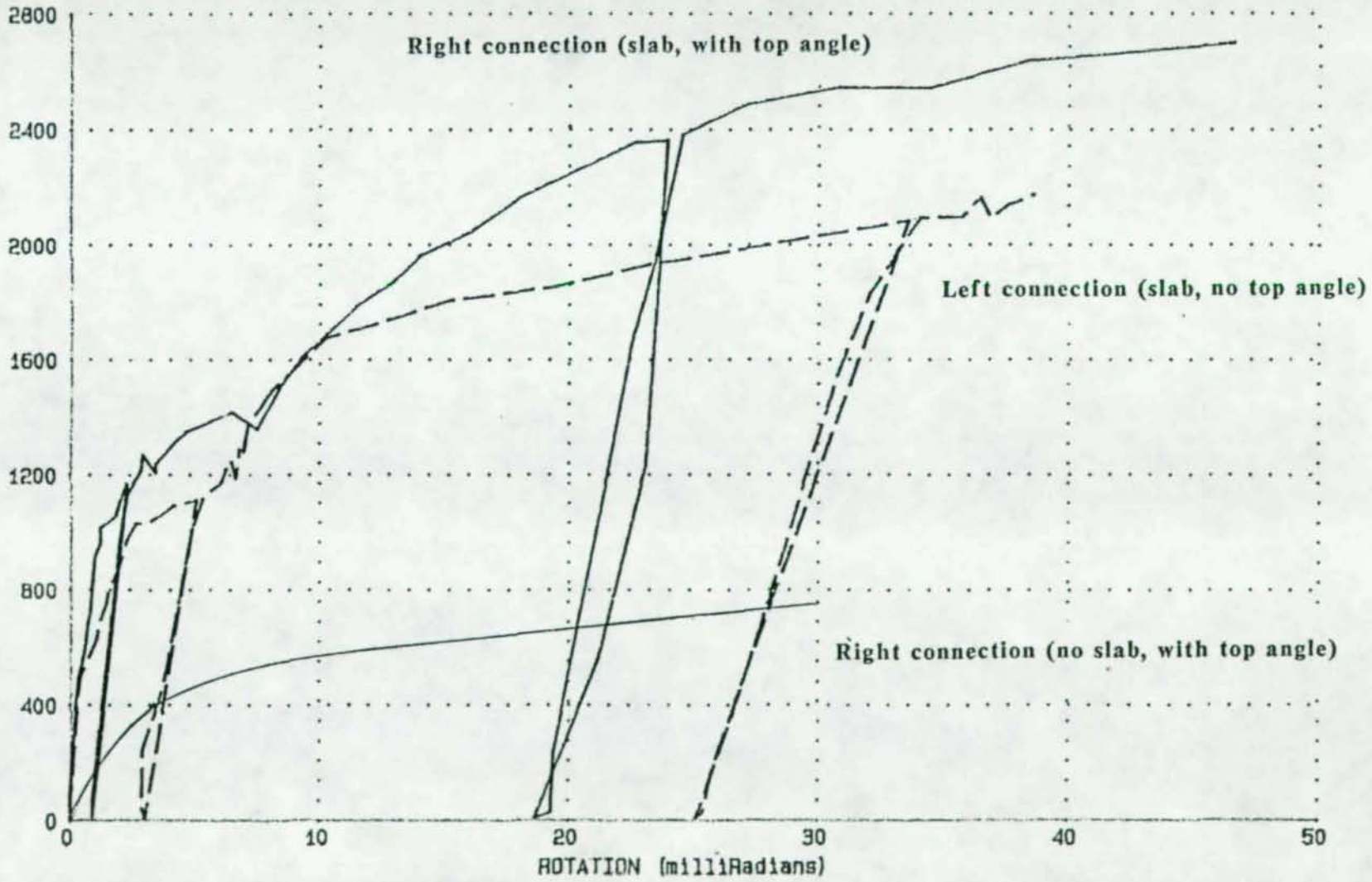

FIGURE 11 - LOAD VS DEFLECTION - GL2 - LOAD STAGES 1 TO 20

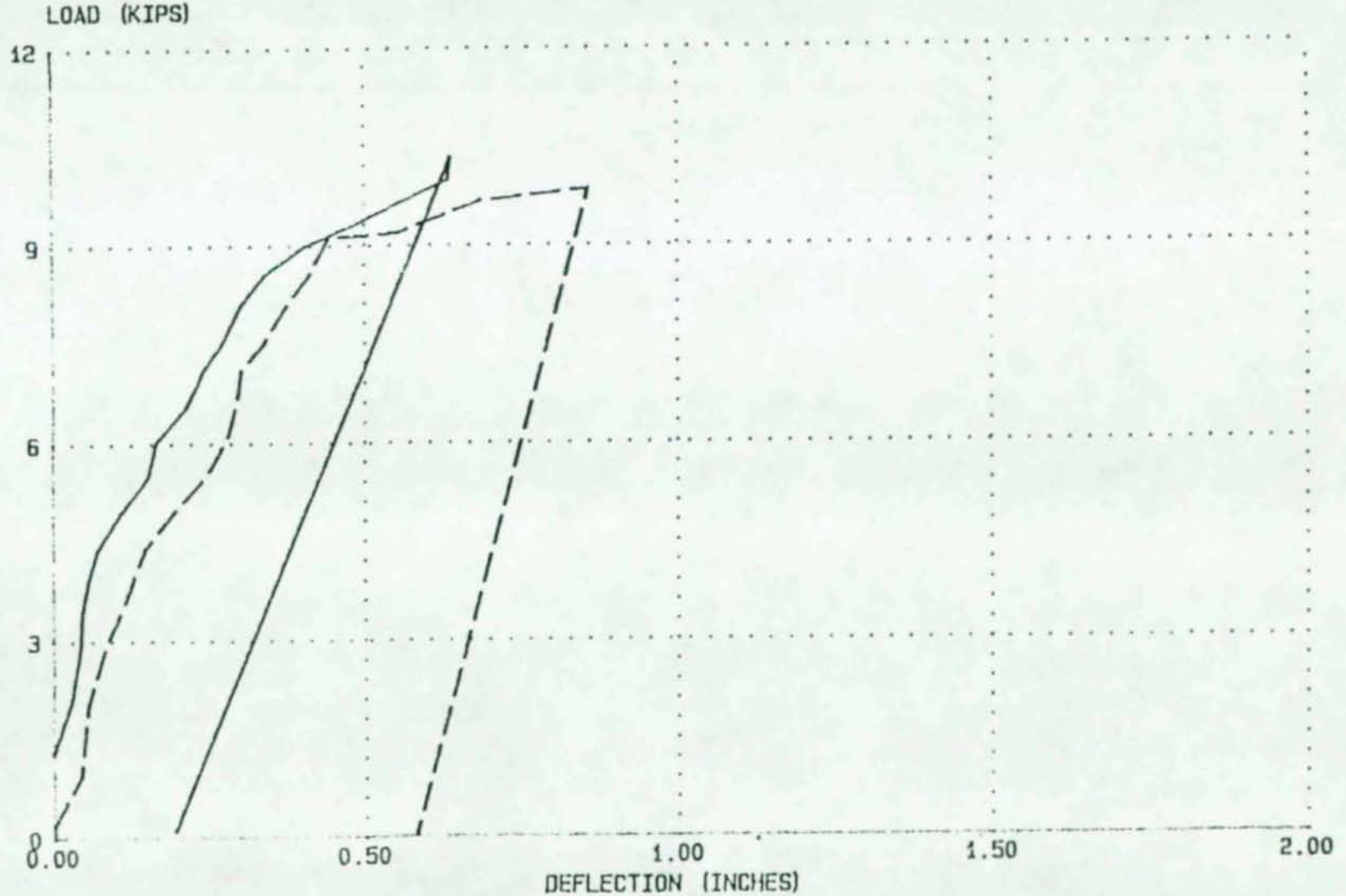

FIGURE 12 - MOMENT VS. ROTATION - GL2 - LOAD STAGES 1 TO 20

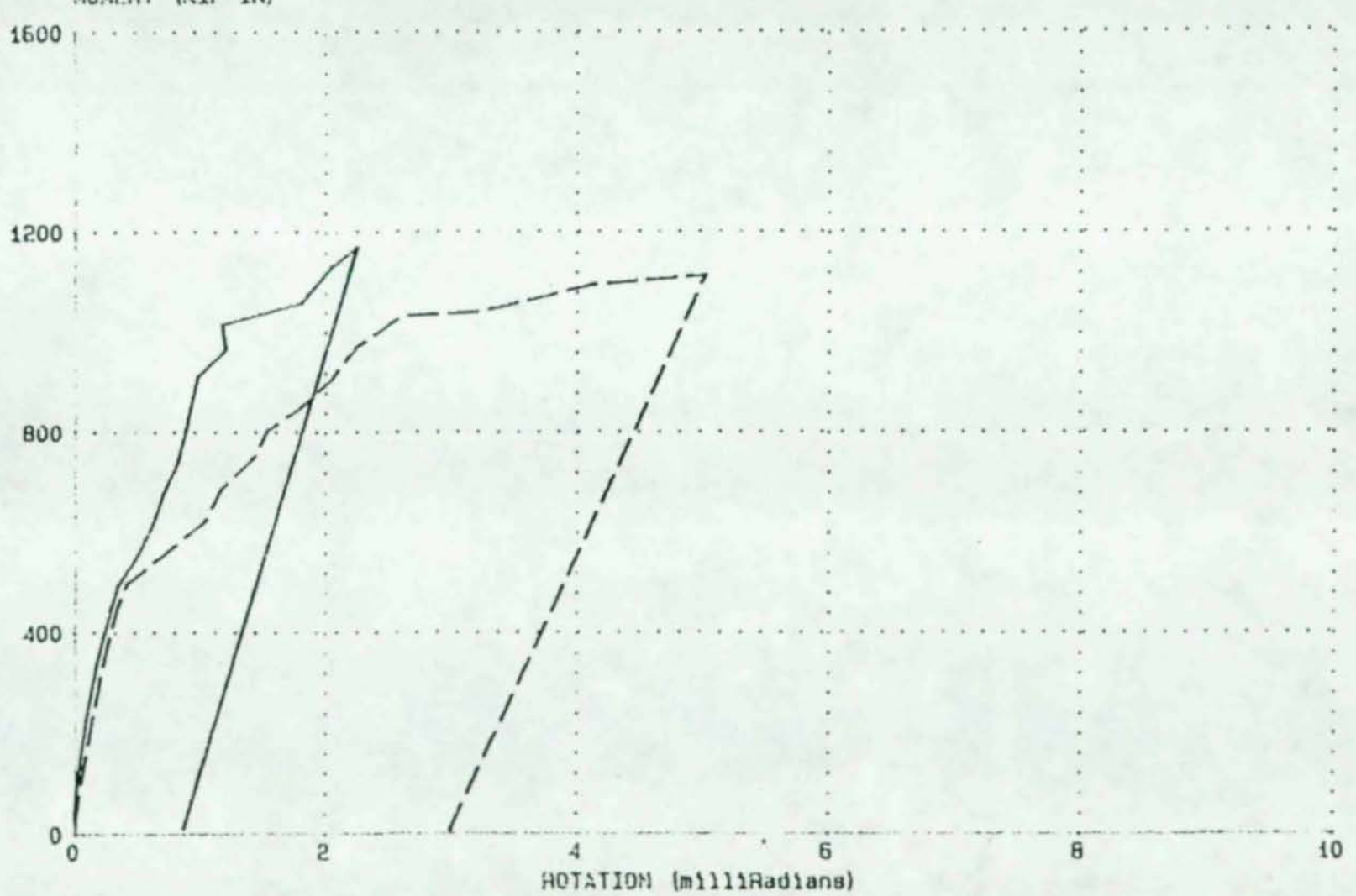

FIGURE 13 - LOAD VS. DEFLECTION - GL3 - LOAD STAGES 21 TO 52

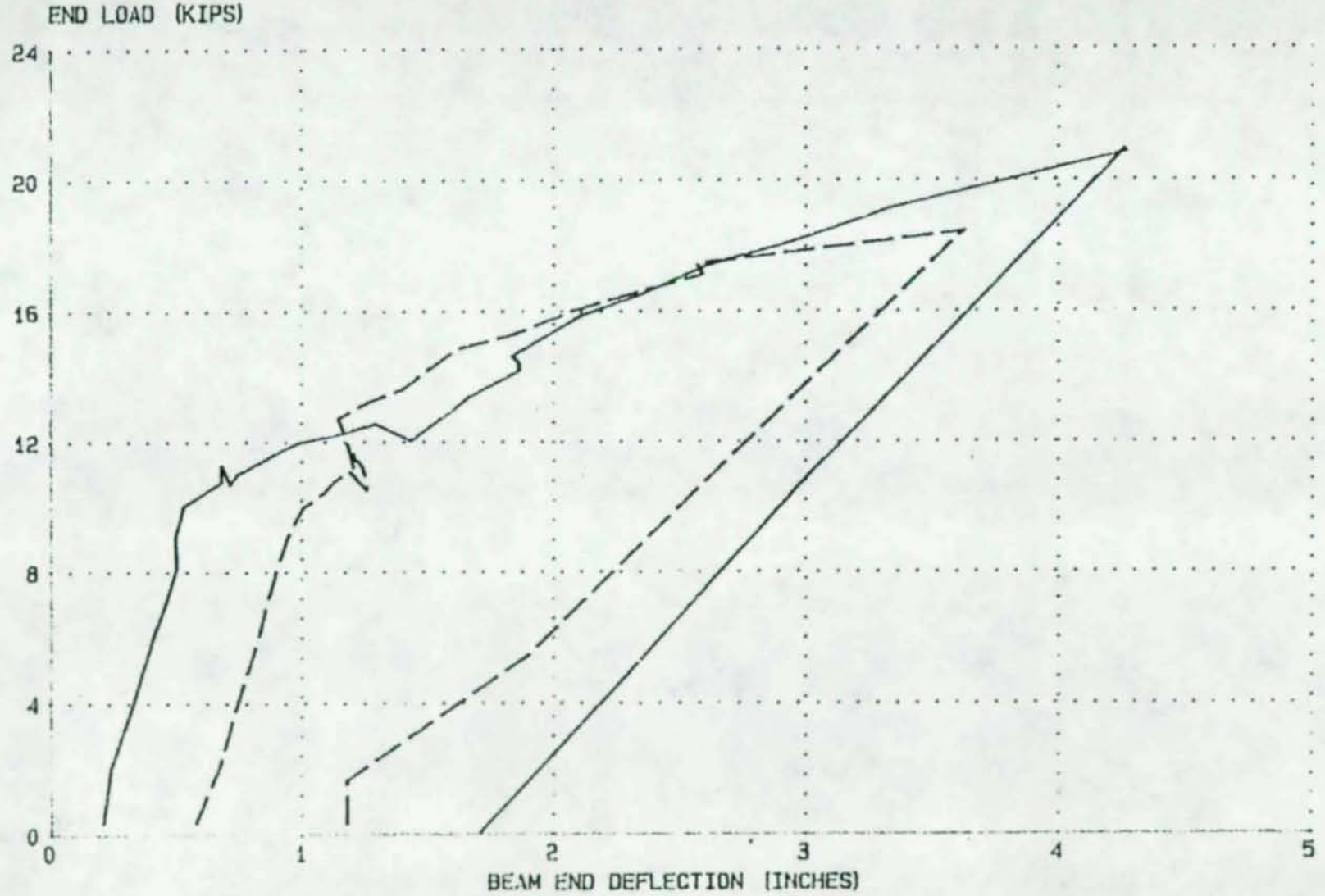

FIGURE 14 - MOMENT VS. ROTATION - GL3 - LOAD STAGES 21 TO 52

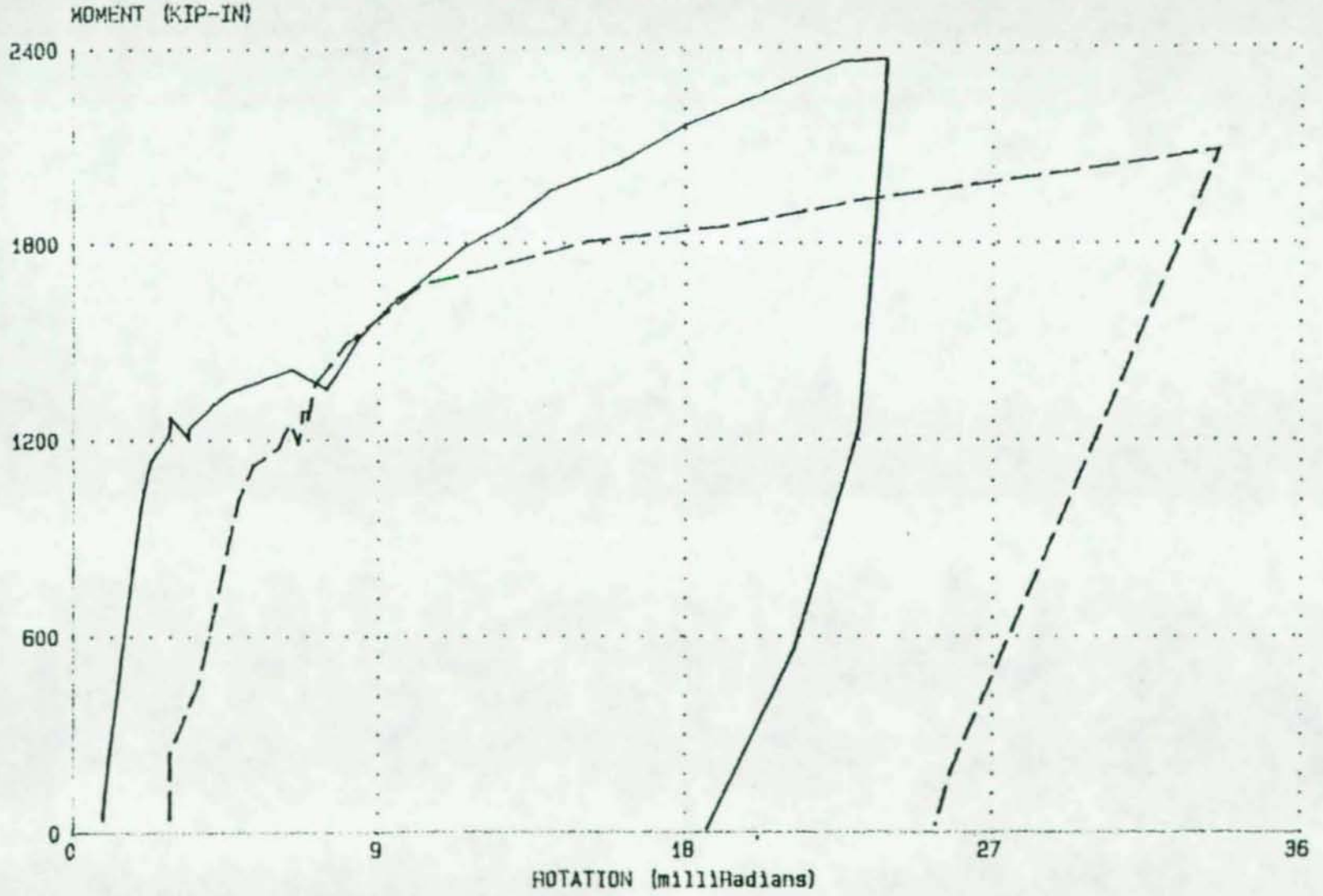

00785

FIGURE 15 - LOAD VS. DEFLECTION - GL4 - LOAD STAGES 53 TO 64

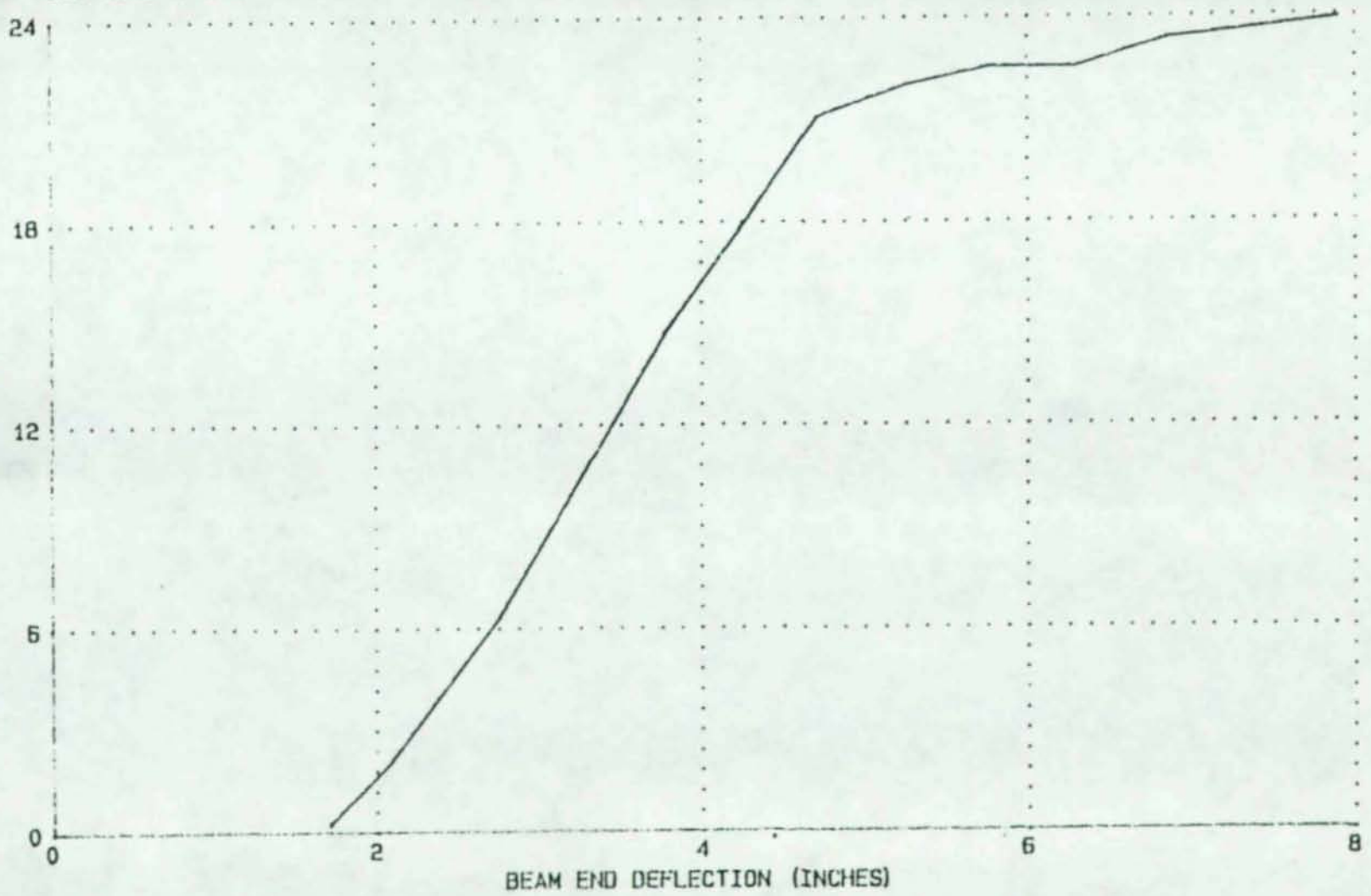

00786

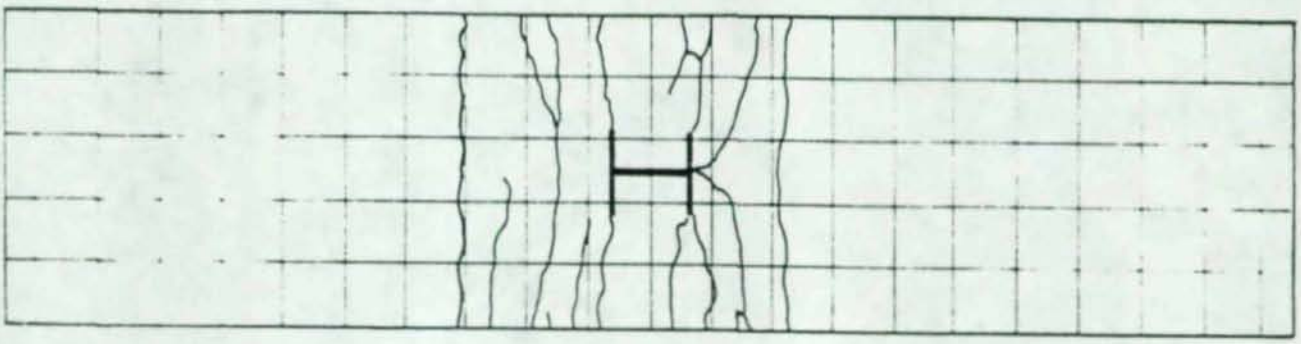

(a) Cracking in the slab at the end of test GL2

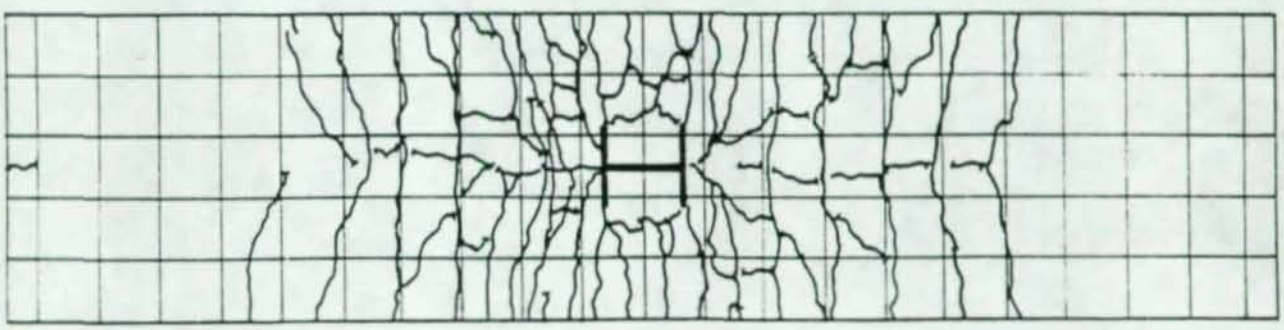

(b) Cracking in the slab at the end of test GL4

Figure 16 - Cracking patterns in the slab at GL2 and GL4

00787

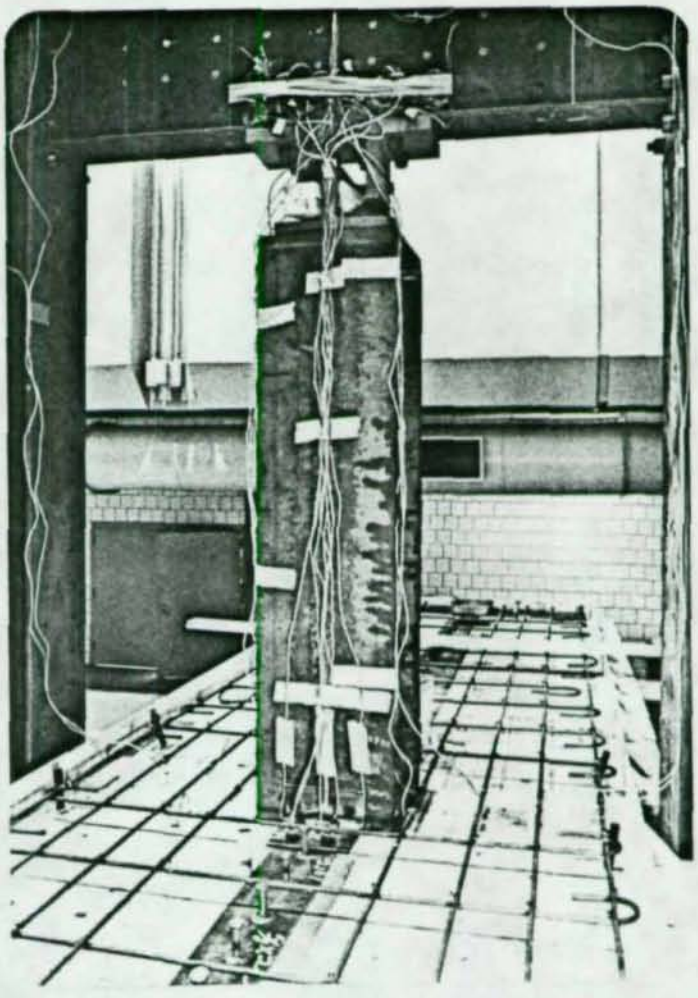

Figure 17 - Specimen before slab was cast

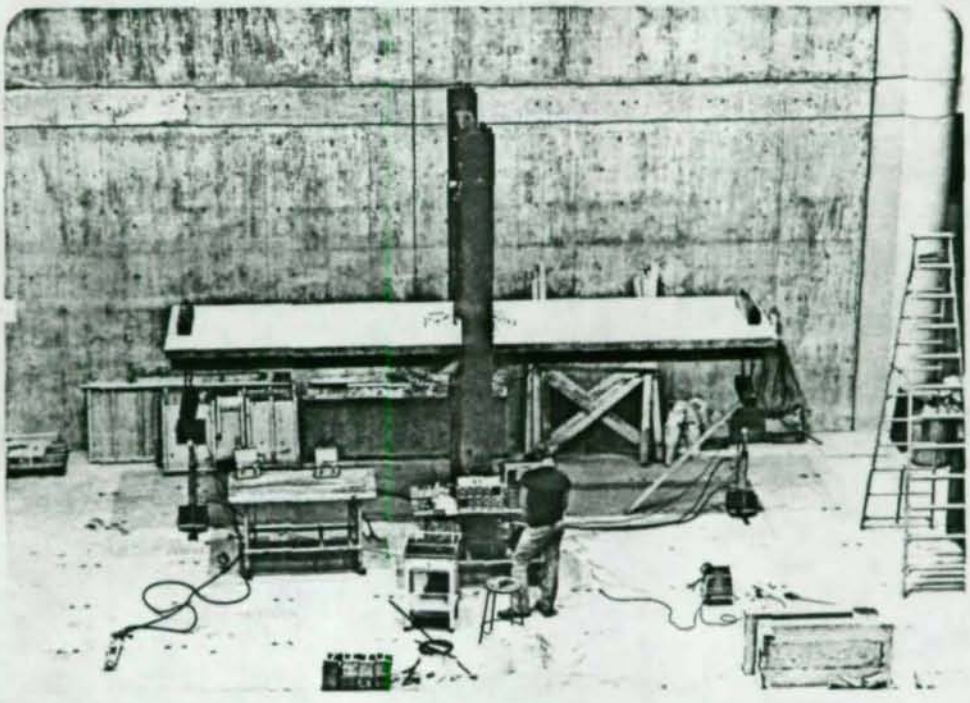

Figure 18 - Specimen in loading frame

000788

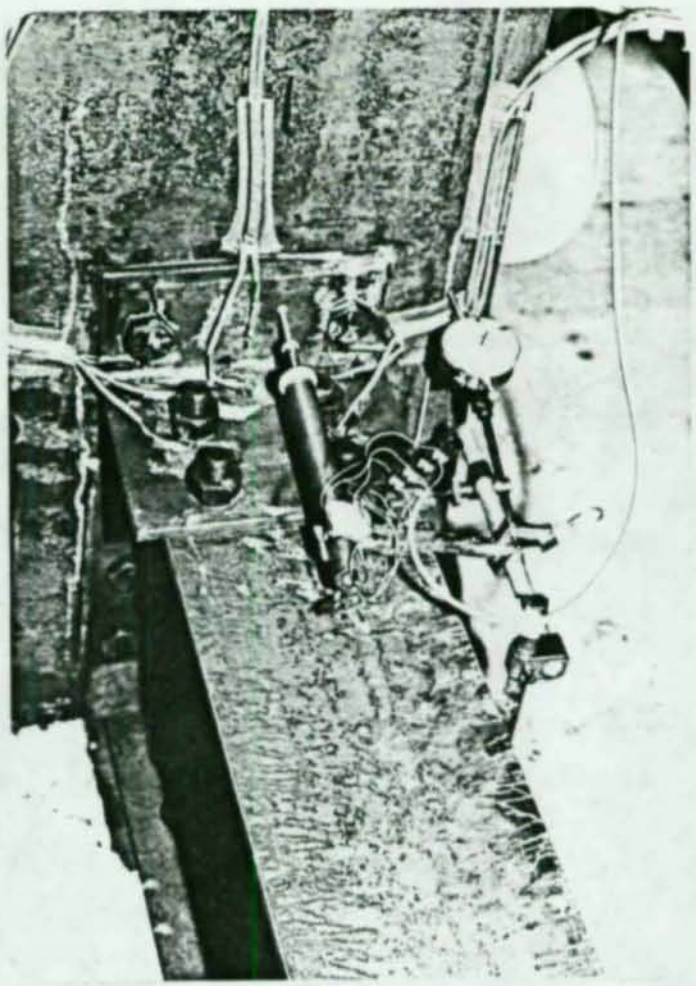

Figure 19 - Instrumentation in the connection area

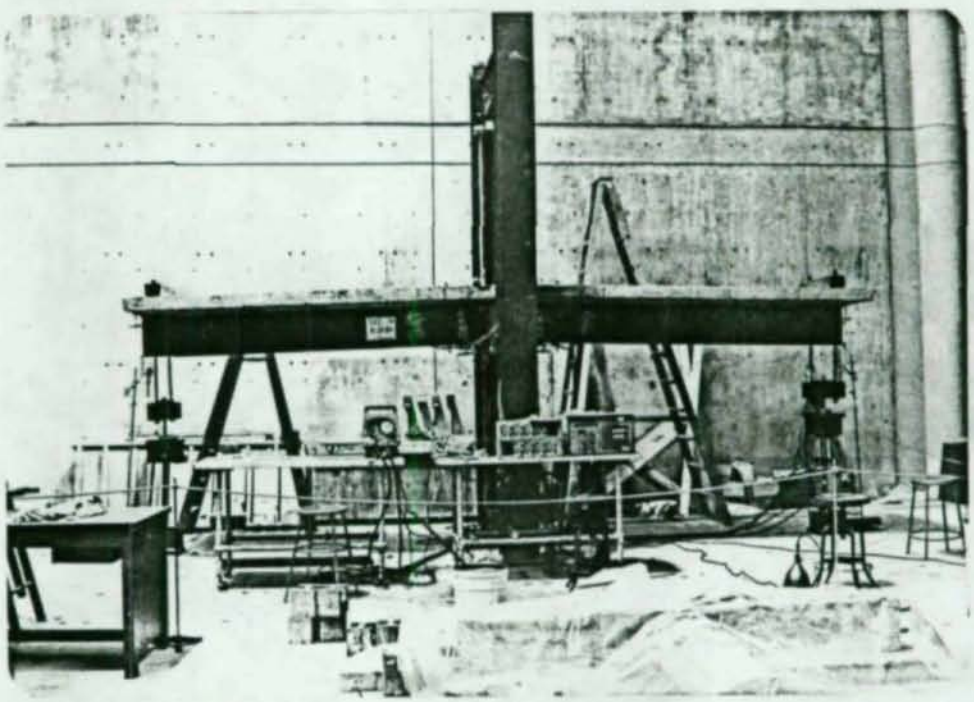

Figure 20 - Specimen deformed at the end of GL2

007789

Figure 21 - Right connection at the end of GL2

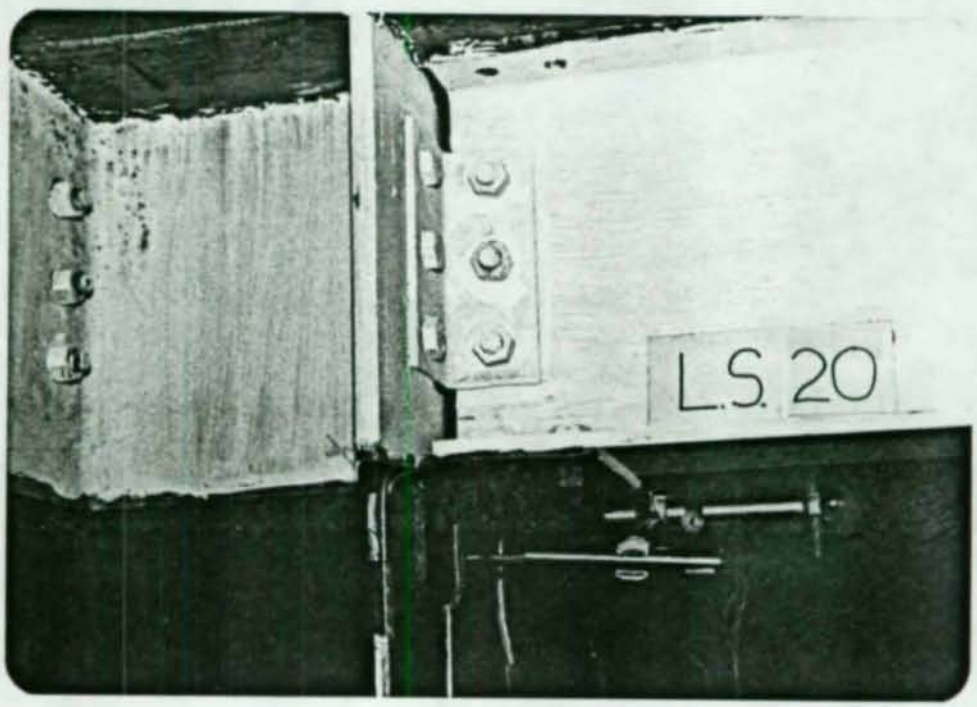

Figure 22 - Left connection at the end of GL2. Note that neither connection shows evidence of yielding or distress

00790

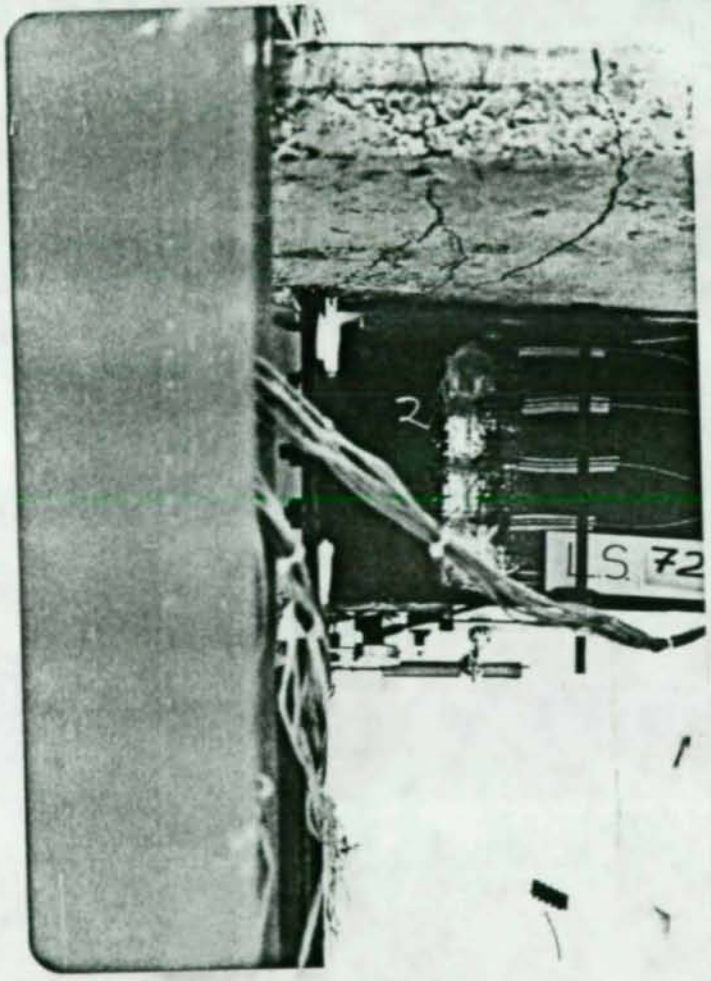

Figure 23 - Right connection at the end of GL4. Note that the bottom bolts have sheared, and the beam flange is bearing against the column flange

Figure 24 - Left connection at the end of GL4. Note that the opening at the top is very wide, and the top of the web angles have begun to seperate from the column.

00791

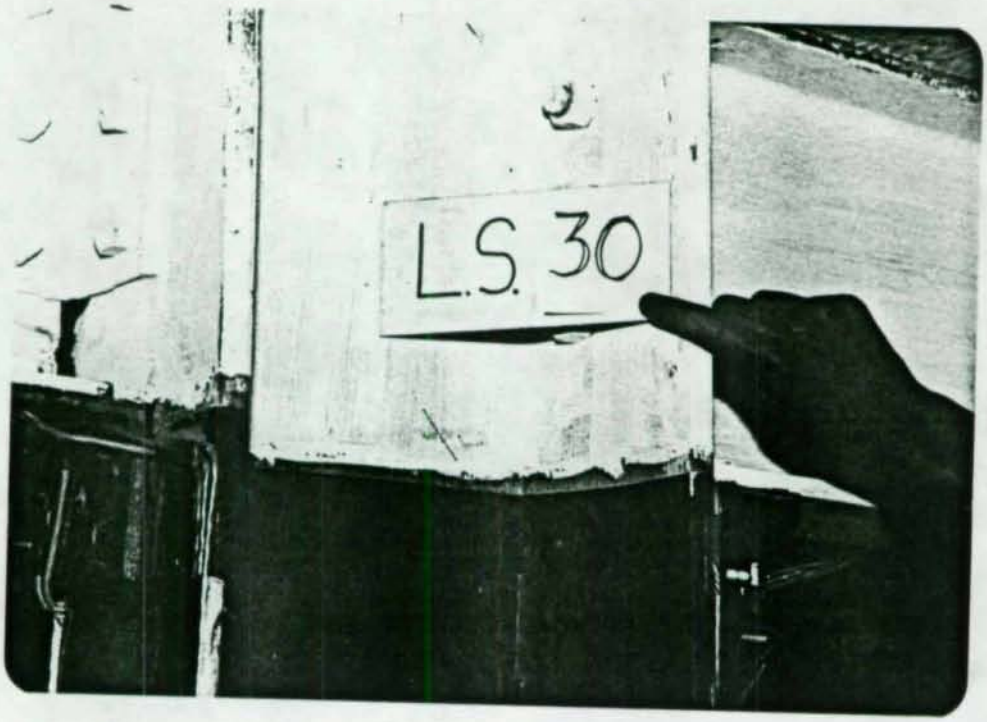

Figure 25 - Column web yielding at LS30

00792

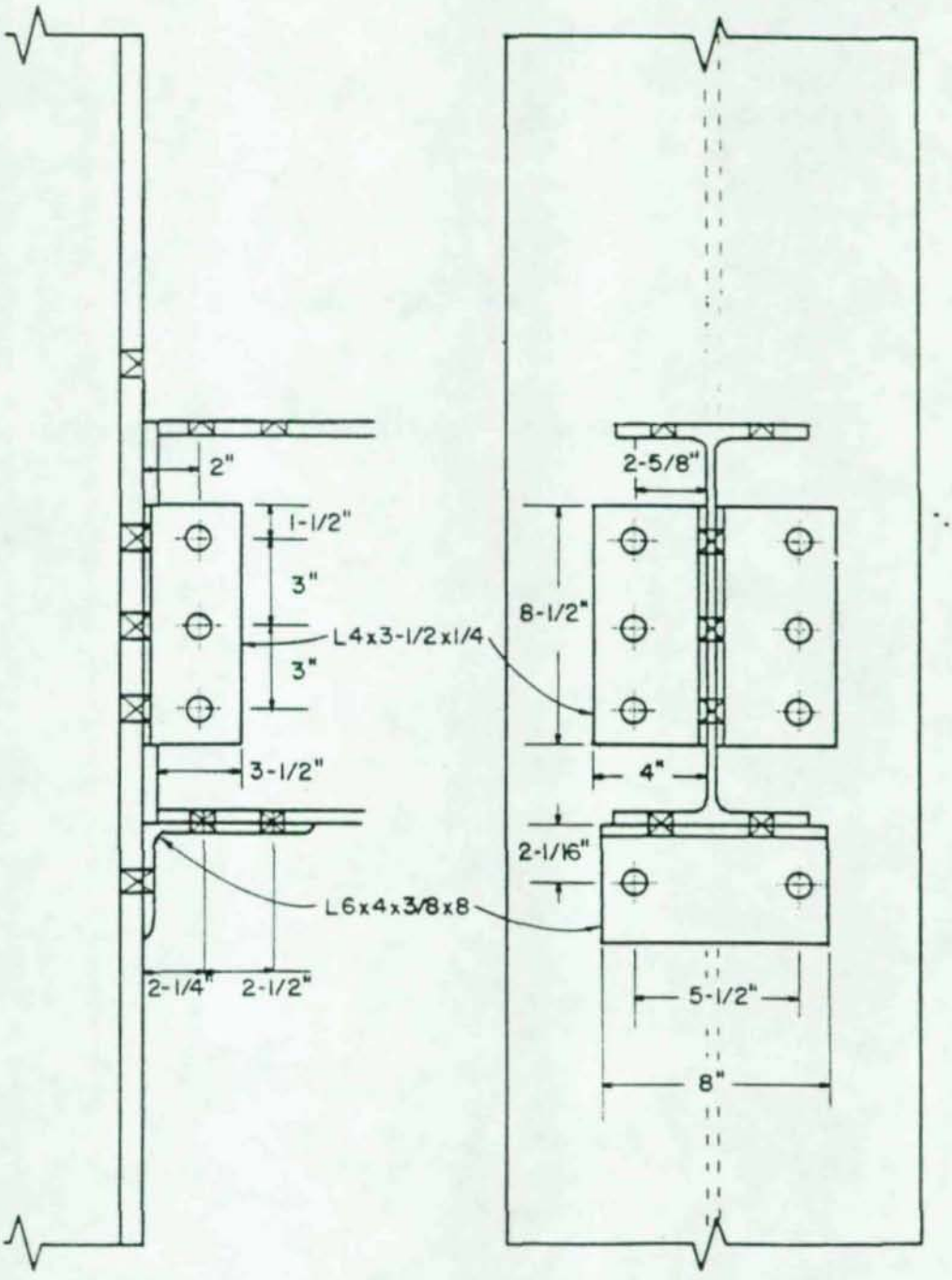

Figure 26 - Details of connection SRCC1C; slab not shown.

00793

FIGURE 27 - LOAD HISTORY FOR CYCLIC TEST SRCC1C

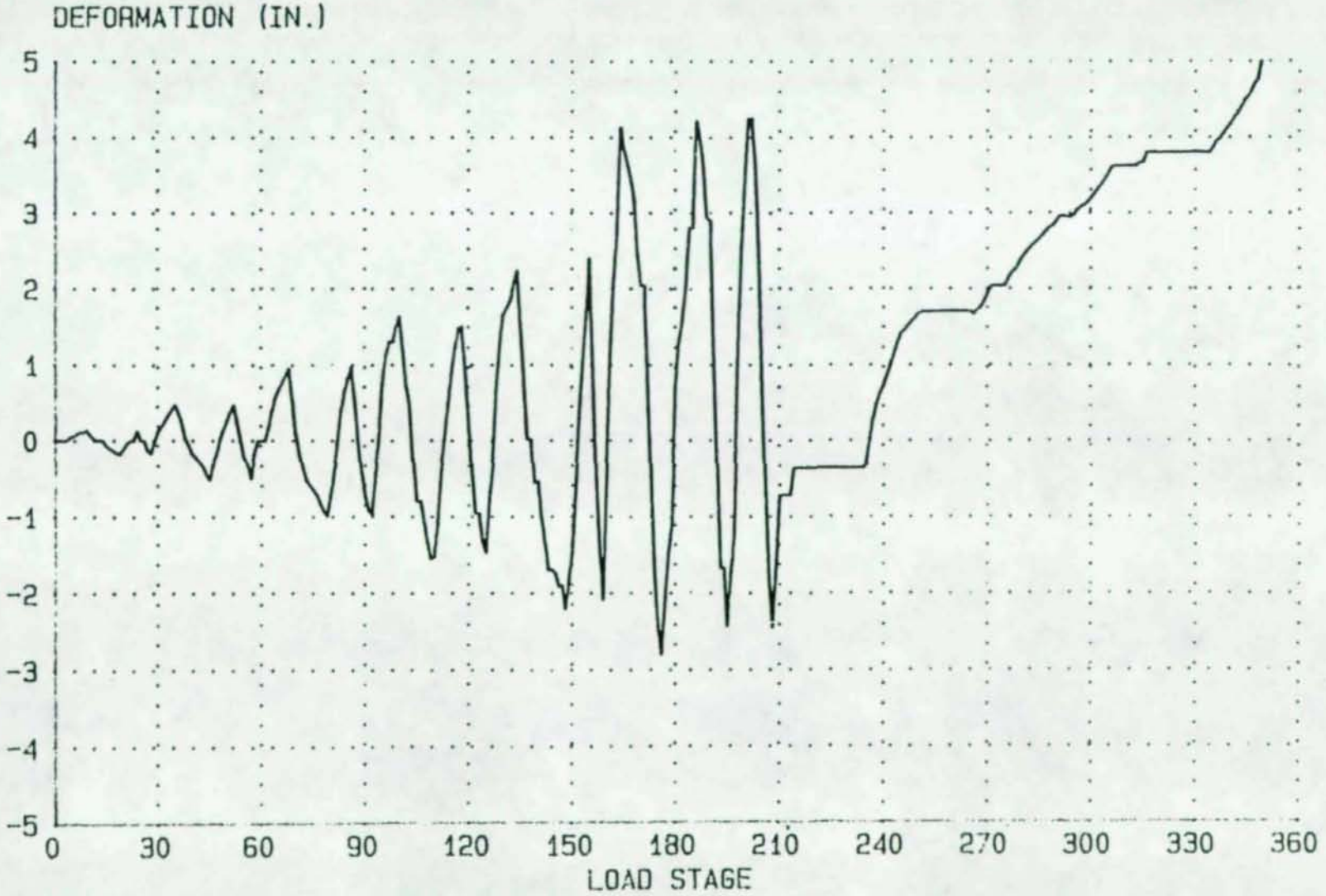

00794

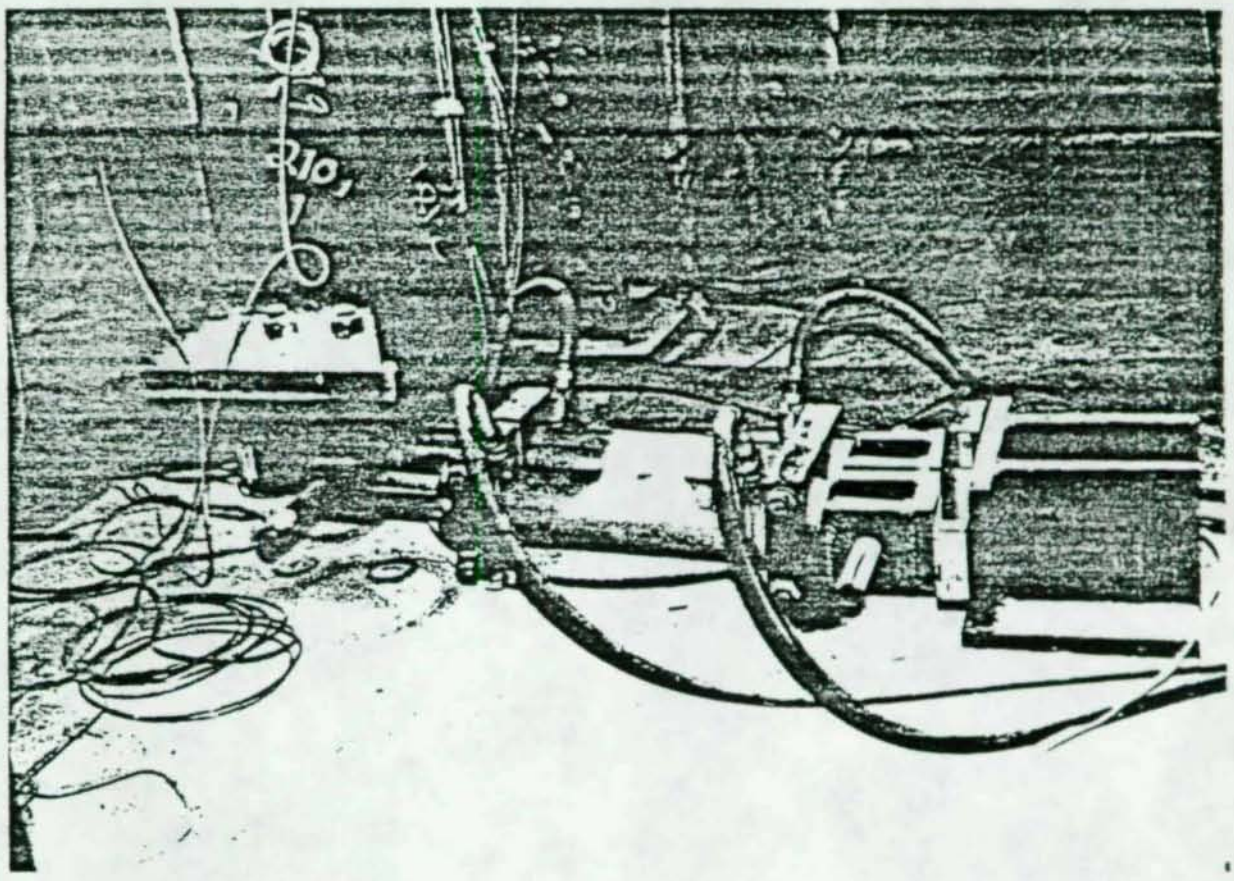

Figure 28 - Loading scheme for test SRCC1C

00795

FIGURE 29 - COMPLETE LOAD VS. STORY DRIFT CURVE FOR CYCLIC TEST SRCC1C

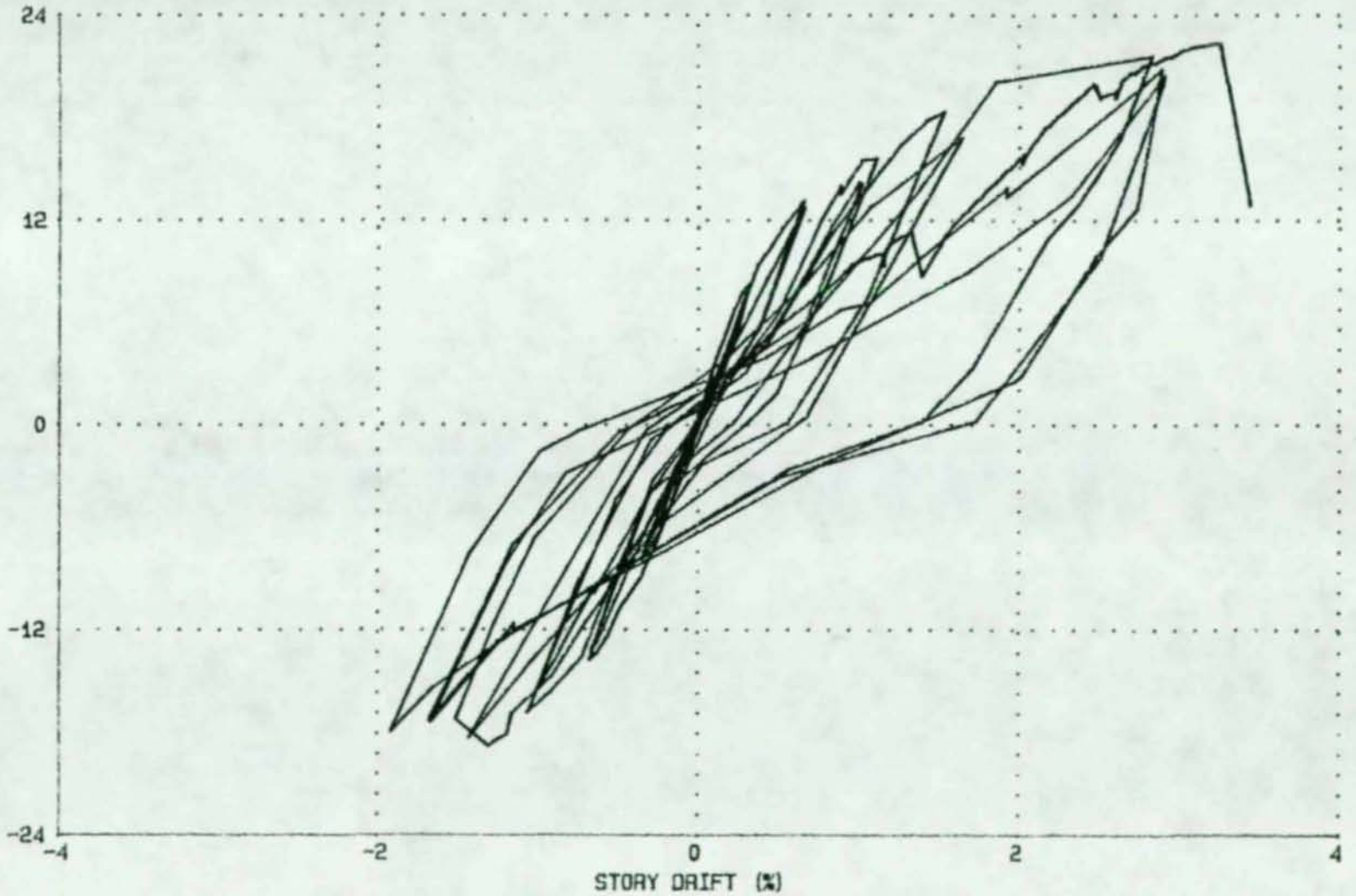

96Z00

FIGURE 30 - LOAD VS. STORY DRIFT - LL1 - LOAD STAGES 1 TO 61

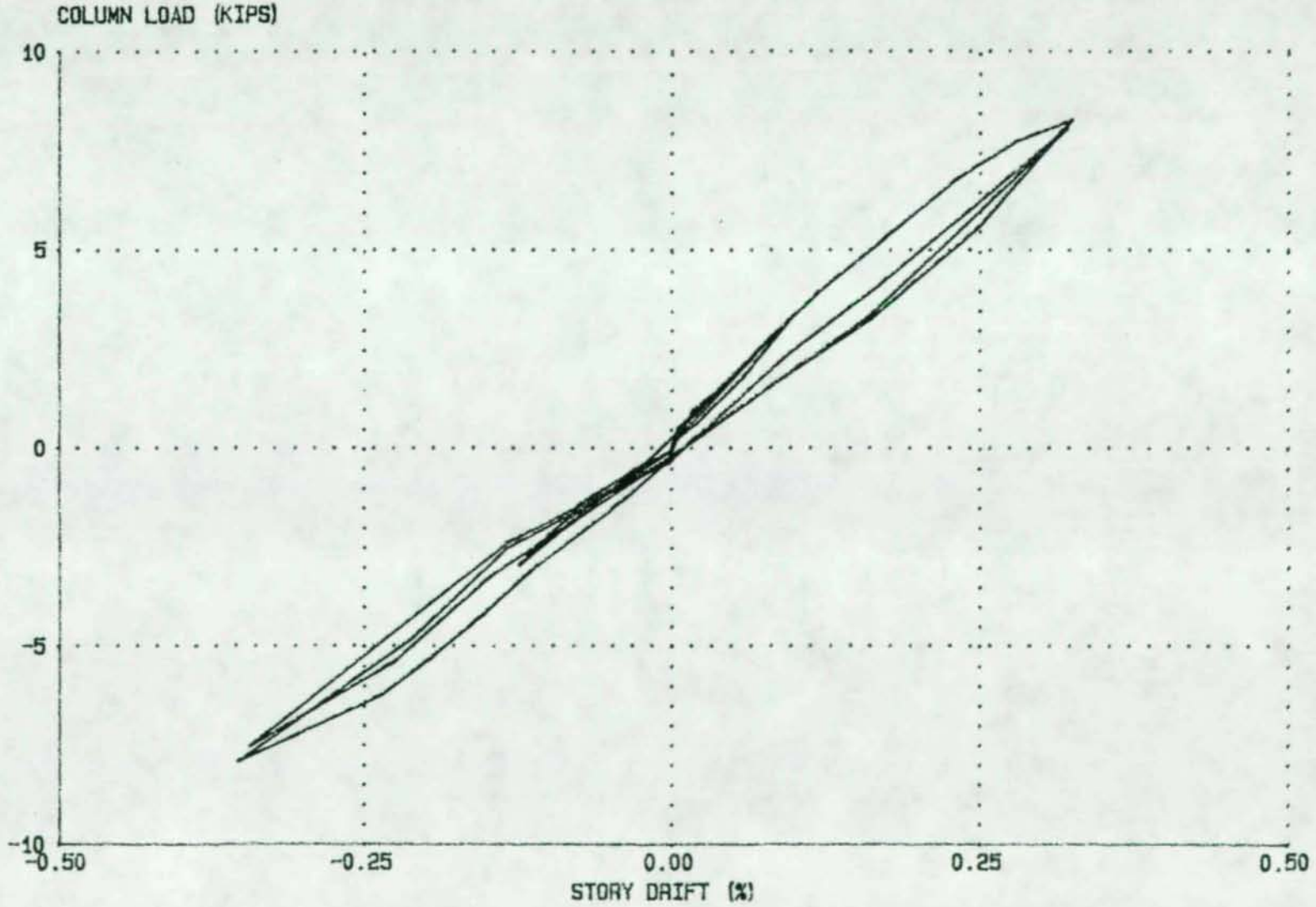

00797

FIGURE 31 - LOAD VS. STORY DRIFT - LL2 - LOAD STAGE 61 TO 160

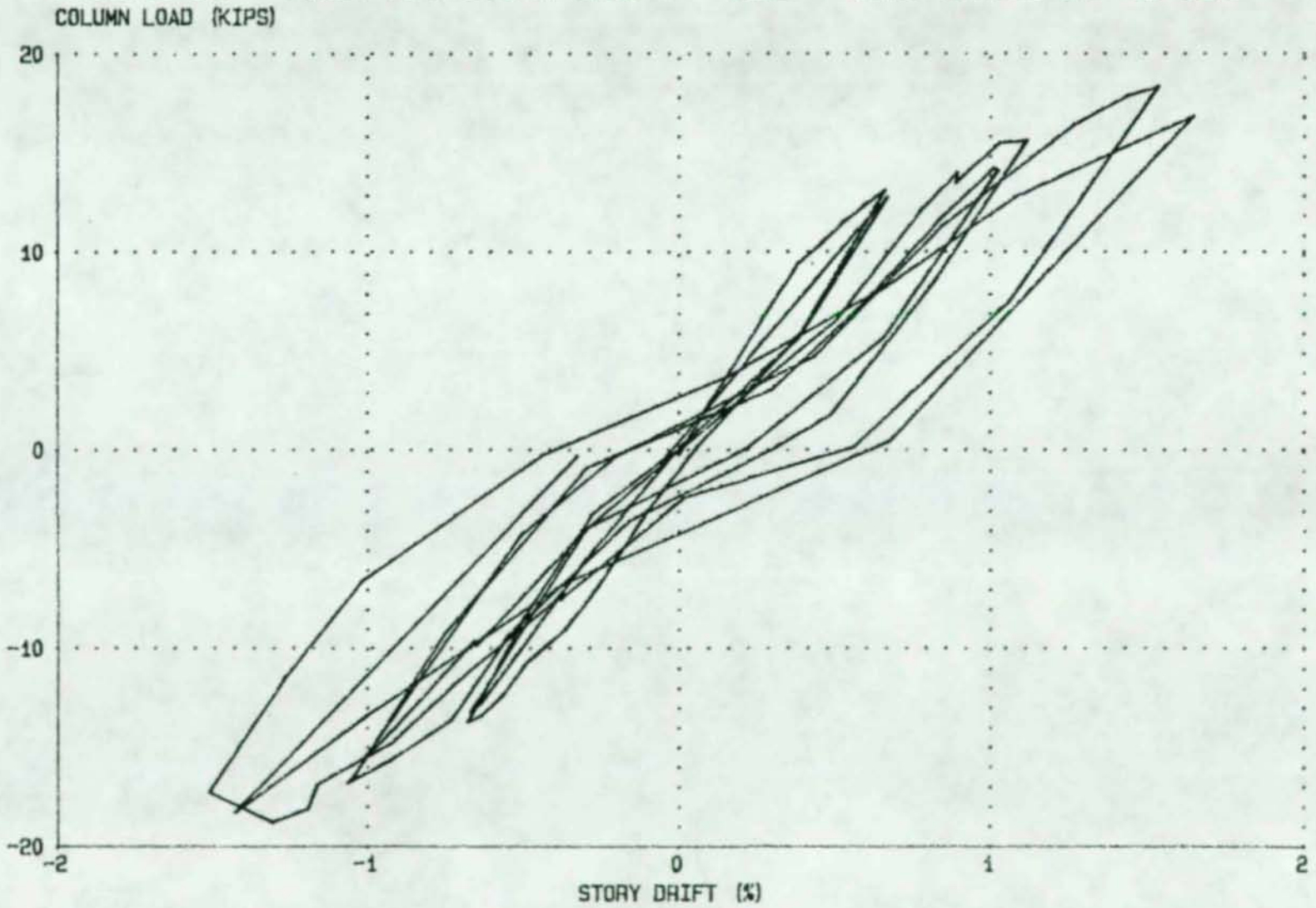

FIGURE 32 - LOAD VS. STORY DRIFT - LL2 - LOAD STAGES 61 TO 94

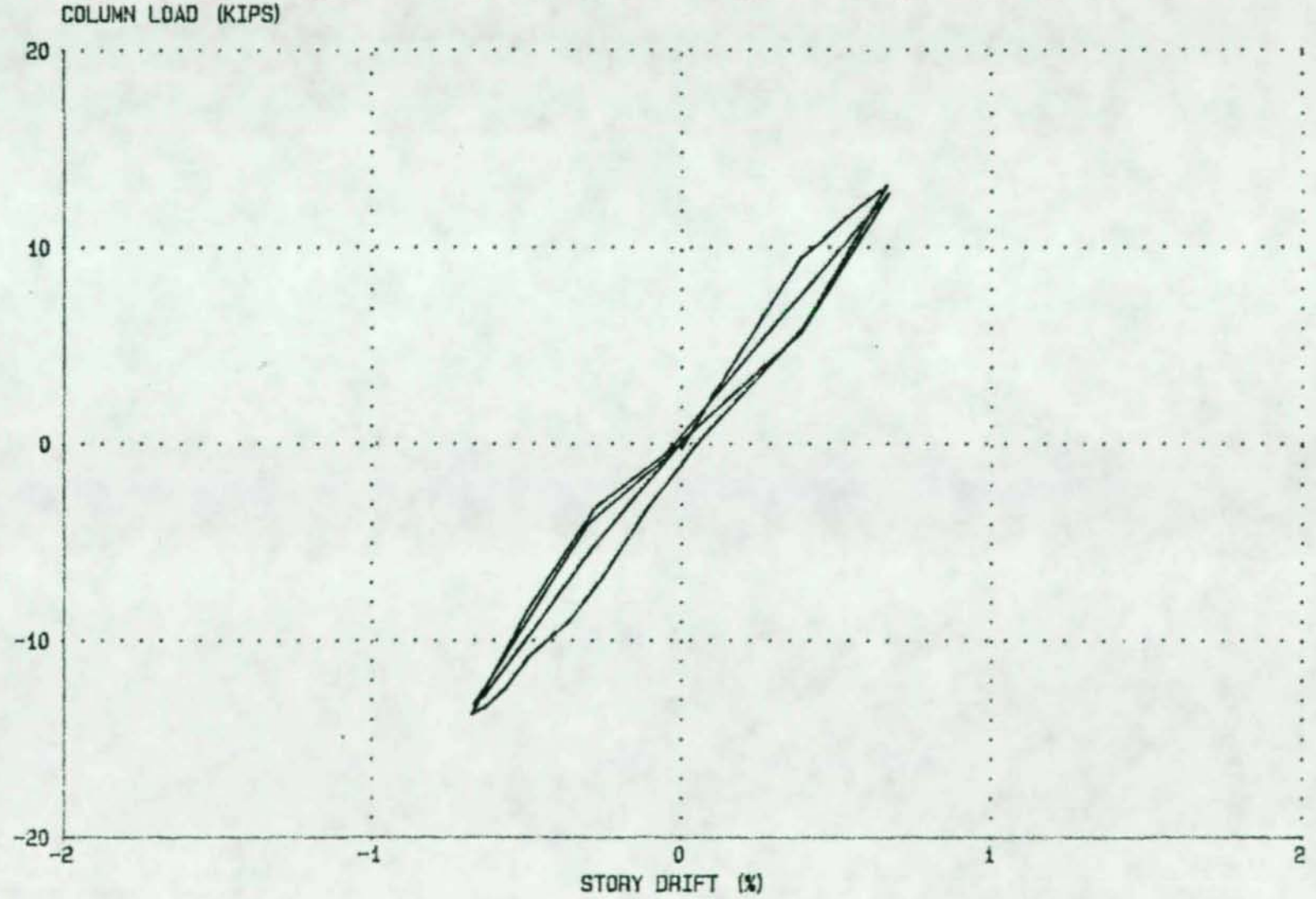

66700

FIGURE 33 - LOAD VS. STORY DRIFT - LL2 - LOAD STAGE 94 TO 127

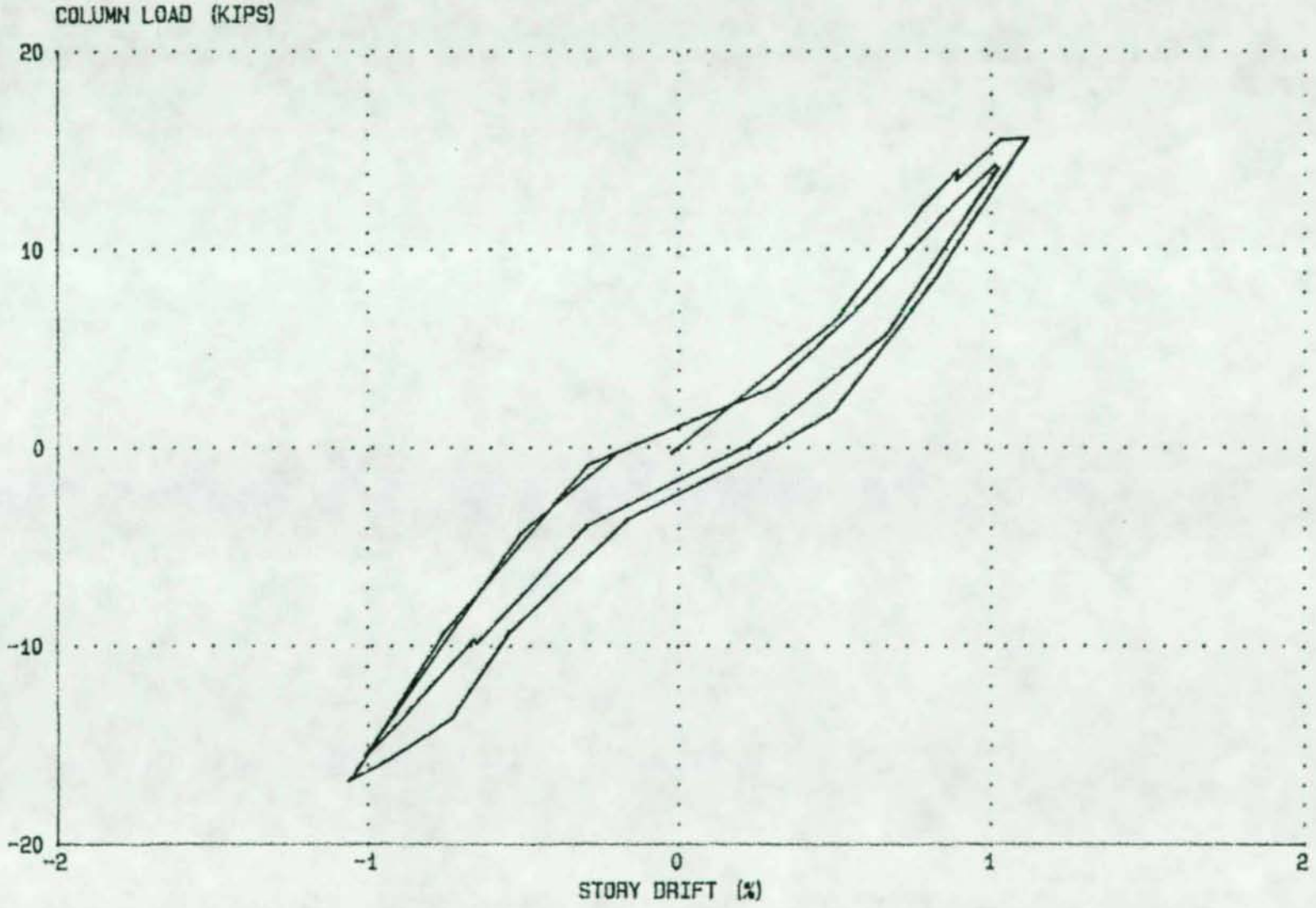

FIGURE 34 - LOAD VS. STORY DRIFT - LL2 - LOAD STAGE 127 TO 160

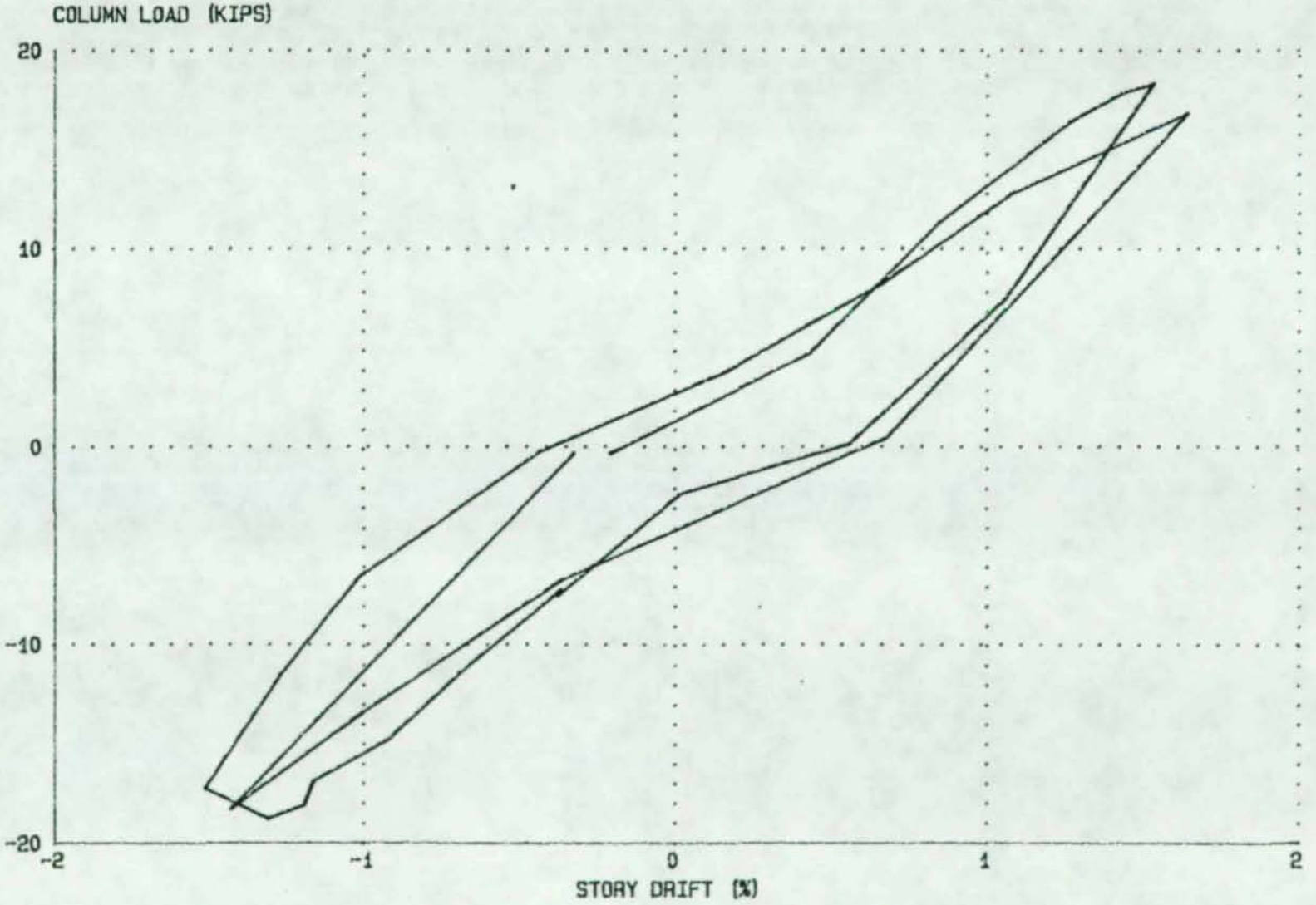

I0800

FIGURE 35 - LOAD VS. STORY DRIFT - LL3 - LOAD STAGE 160 TO 213

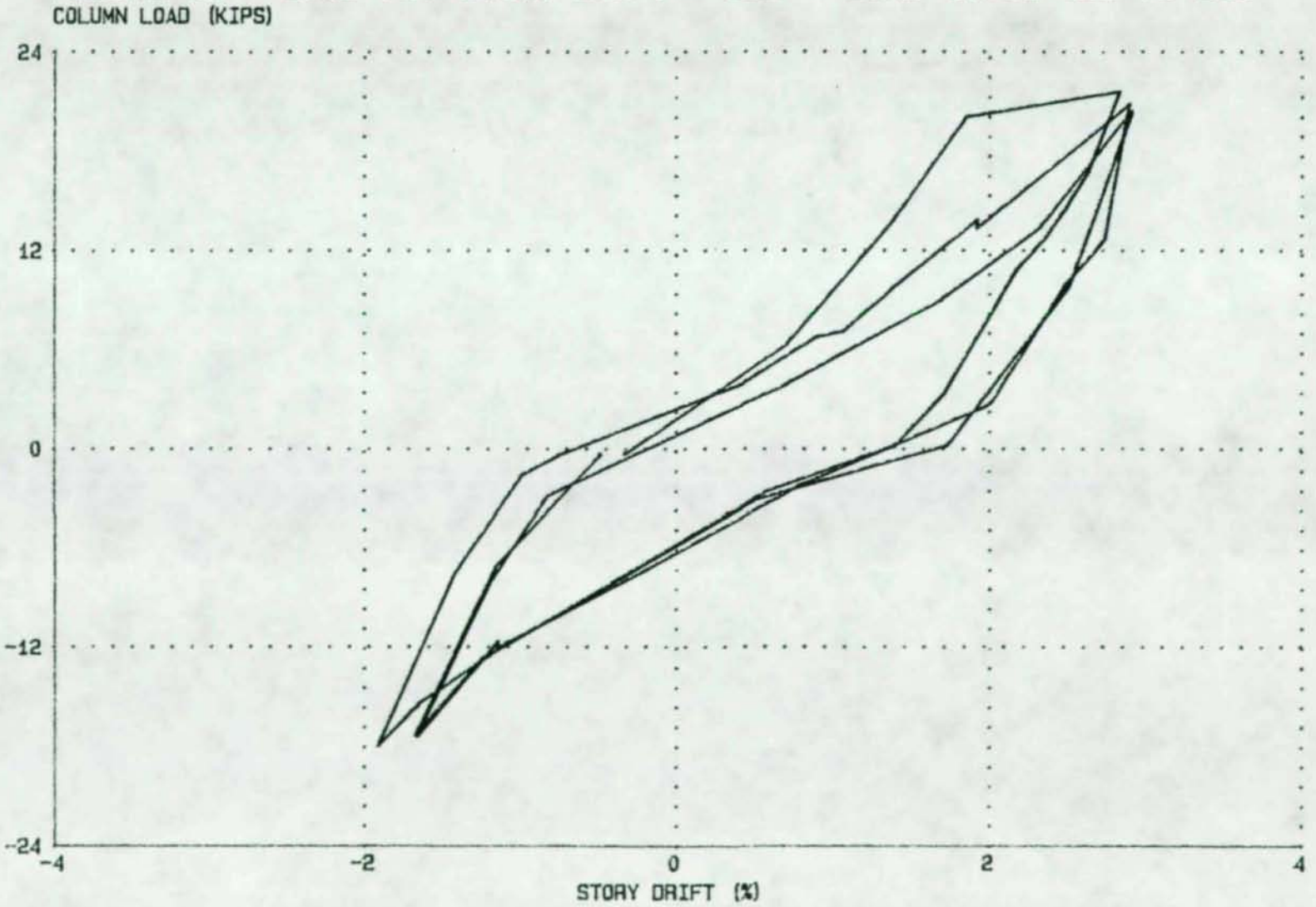

00802

FIGURE 36 - LOAD VS. STORY DRIFT - LL4 - LOAD STAGE 213 TO 353

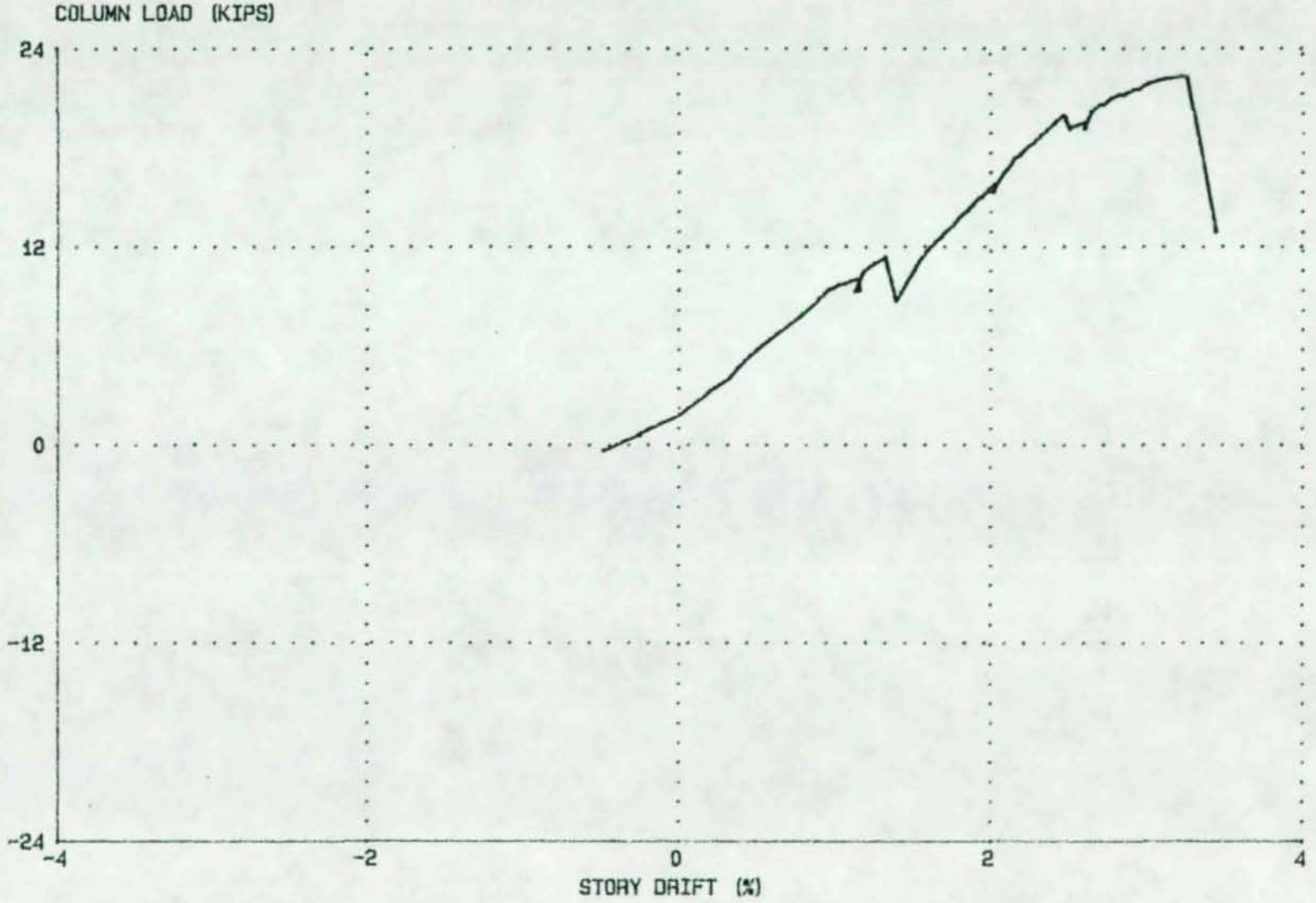

00803

FIGURE 37 - COMPLETE MOMENT VS. ROTATION CURVE FOR SRCC1CL

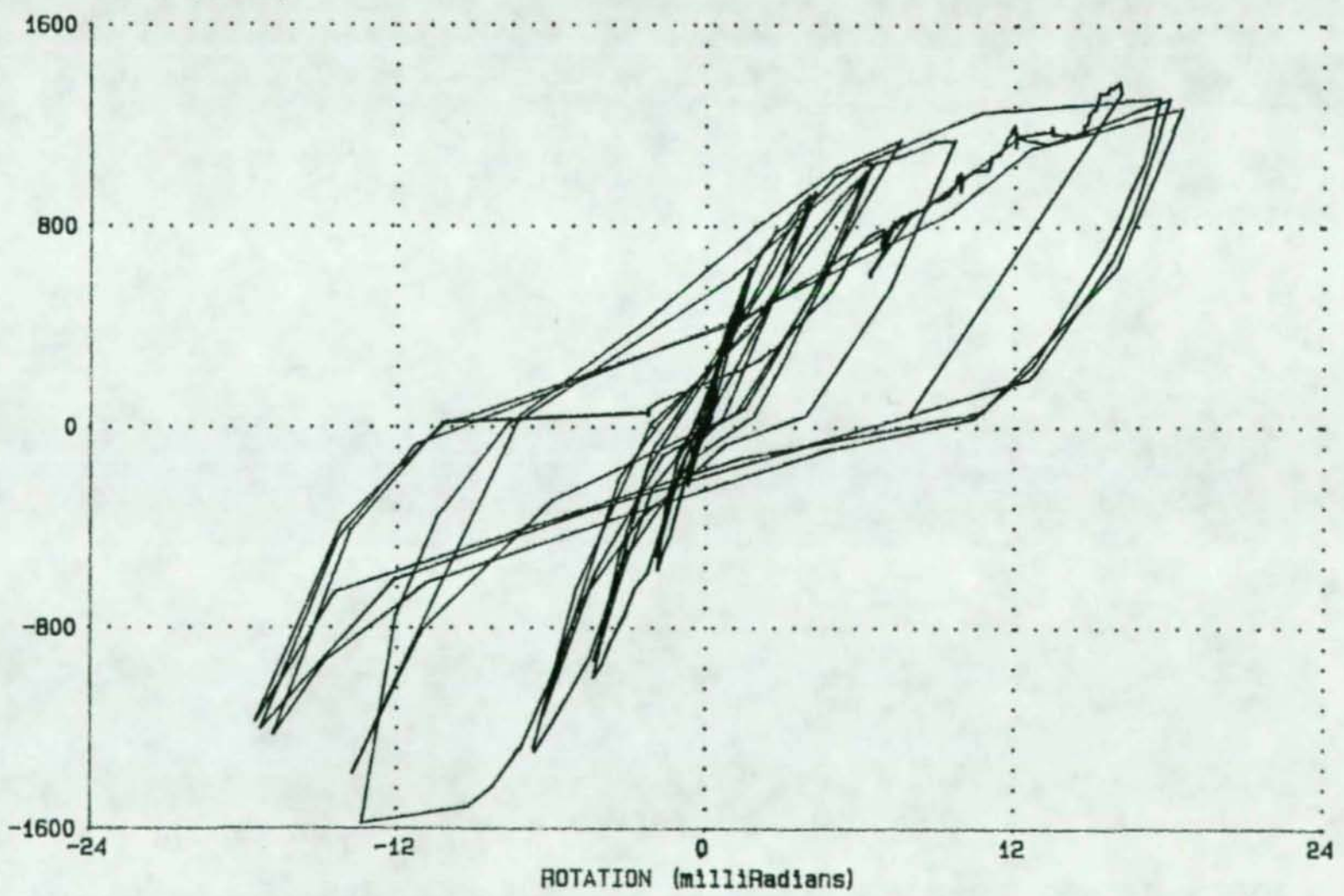

FIGURE 38 - MOMENT VS. ROTATION - LEFT CONNECTION - LL1 - LS 1 TO 61

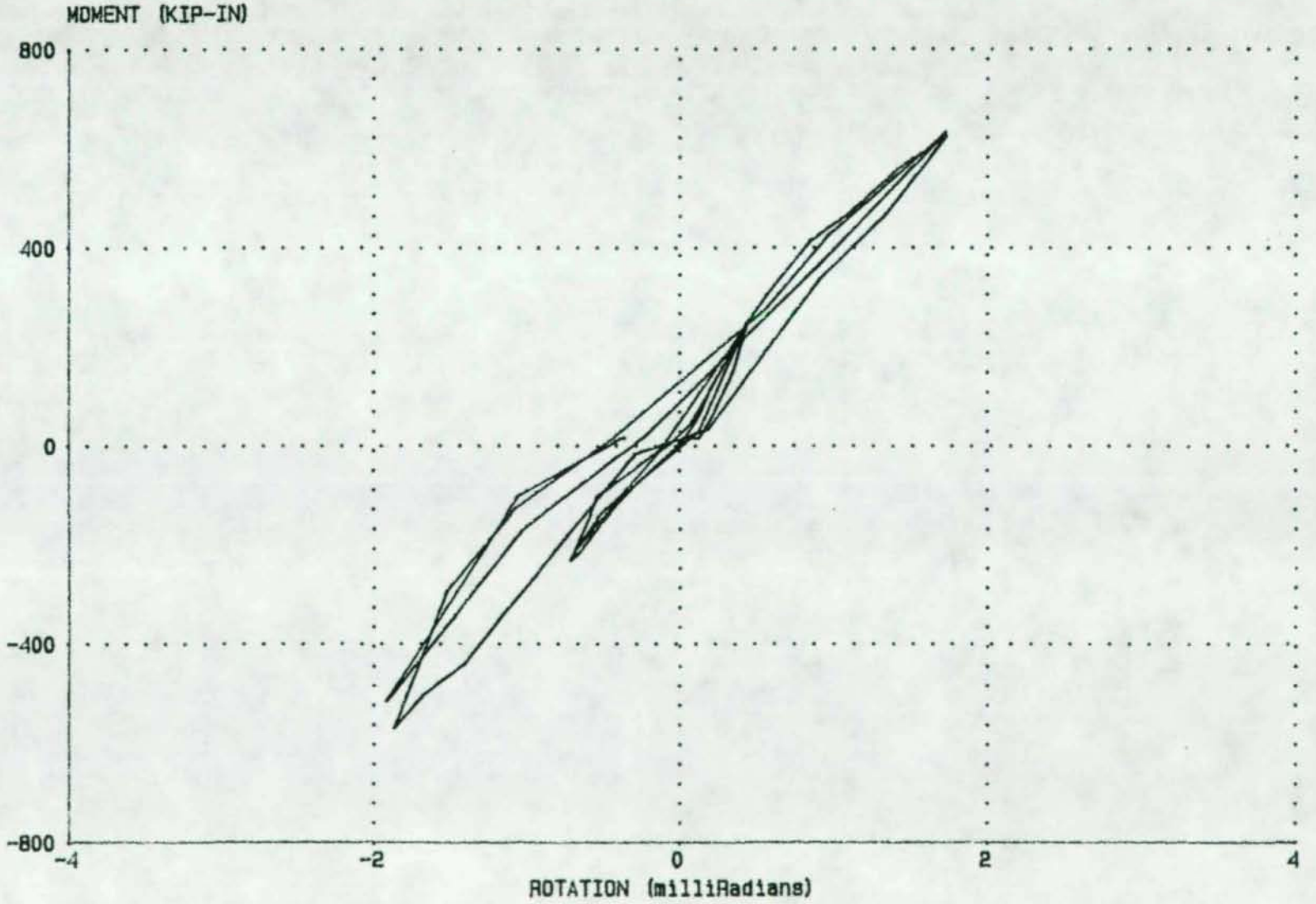

FIGURE 39 - MOMENT VS. ROTATION - LEFT CONNECTION - LL2 - LS 61 TO 160

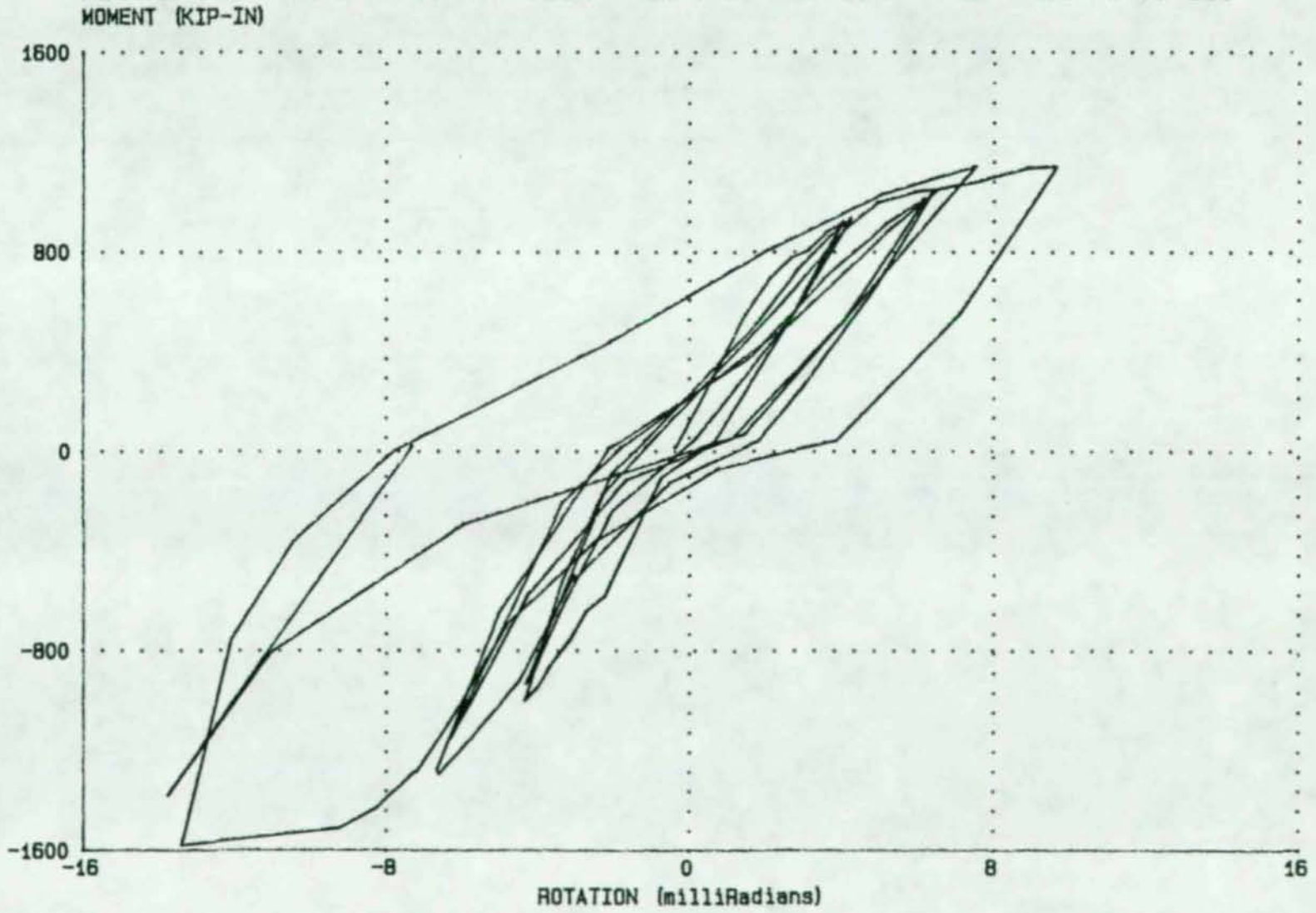

FIGURE 40 - MOMENT VS. ROTATION - LEFT CONNECTION - LL2 -- LS 61 TO 94

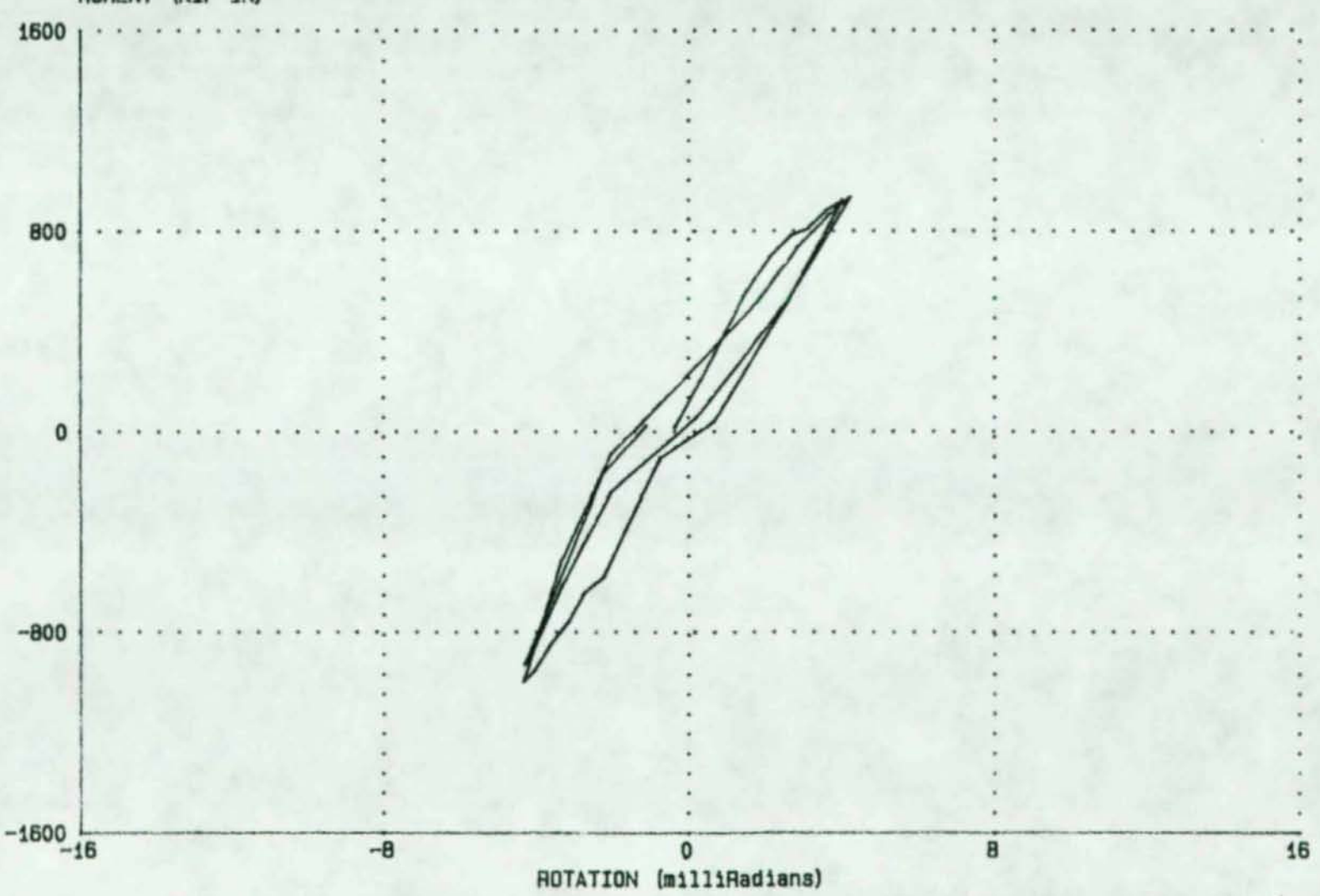

FIGURE 41 - MOMENT VS. ROTATION - LEFT CONNECTION - LL2 - LS 94 TO 127

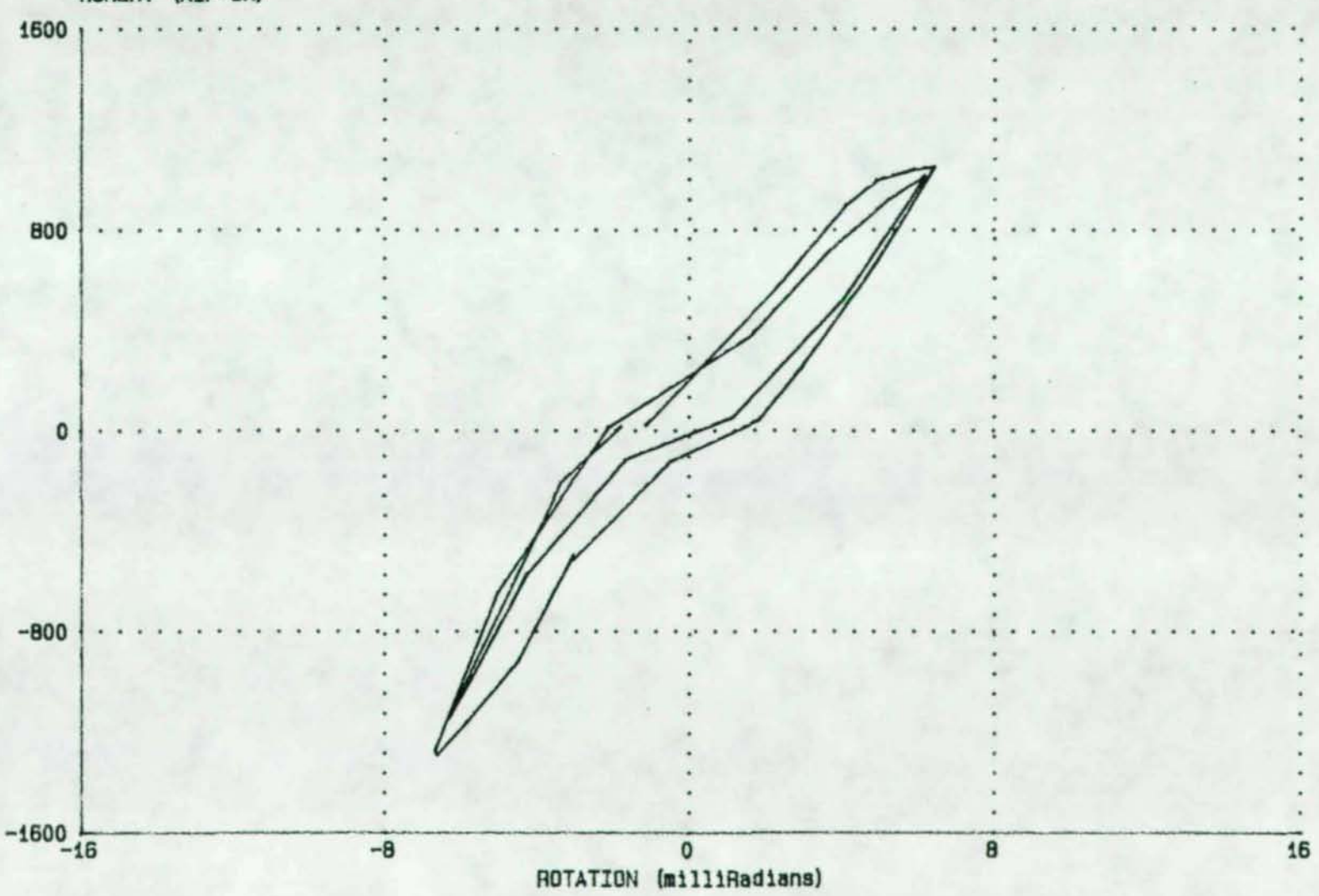

FIGURE 42 - MOMENT VS. ROTATION - LEFT CONNECTION - LS 127 TO 160

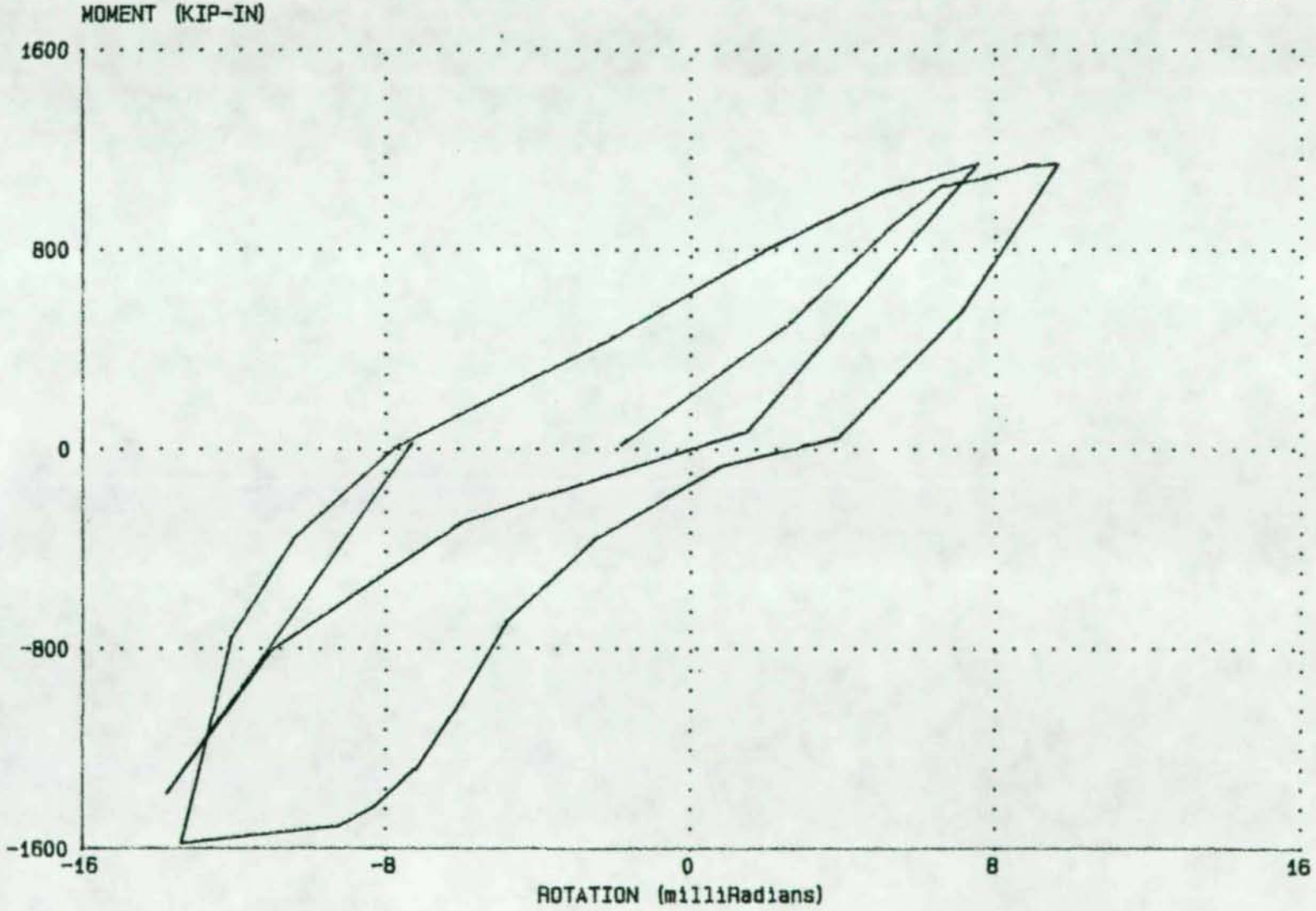

FIGURE 43 - MOMENT VS. ROTATION - LEFT CONNECTION - LL3 - LS 160 TO 213

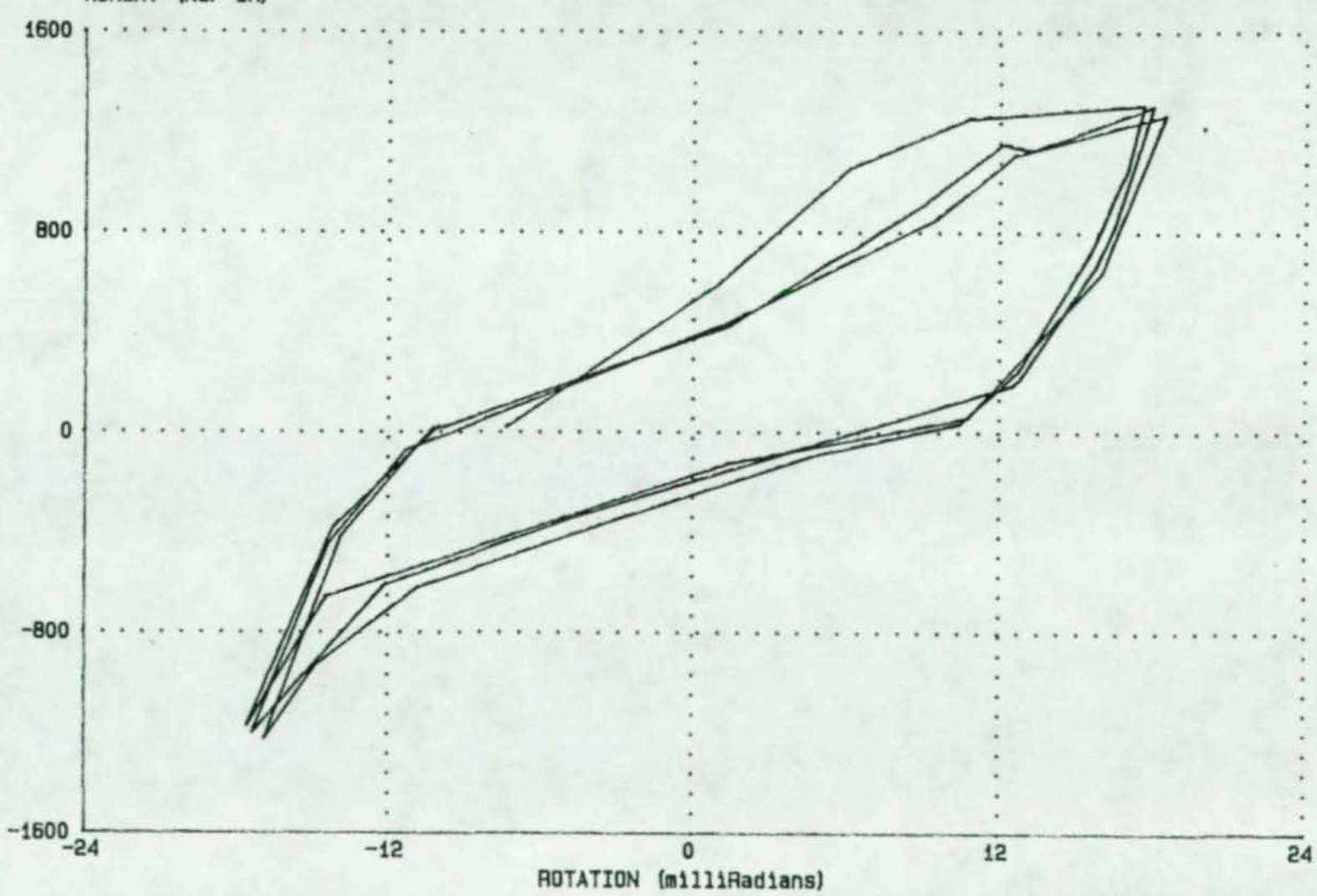

FIGURE 44 - MOMENT VS. ROTATION - LEFT CONNECTION - LL4 -LS 213 TO 353

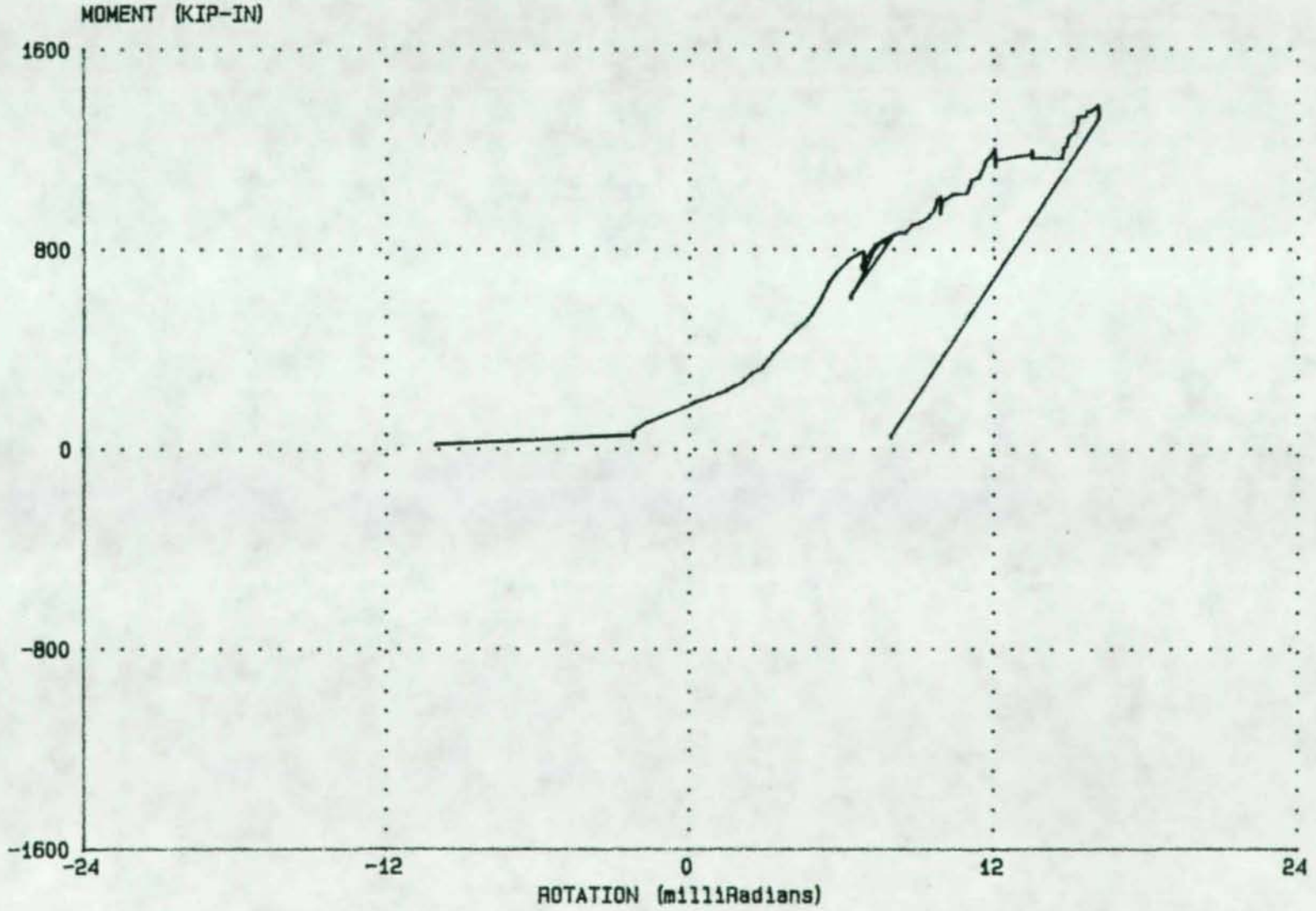

FIGURE 45 - COMPLETE MOMENT VS. ROTATION CURVE FOR SRCC1CR

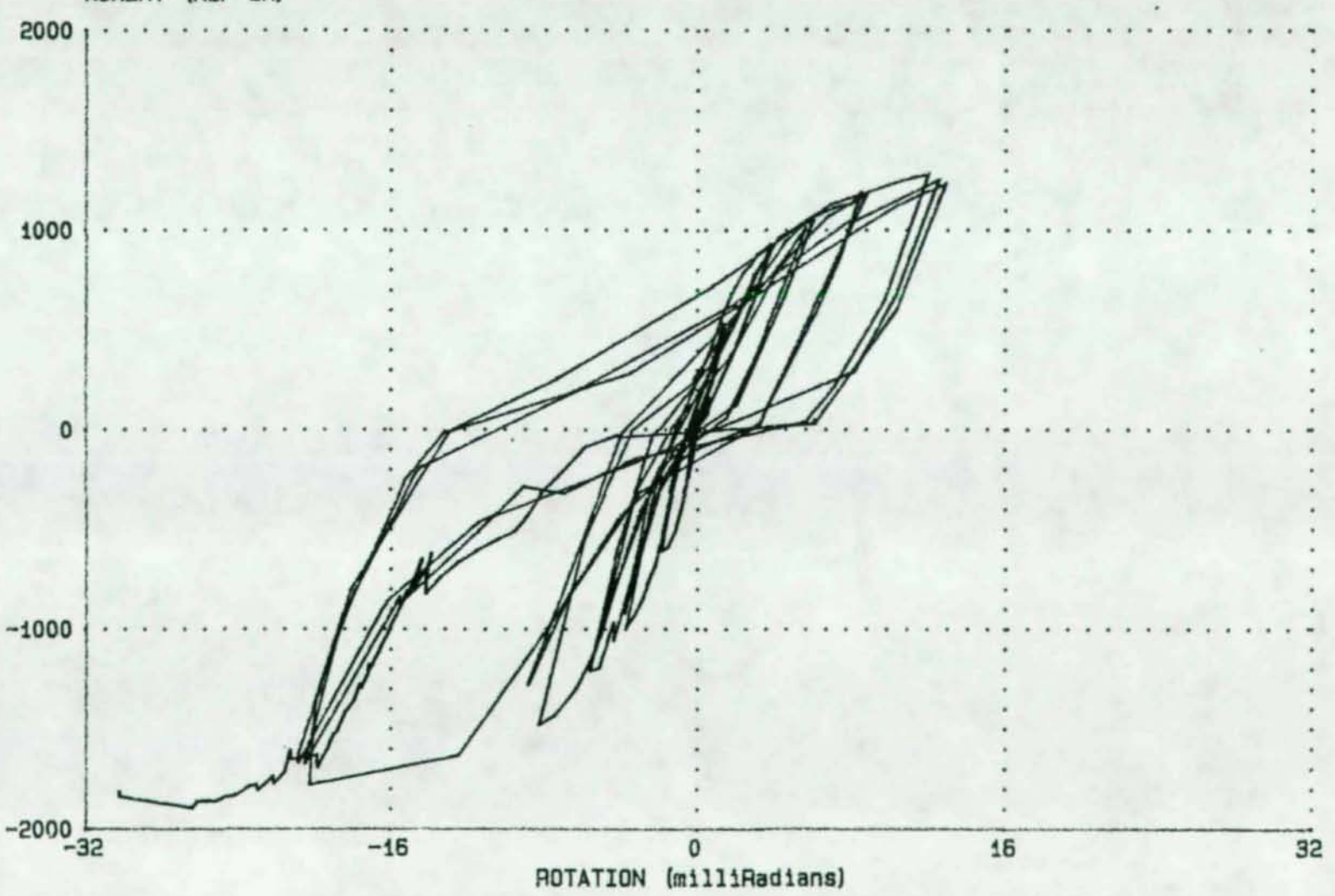

FIGURE 46 - MOMENT VS. ROTATION - RIGHT CONNECTION - LL1 - LS 1 TO 61

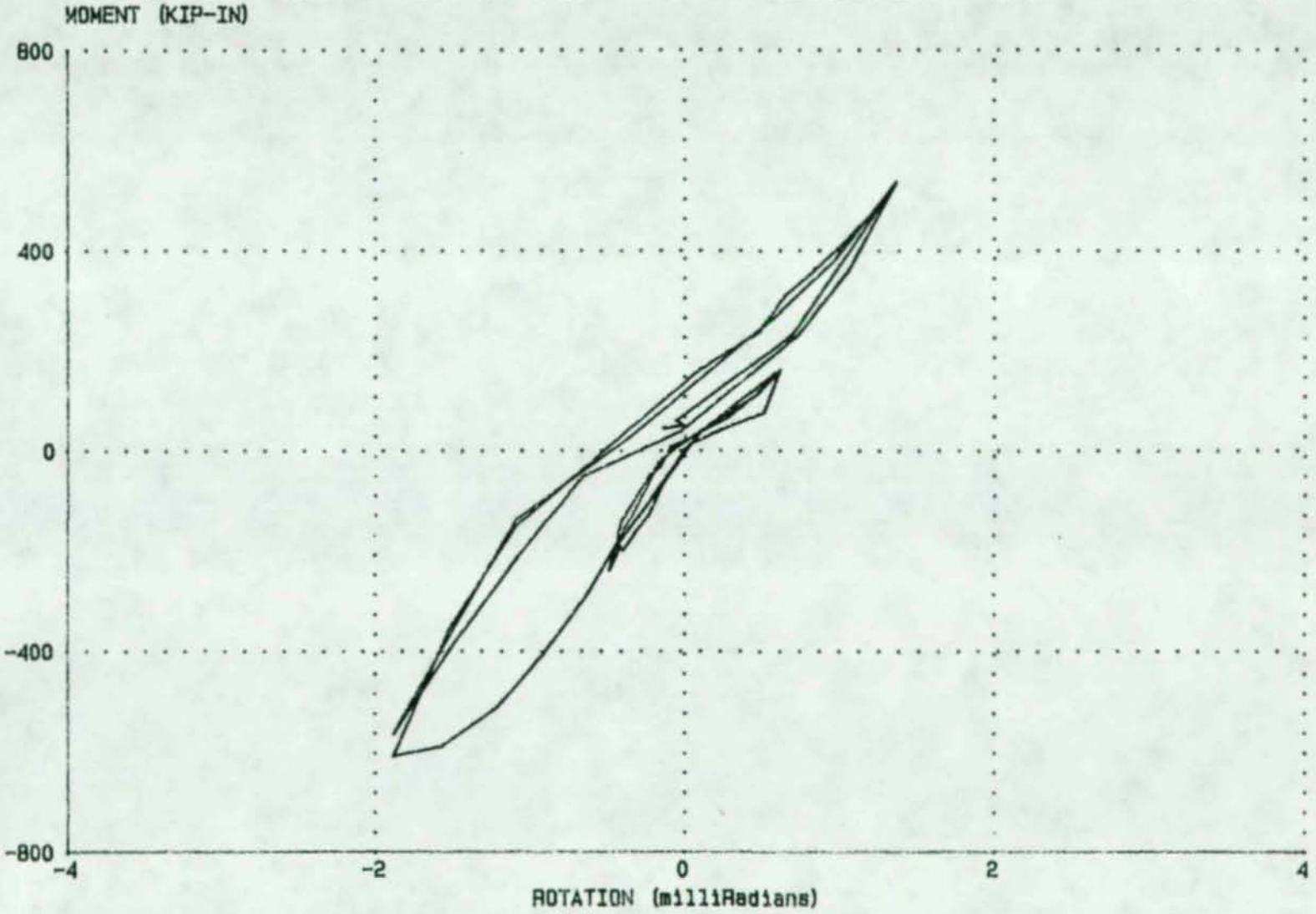

FIGURE 47 - MOMENT VS. ROTATION - RIGHT CONNECTION - LL2 - LS 61 TO 160

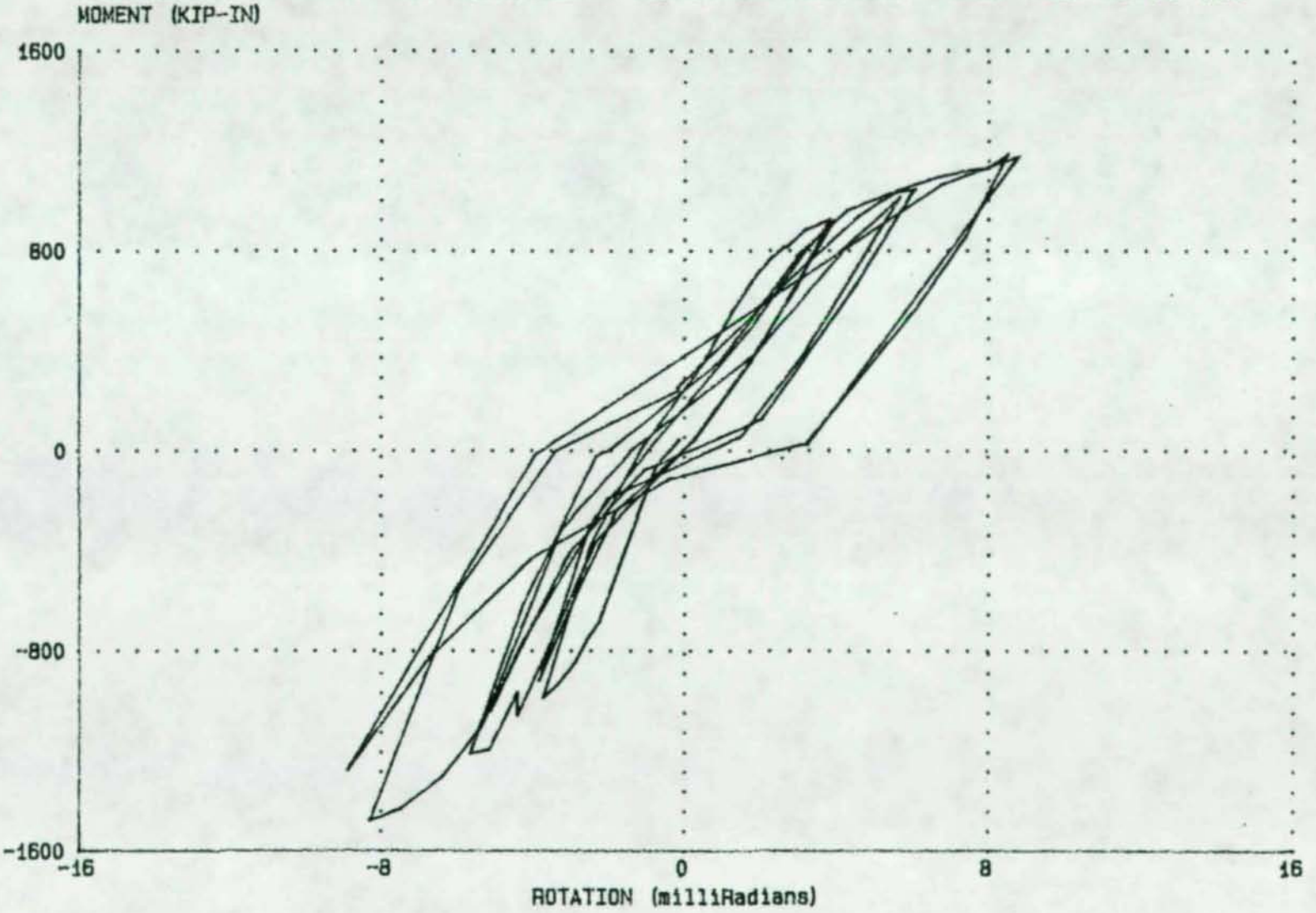

FIGURE 48 - MOMENT VS. ROTATION - RIGHT CONNECTION - LL2 - LS 61 TO 94

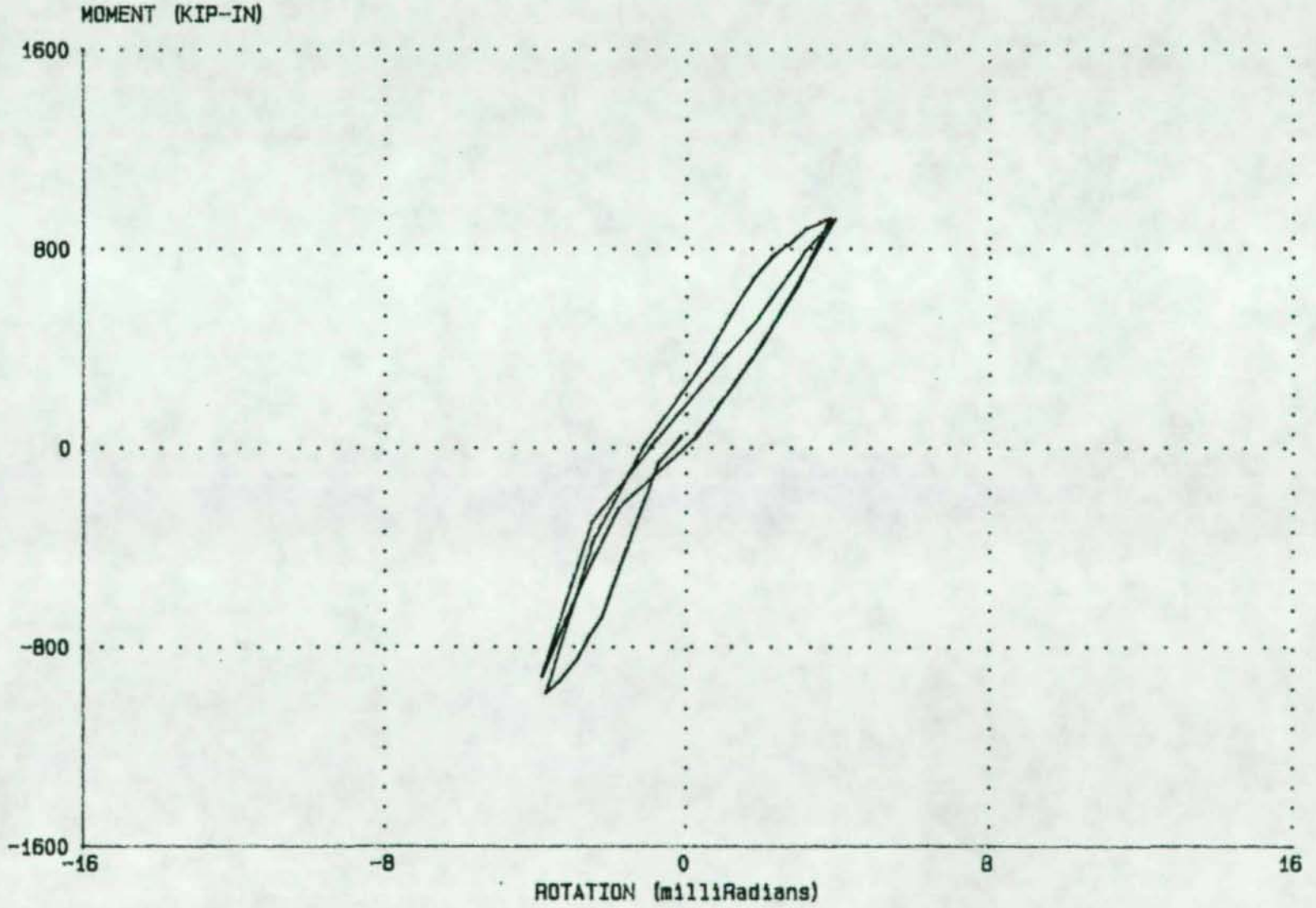

FIGURE 49 - MOMENT VS. ROTATION - RIGHT CONNECTION - LL2 - LS 94 TO 127

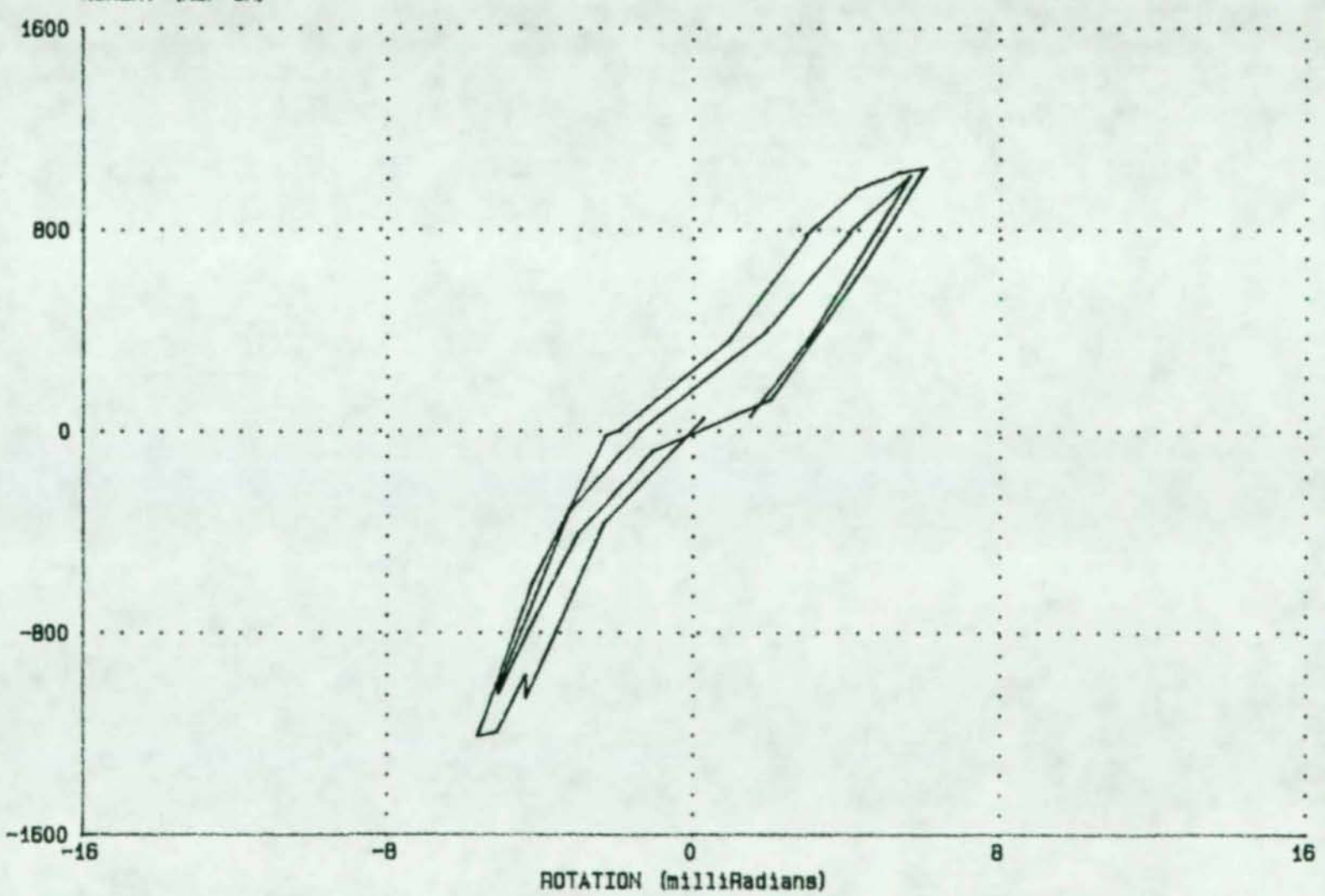

FIGURE 50 - MOMENT VS. ROTATION - RIGHT CONNECTION - LL2 - LS 127 TO 160

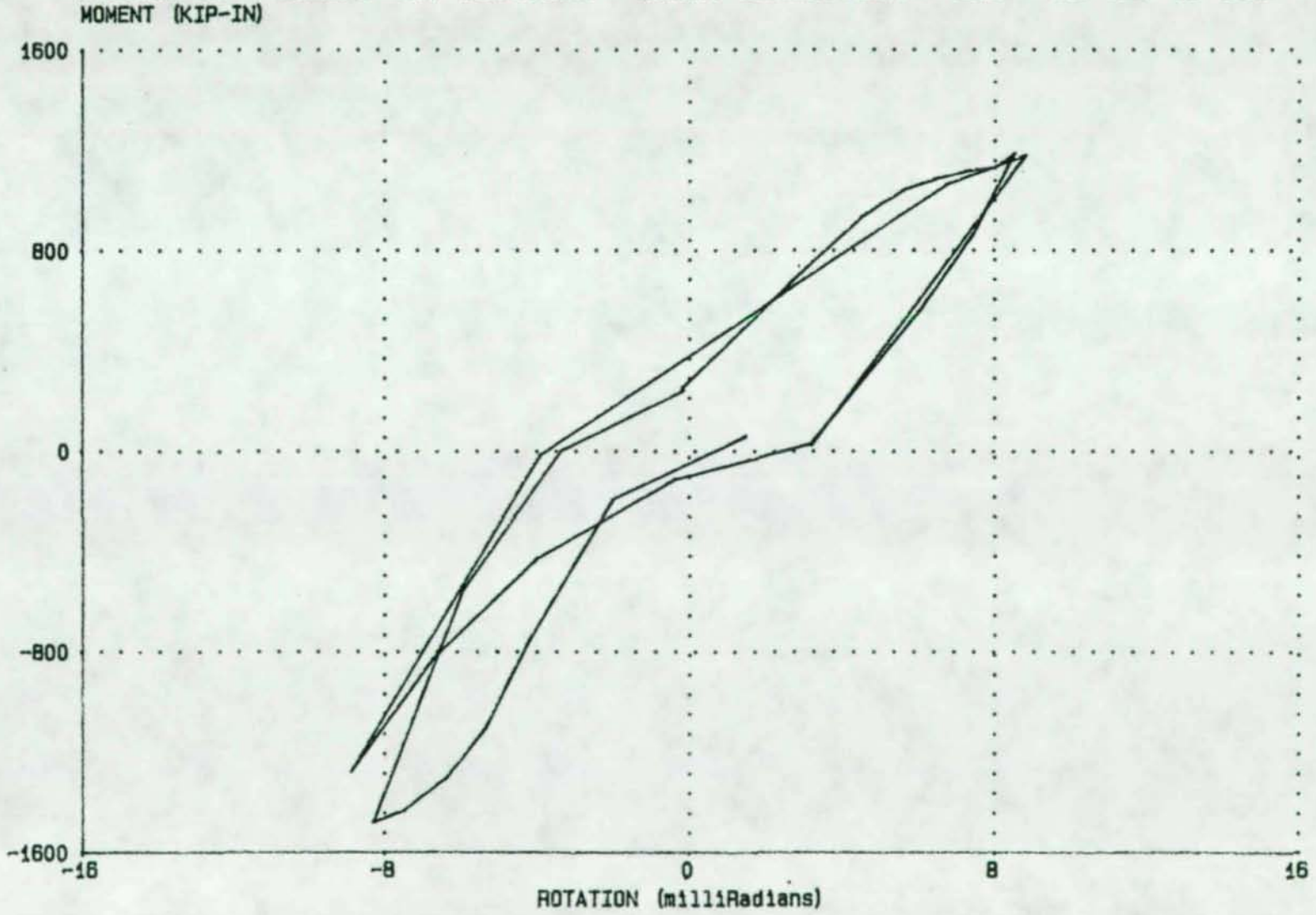

FIGURE 51 - MOMENT VS. ROTATION - RIGHT CONNECTION - LL3 - LS 160 TO 213

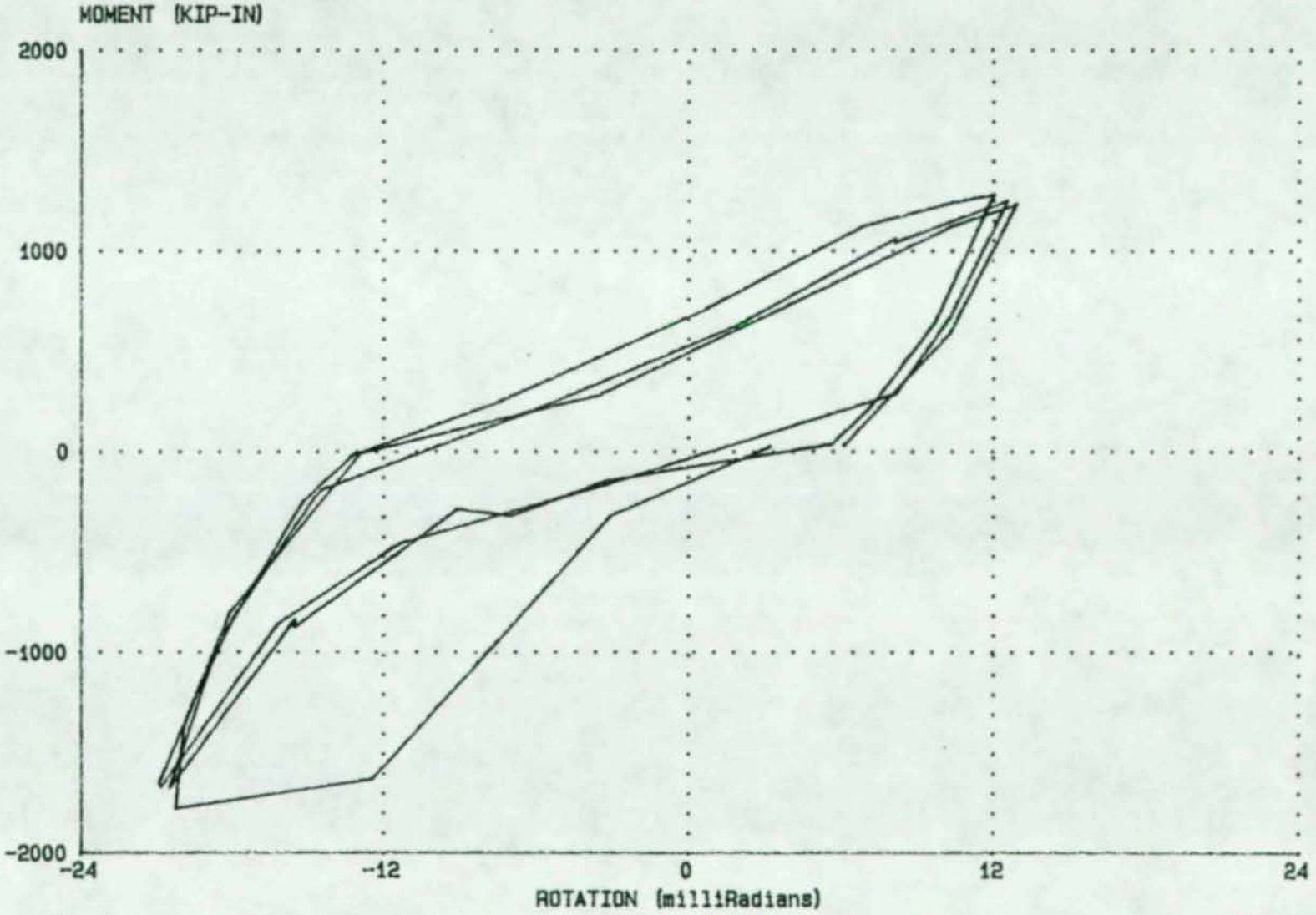

FIGURE 52 - MOMENT VS. ROTATION - RIGHT CONNECTION - LL4 - LS 213 TO 353

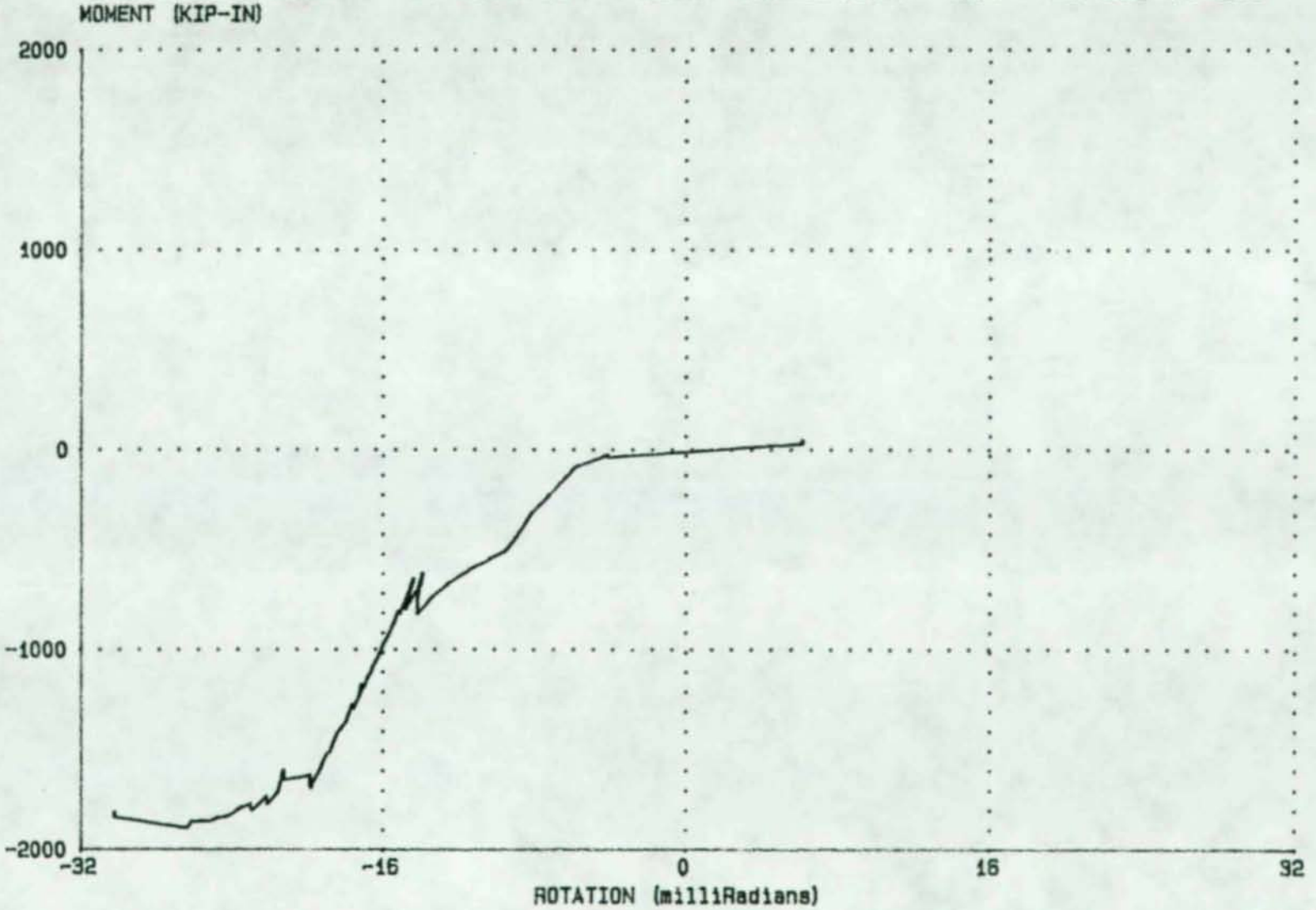

FIGURE 53 - COMPARISON OF MOMENT-ROTATION CURVES - LS 127 TO 151

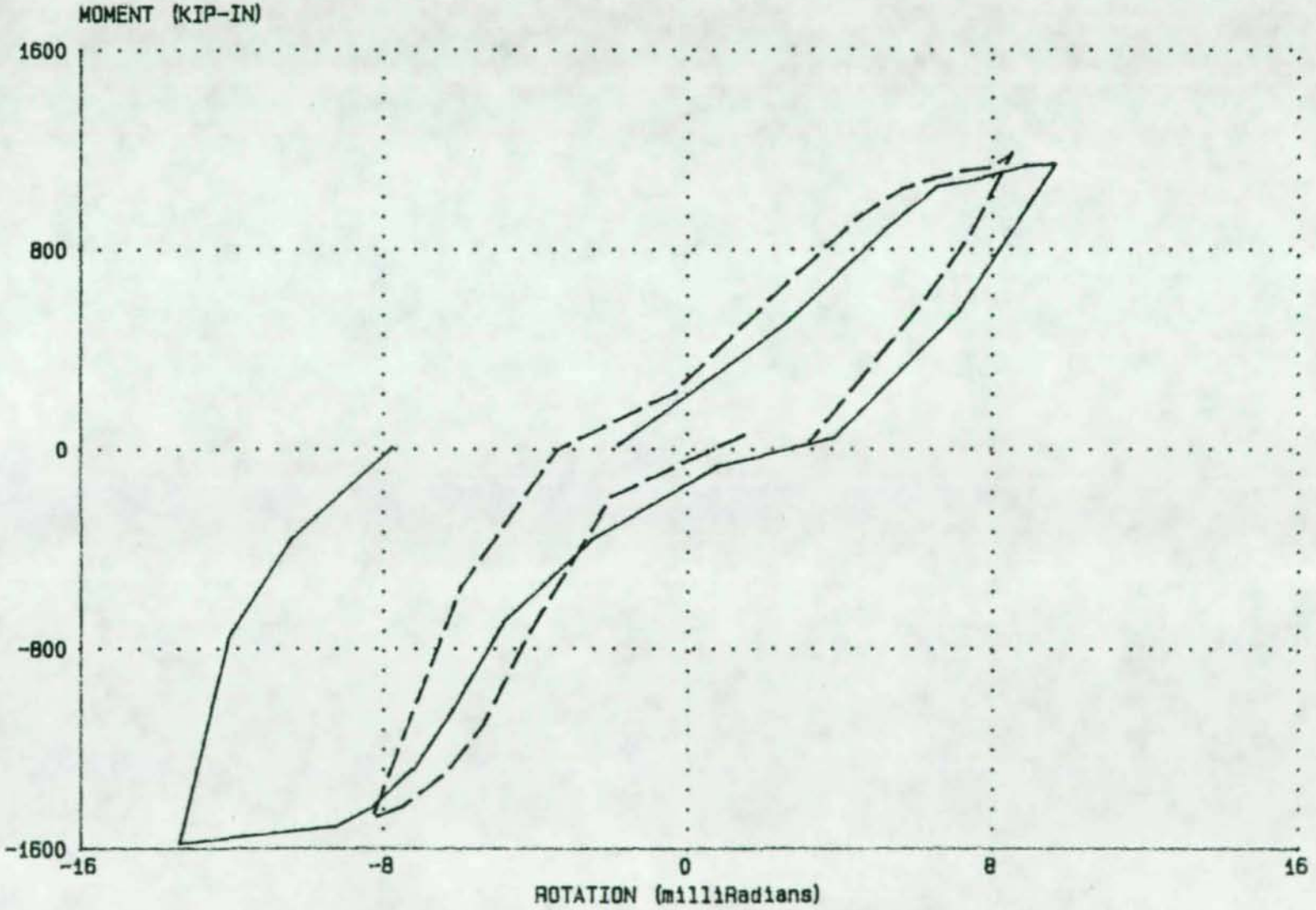

FIGURE 54 - COMPARISON OF MOMENT ROTATION CURVES - LS 160 TO 179

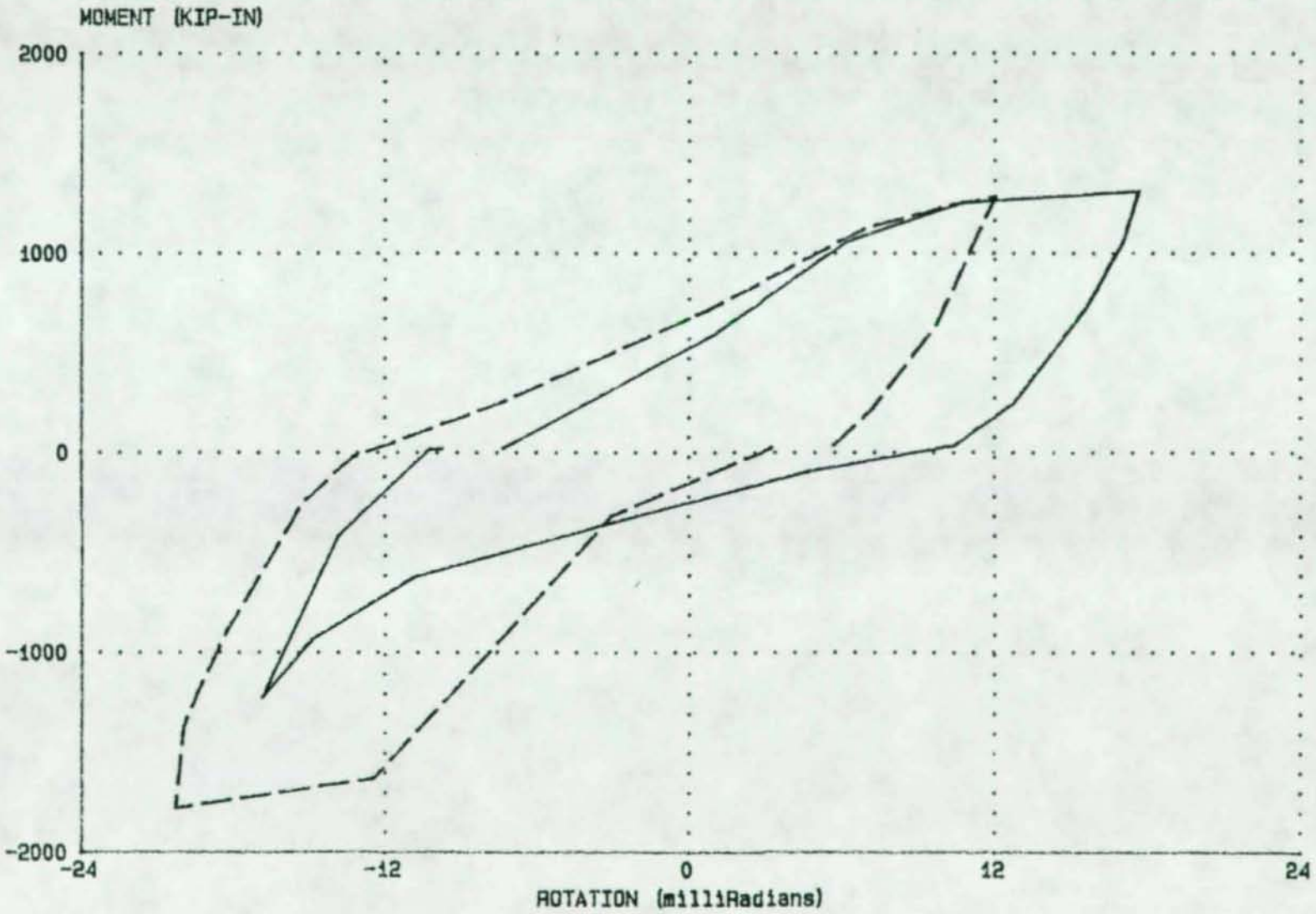

008211

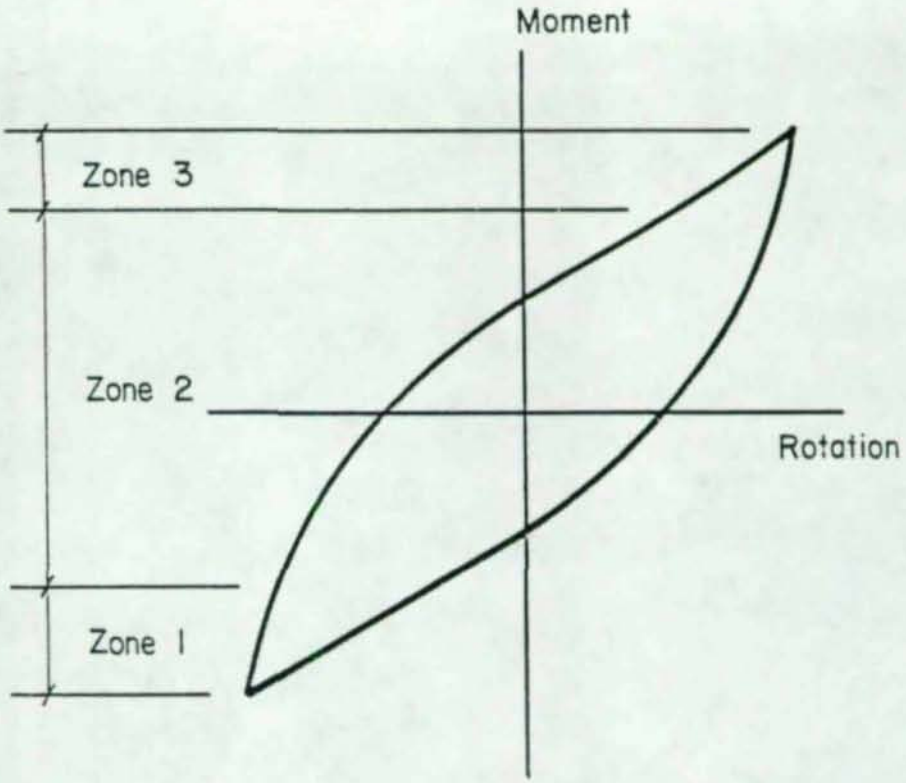

Figure 55 - Idealized loop - bare steel connection

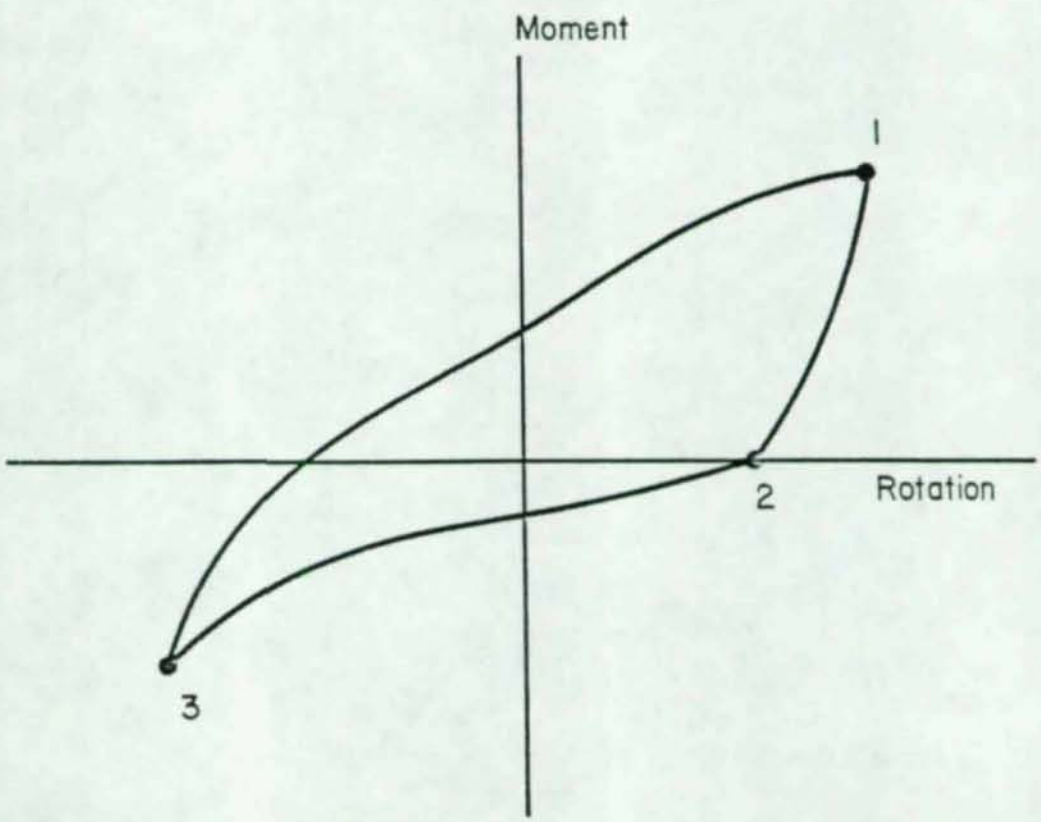

Figure 56 - Idealized loop - composite conneciton

00822

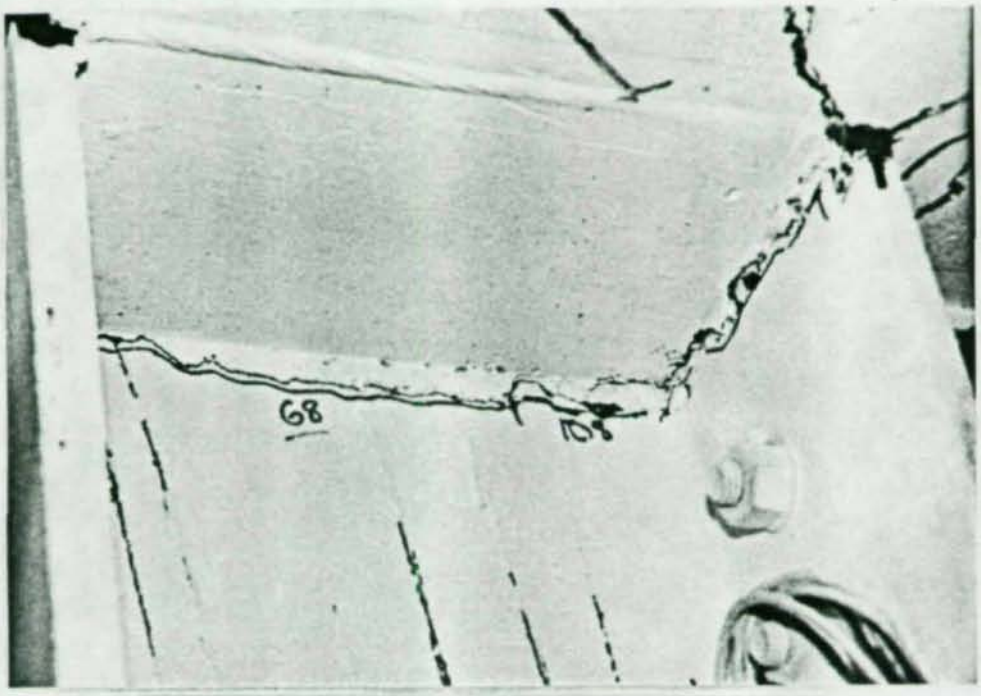

Figure 57 - Yielding of column web (LS108)

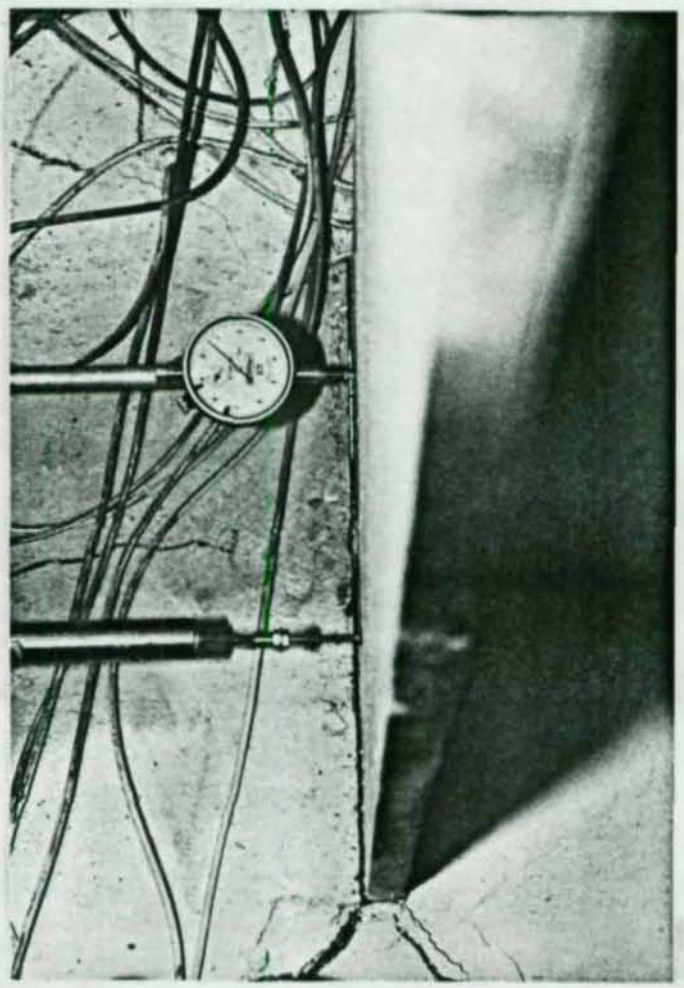

Figure 58 - Opening of slab cracks

00823

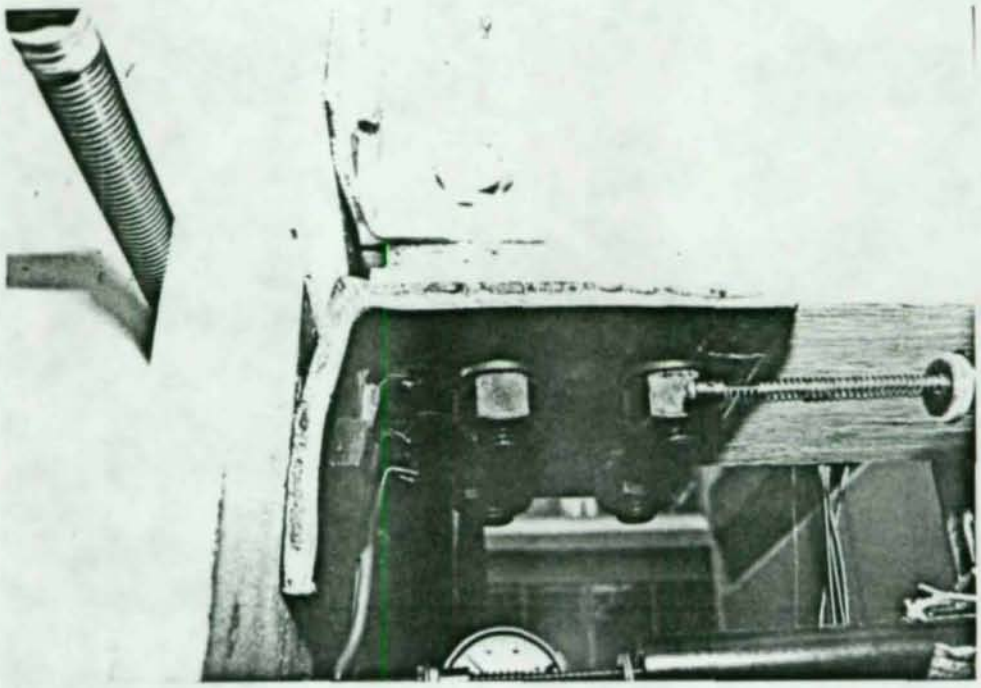

Figure 59 - Seperation of tension angle. Note that the web angles have also seperated from the column flange.

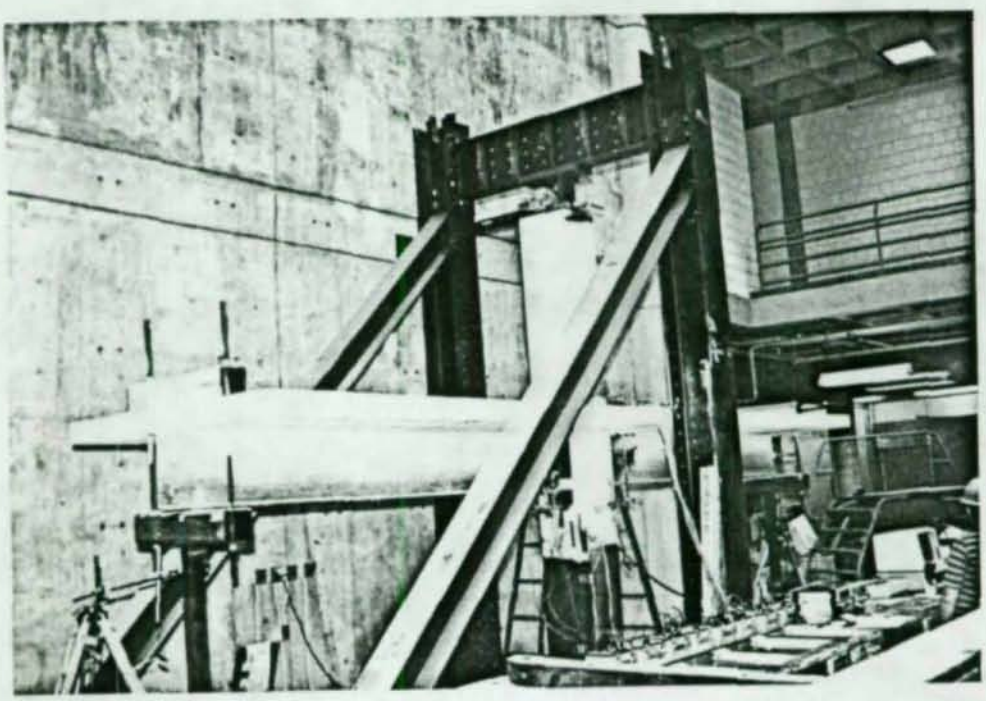

Figure 60 - Specimen in loading frame

00824

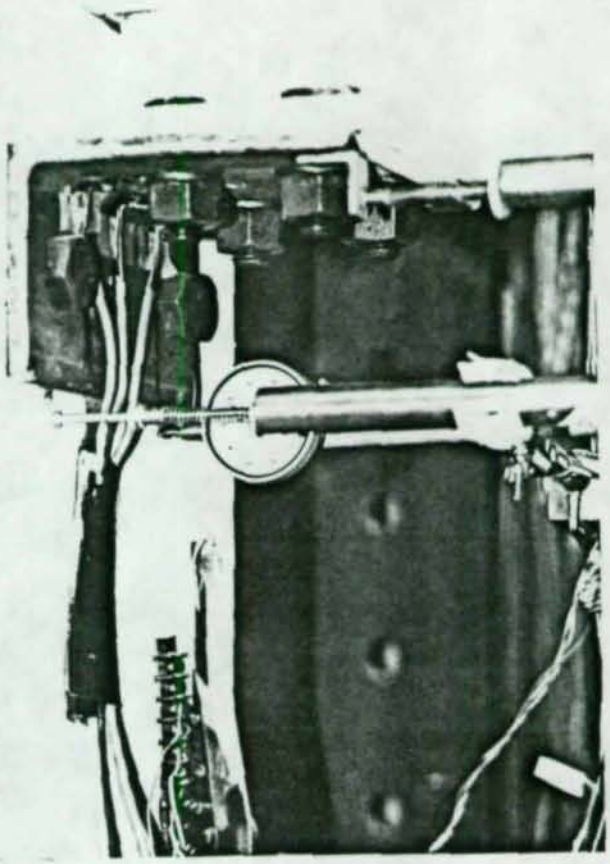

Figure 61 - Instrumentation at flange angle

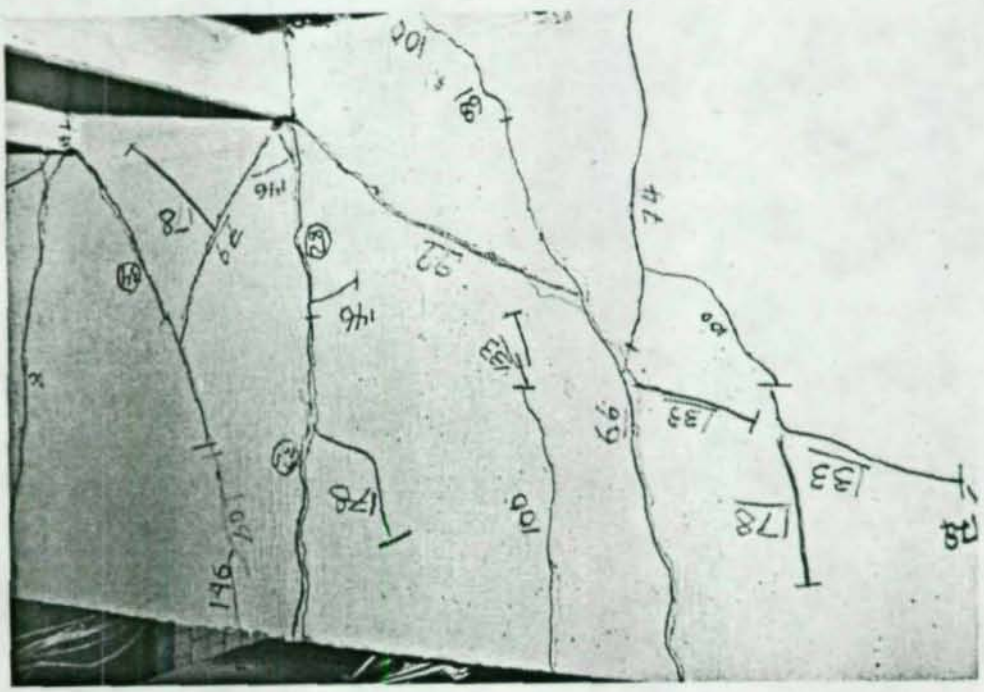

Figure 62 - Cracking of slab at LS178

FIGURE 63 - MOMENT-ROTATION CURVES FOR SRCC1ML AND SRCC1CR

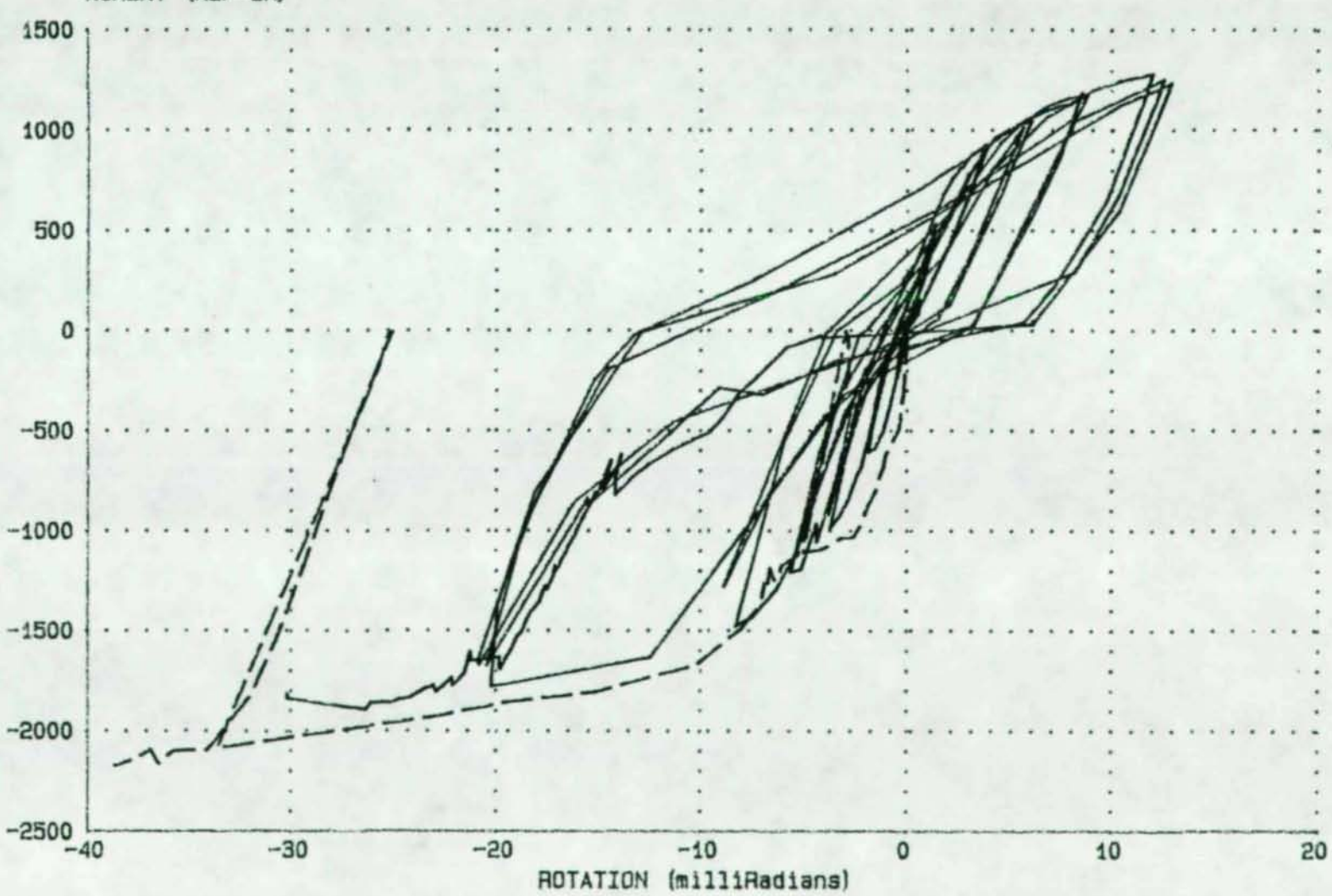

FIGURE 64 - MOMENT VS. ROTATION - GL2 AND GL3 WITH LL1 AND LL2

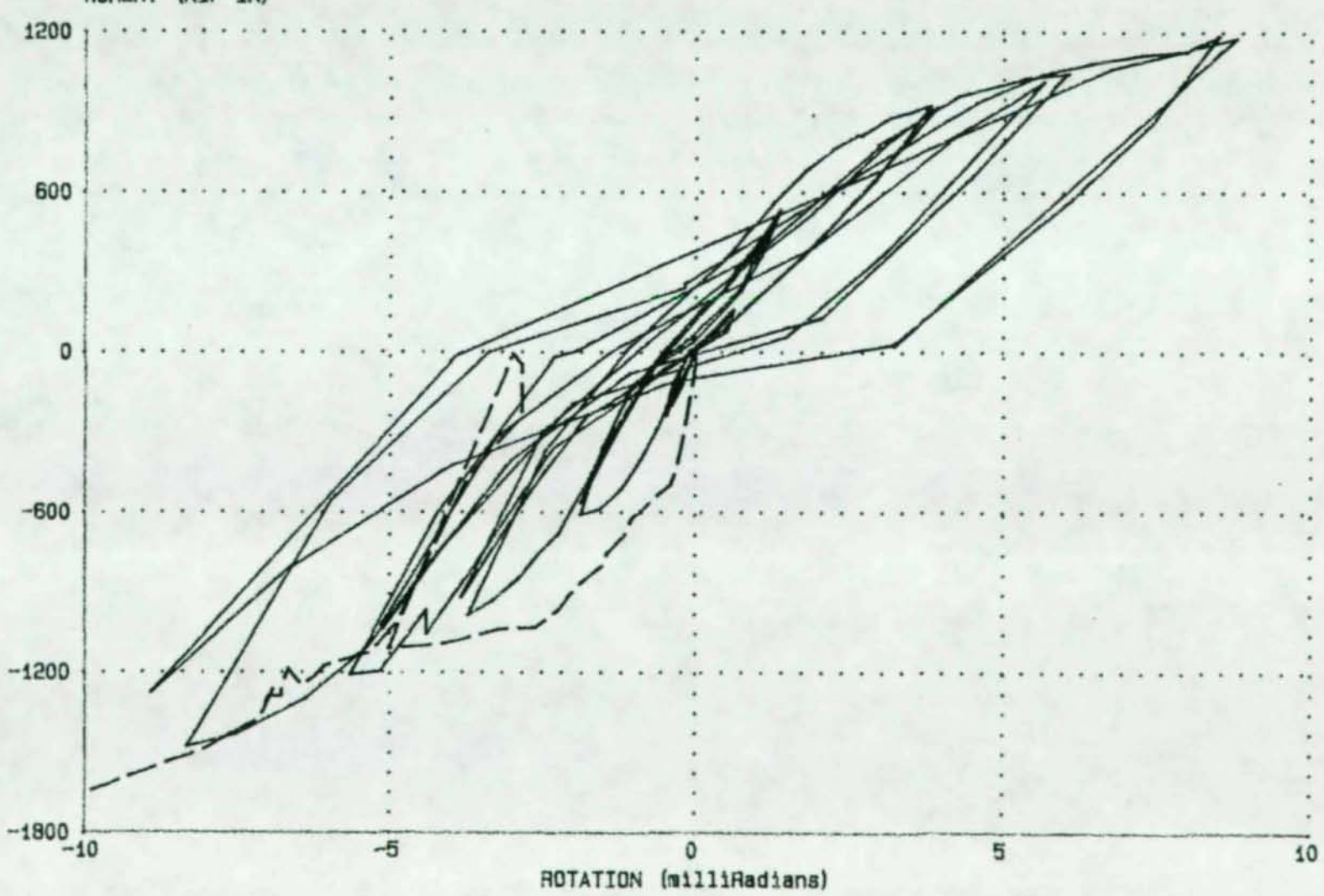

008277

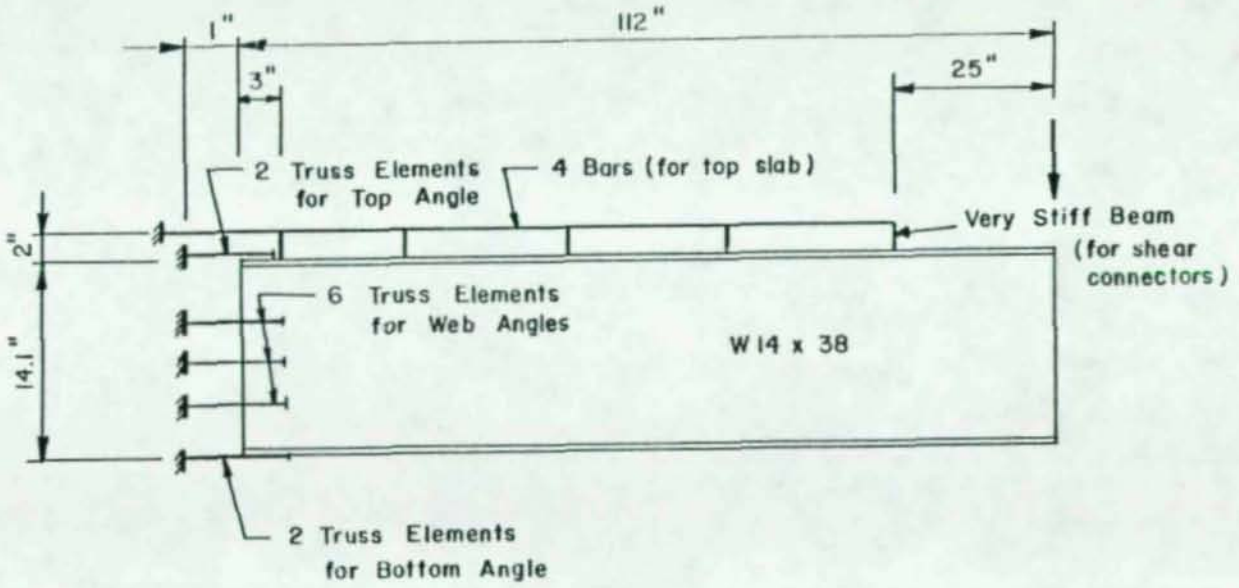

Figure 65 - Finite Element model for semi-rigid conneciton

00828

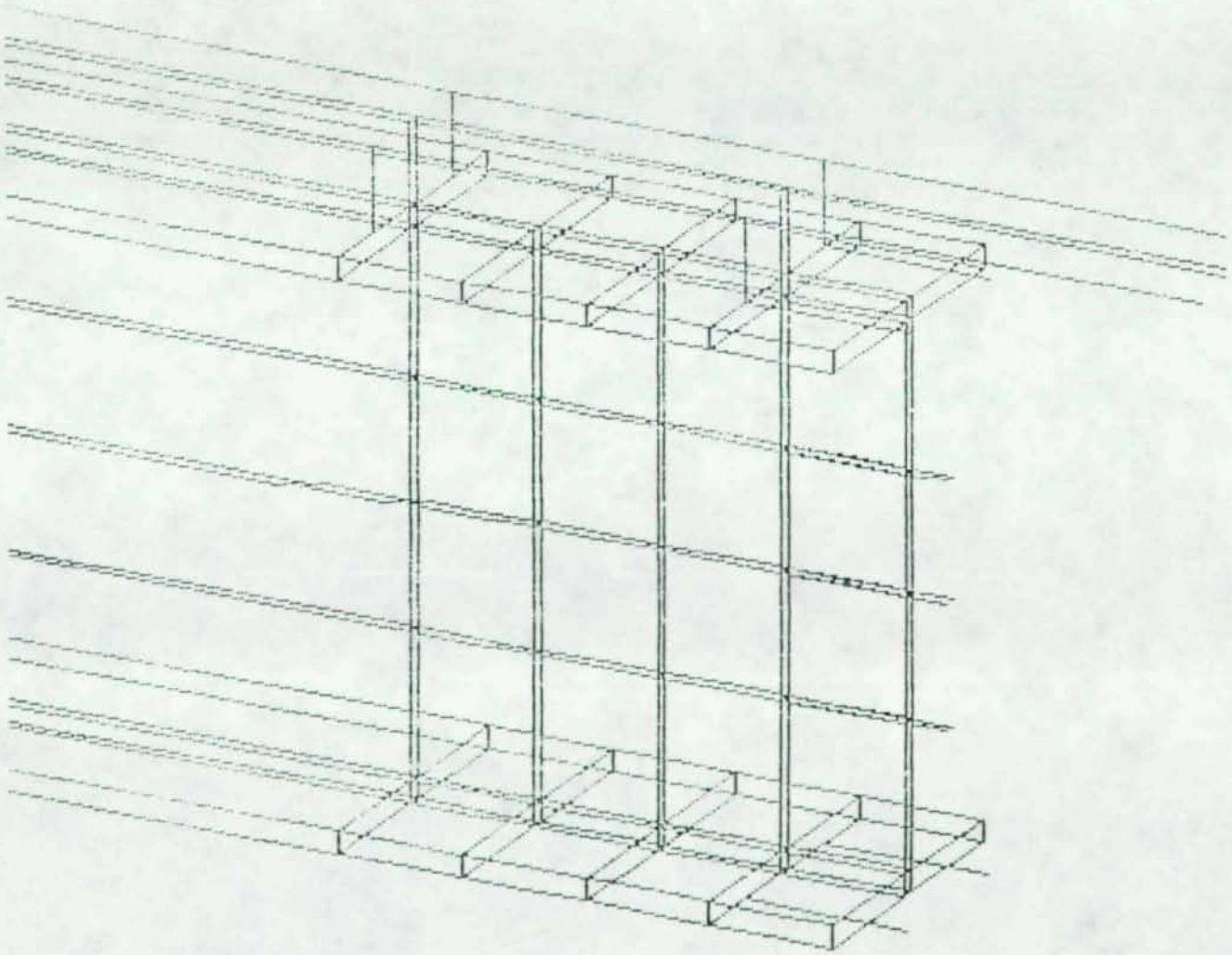

Figure 66 - Finite Element mesh of conneciton

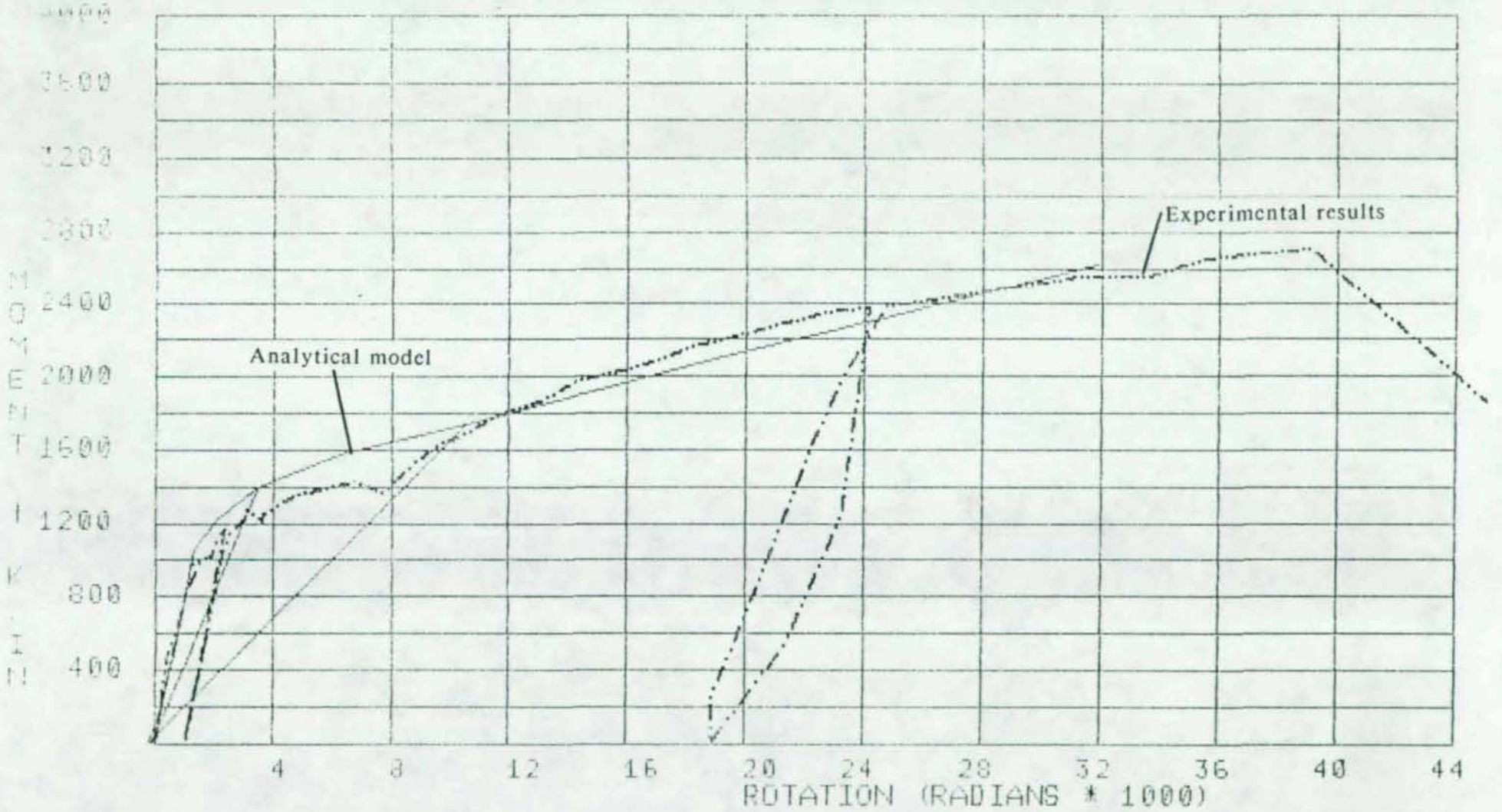

Figure 67 - Experimental and Analytical moment-rotation curves

00830

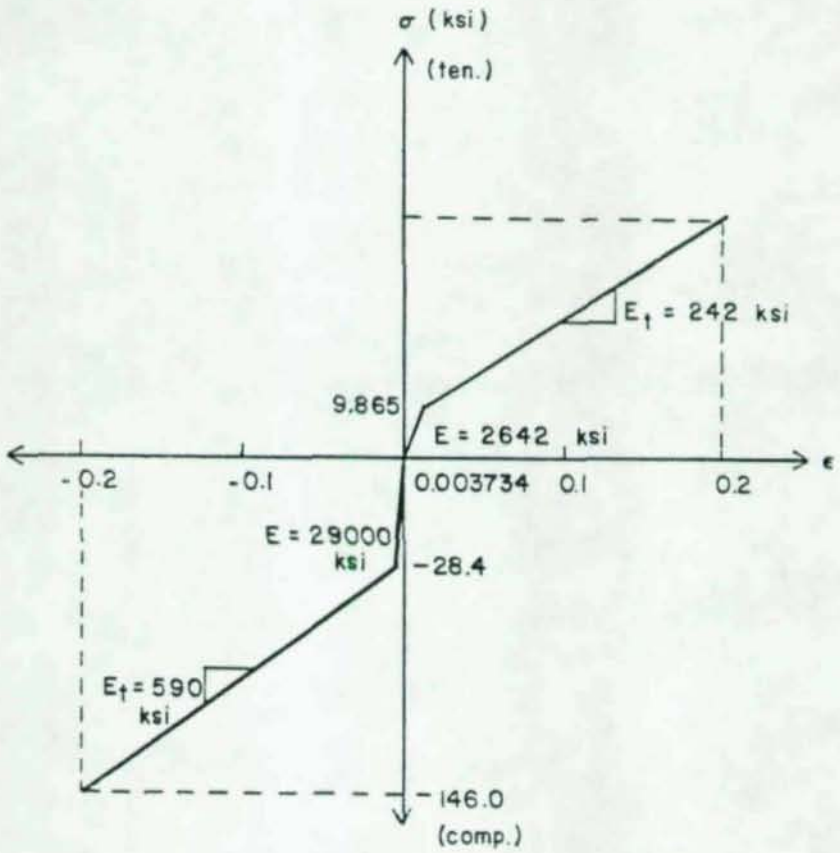

Figure 68 - Stress-Strain model for seat angles

00831

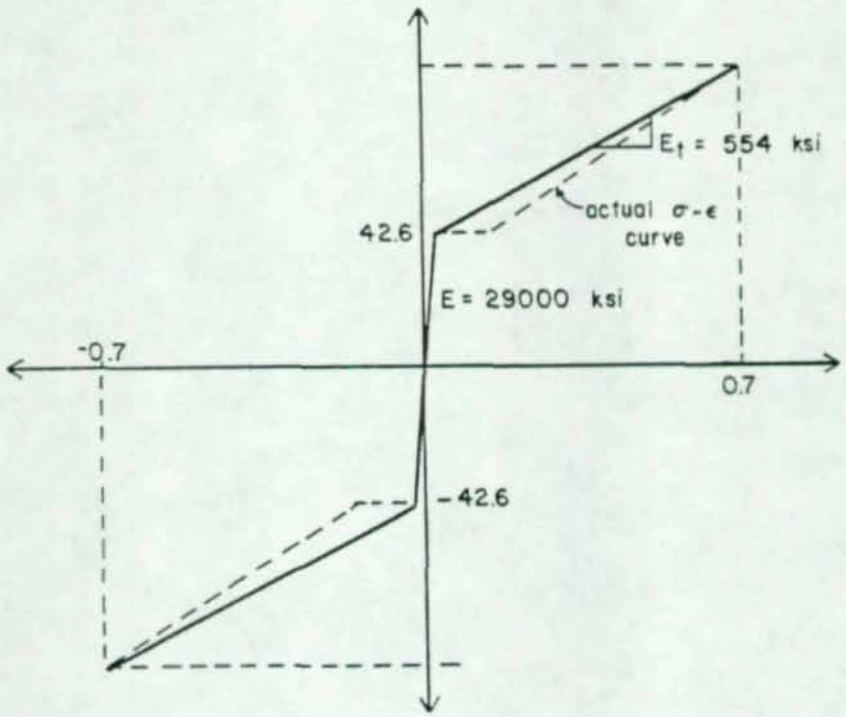

Figure 69 - Stress-Strain model for web angles

00832

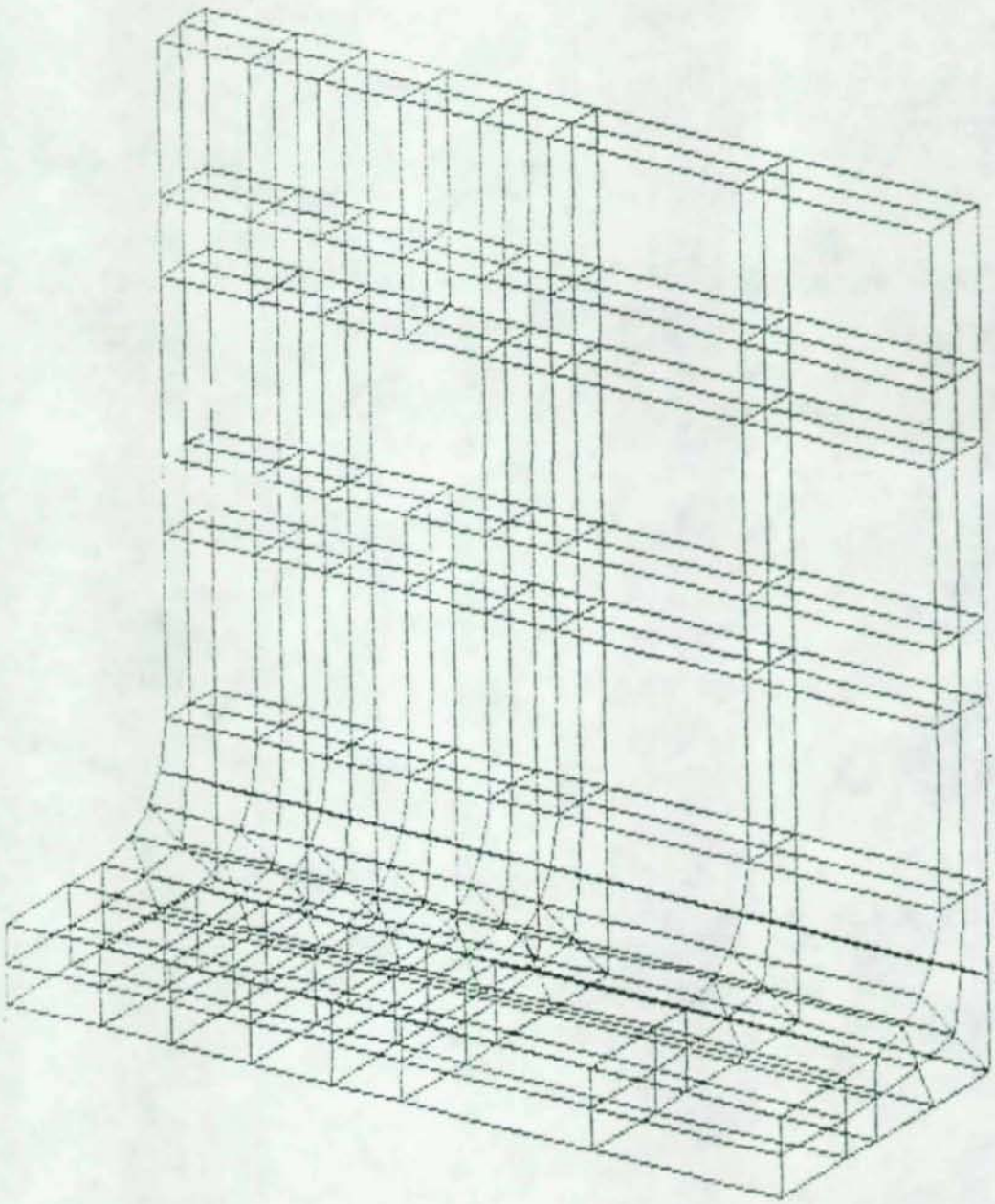

Figure 70 - Finite element mesh for seat angle. Note that only 1/2 of the angle needs to be modeled due to symetry.

00833

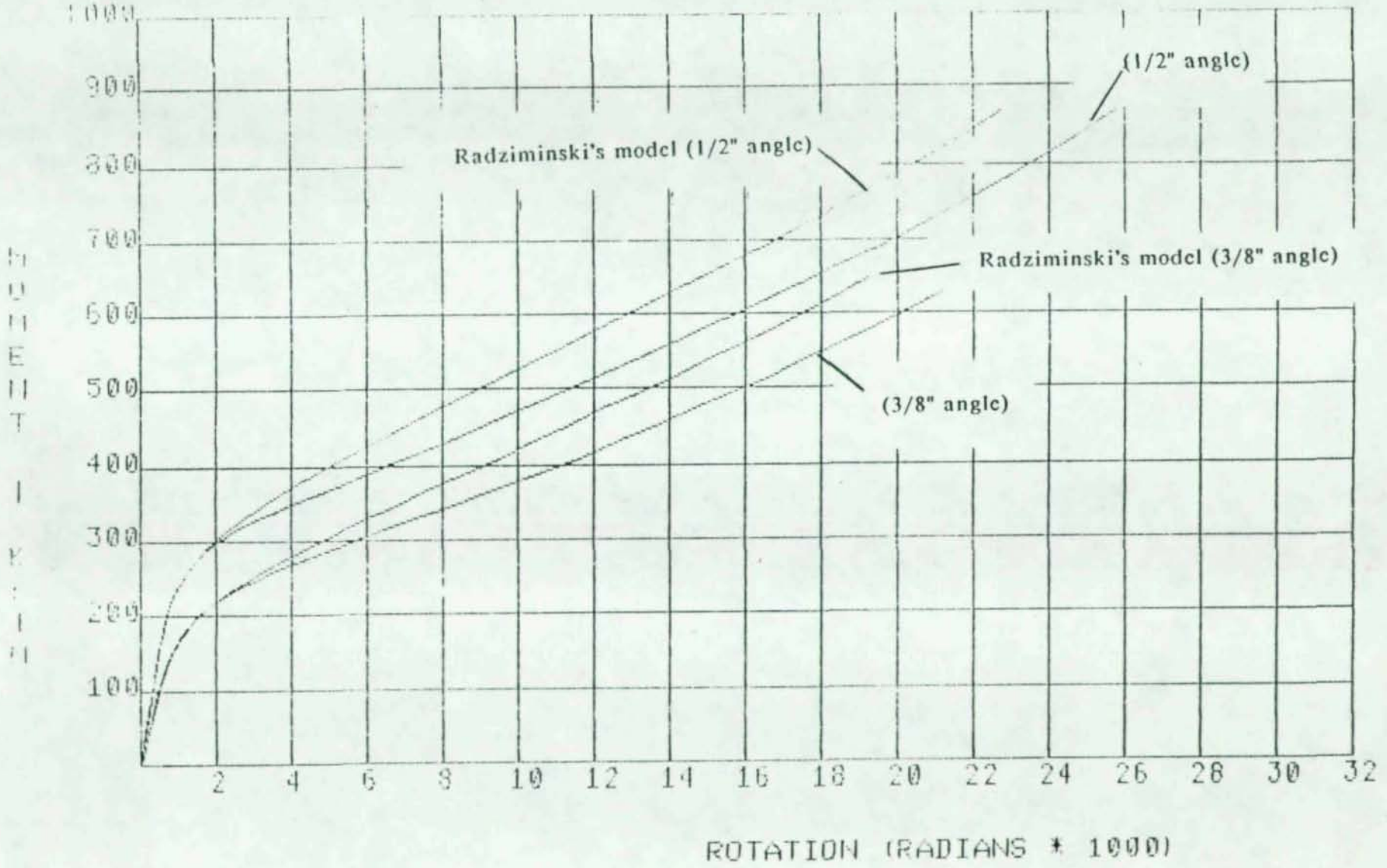

Figure 71 - Moment-Rotation curves for bare connection

00834